Air Force Institute of Technology
AFIT Scholar

Theses and Dissertations | Student Graduate Works

12-22-2011

Investigation of Gallium Nitride Transistor Reliability through Accelerated Life Testing and Modeling

Bradley D. Christiansen

Follow this and additional works at: https://scholar.afit.edu/etd

Part of the Engineering Science and Materials Commons

Recommended Citation

Christiansen, Bradley D., "Investigation of Gallium Nitride Transistor Reliability through Accelerated Life Testing and Modeling" (2011). *Theses and Dissertations*. 1092.
https://scholar.afit.edu/etd/1092

This Dissertation is brought to you for free and open access by the Student Graduate Works at AFIT Scholar. It has been accepted for inclusion in Theses and Dissertations by an authorized administrator of AFIT Scholar. For more information, please contact richard.mansfield@afit.edu.

INVESTIGATION OF GALLIUM NITRIDE TRANSISTOR RELIABILITY THROUGH ACCELERATED LIFE TESTING AND MODELING

DISSERTATION

Bradley D. Christiansen, Lieutenant Colonel, USAF

AFIT/DEE/ENG/11-04

DEPARTMENT OF THE AIR FORCE
AIR UNIVERSITY

AIR FORCE INSTITUTE OF TECHNOLOGY

Wright-Patterson Air Force Base, Ohio

APPROVED FOR PUBLIC RELEASE; DISTRIBUTION UNLIMITED

The views expressed in this thesis are those of the author and do not reflect the official policy or position of the United States Air Force, Department of Defense, or the United States Government. This material is declared a work of the U.S. Government and is not subject to copyright protection in the United States.

AFIT/DEE/ENG/11-04

INVESTIGATION OF GALLIUM NITRIDE TRANSISTOR RELIABILITY THROUGH ACCELERATED LIFE TESTING AND MODELING

DISSERTATION

Presented to the Faculty

Graduate School of Engineering and Management

Air Force Institute of Technology

Air University

Air Education and Training Command

In Partial Fulfillment of the Requirements for the

Degree of Doctor of Philosophy

Bradley D. Christiansen, B.S.E.E., M.S.E.E.

Lieutenant Colonel, USAF

December 2011

APPROVED FOR PUBLIC RELEASE; DISTRIBUTION UNLIMITED

AFIT/DEE/ENG/11-04

INVESTIGATION OF GALLIUM NITRIDE TRANSISTOR RELIABILITY THROUGH ACCELERATED LIFE TESTING AND MODELING

Bradley D. Christiansen, B.S.E.E., M.S.E.E.

Lieutenant Colonel, USAF

Approved:

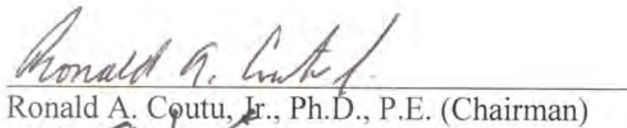
Ronald A. Coutu, Jr., Ph.D., P.E. (Chairman) — 18 OCT 2011 Date

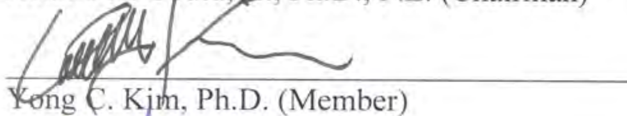
Yong C. Kim, Ph.D. (Member) — 4 Oct 2011 Date

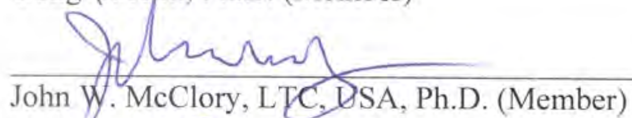
John W. McClory, LTC, USA, Ph.D. (Member) — 4 OCT 2011 Date

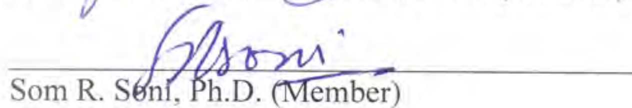
Som R. Soni, Ph.D. (Member) — 4 OCT 2011 Date

Accepted:

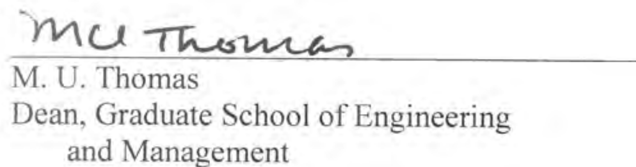
M. U. Thomas
Dean, Graduate School of Engineering and Management — 2 Nov 2011 Date

AFIT/DEE/ENG/11-04

Abstract

Gallium nitride (GaN) high electron mobility transistors (HEMT) are attractive to the United States Department of Defense for their ability to operate at high frequencies, voltages, temperatures, and power. Yet, there are concerns about the reliability, or short lifetimes, of these devices. Various degradation mechanisms and their causes are proposed in the literature. A variety of reliability tests were conducted to understand these mechanisms and causes.

A multi-stressor experiment was performed on AlGaN/GaN HEMTs with high voltage and high power as stressors. The devices tested under high power generally degraded more than those tested under high voltage. In particular, the devices tested at high voltage in the OFF state did not degrade significantly as suggested by some papers in the literature. The same papers in the literature also suggest that high voltages cause cracks and pits in the AlGaN barrier layer. However, the high-voltage-tested devices in this study do not exhibit cracks or pits in transmission electron microscope images, while the high-power-tested devices do exhibit pits.

The validity of Arrhenius accelerated-life testing when applied to GaN HEMT lifetime assessments was investigated. Temperature alone could not explain the differences in observed degradation. GaN HEMT reliability evaluations will benefit if other accelerants, such as voltage, are used. Such evaluations will consider failure mechanisms that are not primarily thermally accelerated in the complex electrothermomechanical system that is GaN.

Reports to date of GaN HEMTs subjected to forward gate bias stress include varied extents of degradation. Reported herein is an extremely robust GaN HEMT technology that survived high forward gate bias (+6 V) and current (>1.8 A/mm) for >17.5 hours, exhibiting only a slight change in gate diode characteristic, little decrease in maximum drain current, with only a 0.1-V positive threshold voltage shift, and, remarkably, a persisting breakdown voltage exceeding 200 V.

Several experiments to examine the time-dependence of GaN HEMT degradation were performed. The data fit best to an exponential model, unlike other reports. Also discovered was that the characterization temperature affects the level of degradation observed.

Results of device testing under continuous- and pulsed-direct current (DC) stressing were compared. The comparison indicates that a pulse width of sufficient brevity is less stressful than continuous DC, possibly due to the device not reaching a higher steady-state channel temperature within the pulse ON time. For longer pulse widths that may attain the higher steady-state channel temperature, thermal cycling between the extremes of the temperature range may induce more degradation than continuous DC.

For my loving, devoted, and encouraging wife

Acknowledgments

I have accumulated a great debt of gratitude over my lifetime and especially over the past 3 years. I'll begin my repayment by starting at the beginning.

I thank God for His sustaining hand. The following passages of scripture have comforted and strengthened me. "Now when our hearts were depressed, and we were about to turn back, behold, the Lord comforted us, and said: Go…and bear with patience thine afflictions, and I will give unto you success" (Alma 26:27). "I do not boast in my own strength, nor in my own wisdom; but behold, my joy is full, yea, my heart is brim with joy, and I will rejoice in my God. Yea, I know that I am nothing; as to my strength I am weak; therefore I will not boast of myself, but I will boast of my God, for in his strength I can do all things; yea, behold, [the miracle of graduation], for which we will praise his name forever" (Alma 26:11-12).

I thank my parents for my life and their love, encouragement, and prayers. I thank my siblings for their love, support, and prayers.

I am grateful to my initial math teacher in middle school who saw in me greater potential than my parents or I did, and recommended to my mother that I be advanced from his math class. I am grateful to my paternal grandmother who fostered my interest in computers by paying for me to attend computer programming classes.

My wife has provided constant encouragement. She has loved me when I haven't felt deserving of her love. She has kept me on track when I didn't want to be on track. I truly would not be at this point in time without her. I thank her for her patience with me.

My children are an inspiration to me. I thank them for their hugs, kisses, and sweet prayers.

I thank the United States Air Force for the opportunity to pursue a doctorate. I thank AFRL/RYD and another external agency for funding.

I am grateful to Dr. Coutu for his excitement, guidance, and prodding. I thank Dr. Kim, LTC McClory, and Dr. Soni for accepting the invitation to be committee members and improving my defense presentation and this document.

I am grateful to my friends at AFRL for their encouragement, guidance, suggestions, and support: Chris Bozada, Eric Heller, Steve Tetlak, Brian Poling, Dave Via, Jim Theimer, Don Dorsey, Antonio Crespo, Kelson Chabak, and Jim Gillespie. I thank Roger Graham of NanoTEM for TEM imaging.

I thank my Navy collaborators: Dr. Todd Weatherford, Alan Acker, and Jonathon Gregory.

I thank my professors for preparing me for this research. Those not previously mentioned are Dr. Yeo, Lt Col Starman, Dr. Cain, Maj Bush, and Dr. Bulutoglu.

I thank Firooz Faili, Felix Ejeckman, and Daniel Francis of Group4 Labs and Rich Johnston for their support.

My family has been blessed with faithful Home Teachers during this period of time: Rich Davis, Brook Bentley, Jonathon Climer, Josh Gustafson, and Sean Holley.

I have appreciated my associations with classmates and friends: Ben Crossley, Derrick Langley, Will Cobb, Neal Kraft, Scott Callihan, Dane Fuller, Kurt Rouser, Chris Martin, Tom Edelmann, Mike Stackhouse, Nina Weissgerber, Calvin Roman, Jon Potter, Rob Lake, Jeff Baugher, Scott Goodman, Chad Hale, Jason Tellez, Steve Ross, Eugene Heuschel, Jesse Lynn, and Eric Buschelman.

I thank Dave Doak and Don Bodle, Unix administrators, for—besides their normal duties—resetting my password. I thank Rich Mansfield and Patrick Colucci, librarians, for locating useful items for me. I thank Bob Memering for making a poster for me.

Indeed, I have been blessed to have crossed the paths of so many good people.

Bradley D. Christiansen

Table of Contents

Page

Abstract iv
Table of Contents ix
List of Figures xiv
List of Tables xxi
List of Abbreviations xxiv
I. Introduction 1
1.1. Motivation 1
1.1.1. Desirable Performance Attributes 2
1.1.2. Circuits and Applications 3
1.2. Accelerated Testing Research 3
1.2.1. Problem Statement 4
1.2.2. Thesis Statement 4
1.2.3. Contributions 4
1.3. Modeling Research 5
1.3.1. Problem Statement 5
1.3.2. Thesis Statement 5
1.3.3. Contribution 6
1.4. Publications 6
1.5. Purpose 7
1.6. Document Overview 7
II. Background 9
2.1. Brief History 9
2.2. Definitions 10

2.3. Fabrication Processes 14

2.4. GaN HEMT Structure 17

2.5. Physics 19

2.5.1. Basic Operation 19

2.5.2. DC Performance 19

2.5.3. AC Performance 23

2.6. Accelerated Life Testing 25

2.6.1. Types of Stress Testing 25

2.6.2. Causes of GaN HEMT Failure in the Literature 26

2.6.3. Arrhenius Relationship 32

2.6.4. Eyring Model 34

2.6.5. Parameter Definitions and Failure Criteria 35

2.7. Modeling 36

2.7.1. Recent Examples 36

2.7.2. Current Industry Software – Synopsys TCAD 37

2.8. Chapter Summary 38

III. Modeling Research 39

3.1. Introduction 39

3.2. General Motivation for Modeling Microelectronic Devices 39

3.3. Approach 41

3.4. Modeling at AFIT 43

3.5. Future Work 47

3.6. Chapter Summary 48

IV. Experimental Procedures 49
4.1. Introduction 49
4.2. Voltage Step-Stress 49
4.3. 300-hour Test 51
4.4. 1000-hour Test 54
4.5. 600-hour Test 54
4.6. Gate Bias Test 55
4.7. Chapter Summary 57
V. Reliability Testing of AlGaN/GaN HEMTs under Multiple Stressors 58
5.1. Introduction 58
5.2. Experiment Description 58
5.3. Results and Discussion 59
5.4. Conclusion 66
VI. Benefits of Considering More Than Temperature Acceleration for GaN HEMT Life Testing 67
6.1. Introduction 67
6.2. Experiment Description 70
6.3. Results and Discussion 70
6.3.1. 300-hour Test 70
6.3.2. 600-hour High-Power Test 83
6.3.3. Discussion 87
6.4. Conclusion 89
VII. A Very Robust AlGaN/GaN HEMT Technology to High Forward Gate Bias and Current 91

7.1. Introduction 91

7.2. Experiment Description 92

7.3. Results 92

7.4. Conclusion 95

VIII. Time-dependent Electrical Degradation of AlGaN/GaN HEMTs Subjected to High DC Power and High Drain Bias 97

8.1. Introduction 97

8.2. Experiment Description 97

8.3. Results and Discussion 98

8.3.1. Voltage Step-Stress Test 98

8.3.2. 1000-hour Test 101

8.3.3. 600-hour Test 108

8.3.4. Discussion 112

8.4. Conclusion 112

IX. Comparison of Pulsed- and Continuous-DC Stressing of AlGaN/GaN HEMTs 114

9.1. Introduction 114

9.2. Experiment Description 114

9.3. Results and Discussion 115

9.4. Conclusion 116

X. Conclusions 118

10.1. Overall Summary 118

10.2. Contributions 118

10.3. Ideas for Future Research 120

Appendix A. Pictorial Presentation of Test Preparation and Setup 124

Appendix B. Scripts, Command Files, and Macros 127
B.1. Modeling 127
B.1.1. Unix script 127
B.1.2. Sentaurus Structure Editor command files 127
B.1.3. Sentaurus Device command file 138
B.1.4. Sentaurus Device parameter file 139
B.1.5. Tecplot macro 140
B.1.6. MATLAB files 140
B.2. Data Processing 142
B.2.1. Unix scripts 142
B.2.2. MATLAB files 143
B.3. Voltage step-stress Excel macro 146
B.4. Accel-RF test sequence 155
Appendix C. Data Tables 160
Bibliography 172
Vita 181

List of Figures

Page

Figure 1. Relative size comparison of a transistor (left) and a vacuum tube (Nobelprize.org, 2010) ... 3

Figure 2. Cell phone base station (Statemaster.com, 2010) ... 4

Figure 3. National Missile Defense X-band radar (U.S. DoD, 2010) ... 4

Figure 4. AlGaN/GaN HEMT (after (Liddle, 2008)) ... 11

Figure 5. Energy band diagram of AlGaN/GaN hetero-junction with 2DEG area identified (after (McClory, 2008)) ... 11

Figure 6. Illustrations of (a) lattice-matched, (b) strained, and (c) unstrained (relaxed) heteroepitxial structures (May, 2004:153) ... 12

Figure 7. CdS wurtzite structure with lattice constants *a* and *c* (Ullrich, 2010) ... 13

Figure 8. Calculated (solid line) lattice constant (*a* in (a) and *c* in (b)) dependence on aluminum composition (x) in $Al_xGa_{1-x}N$ alloys (Dridi, 2010) ... 14

Figure 9. MOCVD reactor (EENG 596, 2008:slide 9) ... 15

Figure 10. MOCVD multiwafer processing (EENG 596, 2008:slide 13) ... 15

Figure 11. MBE system (May, 2004:149) ... 15

Figure 12. Typical HEMT creation steps (Ali, 1991:85) ... 16

Figure 13. (a) Cross-sectional view of an undercut T-shaped resist cavity with a 0.15-μm bottom opening. Three layers of electron-beam resist are used to form the cavity. (b) Submicron T-gate on the channel of a HEMT after removing the trilayer resist structure shown in (a). (Ali, 1991:88) ... 17

Figure 14. AlGaN/GaN HEMT with gate-integrated and source-connected field plates 18

Figure 15. Drain current versus drain voltage at multiple values of gate voltage for an NMOSFET (Circuits Today, 2010) 21

Figure 16. Drain current versus drain voltage at multiple values of gate voltage for a HEMT used in this research 22

Figure 17. Transfer curve for an NMOSFET (after (Circuits Today, 2010)) 23

Figure 18. Transfer curve for a HEMT used in this research 23

Figure 19. Transfer and transconductance (g_m) curves for a HEMT used in this research 24

Figure 20. Pictorial representation of lattice disruption creation by an etching process as proposed by Smith *et al.* (Smith, 2009). 27

Figure 21. (a) Change in normalized I_{Dmax} in step-stress experiments for three different stress conditions. Dashed line represents the estimated change in I_{Dmax} in the high-power state removing the effect of V_T change. (b) Change in the gate leakage current I_{Goff} (gate current at $V_{DS} = 0.1$ V and $V_{GS} = -5$ V) in the same experiment (Joh, 2008). 28

Figure 22. (a) and (b) Cross-sectional HREM and (c) Z-contrast images of three stressed devices. Material below the horizontal interface is semiconductor; the trapezoidal shape defines the gate metal. Right side is toward the drain, and left side is toward the source in all three images. (a) shows the formation of pits on both the source- and drain-side edges of the gate, (b) shows the formation of a crack, and (c) shows a severe case of degradation where the gate metal (Pt) has diffused into the crack formed (Chowdhury, 2008). (b) and (c) have roughly the same scale. 29

Figure 23. Average percent decrease of the maximum transconductance measured at V_{DS} = 10 V during 10-hour ON-state tests (V_{DS} = 20 V, V_{GS} = 0 V; diamonds), OFF-state tests (V_{DS} = 20 V, V_{GS} = −7.7 V; squares), and semi-ON-state tests (V_{DS} = 20 V, V_{GS} = −5.5 V; triangles) (Meneghesso, 2008) 30

Figure 24. Atomic configurations of triply hydrogenated (a) gallium vacancy,(b) nitrogen antisite, and (c) divacancy. (Puzyrev, 2011) 31

Figure 25. Electron tunneling leakage from the gate electrode and possible current paths (Trew, 2009) 32

Figure 26. Flow chart for automated device modification. (Coutu, 2011) 42

Figure 27. Manual electromigration example. Current densities range from 1 kA/cm^2 (and less) in blue to 100 kA/cm^2 (and greater) in red. The last frame (not shown) is a complete void. 44

Figure 28. Automated electromigration example. Current densities range from 1 kA/cm^2 (and less) in blue to 100 kA/cm^2 (and greater) in red. 46

Figure 29. Transfer and transconductance curves at 0 and 300 hours of typical high-voltage-tested device. Device 7579 was tested at Condition 6. (Christiansen, 2011b) 61

Figure 30. Transfer and transconductance curves at 0, 300, and 1016 hours of exceptional high-voltage-tested device. Device 001 was tested at Condition 6. (Christiansen, 2011b) 61

Figure 31. Representative transfer and transconductance curves at 0, 300, and 343 hours of high-power-tested device. Device 007 was tested at Condition 1. (Christiansen, 2011b) 62

Figure 32. Device 001 (high-voltage-tested) at a baseplate of 85 °C. The upper middle spot was targeted for TEM imaging. (a) IR (radiance) image at 15X magnification. V_{DS} = 40 V, I_D = 10 mA, V_{GS} = −2.42 V, I_G = −5 µA. (b) PE image at 20X magnification. V_{DS} = 100 V, I_D = 11 µA, V_{GS} = −10 V, I_G = −12 µA. (Christiansen, 2011b) 64

Figure 33. Device 007 (high-power-tested) at a baseplate of 85 °C. The lower left spot was targeted for TEM imaging. (a) IR (radiance) image at 15X magnification. V_{DS} = 28 V, I_D = 10 mA, V_{GS} = −1.69 V, I_G = −3.3 µA. (b) PE image at 50X magnification. V_{DS} = 10 V, I_D = 3.2 mA, V_{GS} = −1 V, I_G in nA range. (Christiansen, 2011b).......... 65

Figure 34. TEM images of (a) Device 001 (high-voltage-tested) and (b) Device 007 (high-power-tested). Notice absence of a pit or crack in Device 001 and the presence of a pit in Device 007. (Christiansen, 2011b) 65

Figure 35. Normalized pre- and post-stress values of (a) I_{Dmax} and (b) I_{DSS} for high-power conditions. The top three lines (red) of the legend are Condition 1, the middle three (blue) Condition 2, and the bottom three (green) Condition 3. (Christiansen, 2011a) 74

Figure 36. Normalized pre- and post-stress values of (a) I_{Dmax} and (b) I_{DSS} for high-voltage conditions. The top two lines (red) of the legend are Condition 4 and the bottom two (blue) Condition 6. (Christiansen, 2011a) 76

Figure 37. Comparing acceleration factors based on initial T_{ch} estimates and observed degradation. The reference slope line assumes an activation energy of 2.09 eV. (Christiansen, 2011a) 78

Figure 38. Comparing Agilent power supply measurement error and initial T_{ch} estimates in 300-hour test. (Christiansen, 2011a) ... 80

Figure 39. Magnified portion of Figure 38 but on different scales. (Christiansen, 2011a) ... 81

Figure 40. Normalized values (to the 1-hour, 245-°C measurements) of I_{Dmax} over time during the 600-hour test. (Christiansen, 2011a) ... 84

Figure 41. Normalized values (to the 0-hour, 70-°C measurements) of I_{Dmax} over time during the 300-hour, Condition-1 (lines 2-4 in the legend, in red) and 600-hour, Condition-7 (lines 5-7 in the legend, in green) tests. (Christiansen, 2011a) ... 85

Figure 42. Comparing Agilent power supply measurement error and initial T_{ch} estimates in Conditions 1 and 7. (Christiansen, 2011a) ... 87

Figure 43. Transfer curves (a), and associated gate current in absolute value (b) and transconductance (c) of the device as measured during characterizations between gate stressing events. Insets show detail at regions of interest in the same data sets. Extra gate current is seen in (b) above $V_G \approx -3.5$ V after 210 minutes stress (top curve) that is not seen after longer stress time (second-to-top curve). It is not known if there was a temporary test issue or if that is indeed real. ... 94

Figure 44. Gate diode curves during the stressing. Insets show additional detail for regions of interest of the same curves as the main plot and share the same units (i.e., mA/mm and V) as the main figure. The data was collected at stress times represented in Figure 43. Black curves represent the initial Vg = +2.5 V gate stresses. Red curves represent the gate voltage stress ramps of increasing magnitude collected just prior to the red curves of Figure 43. Green curves are gate voltage

stress ramps collected just after the total stress times represented by the green curves of Figure 43. (Christiansen, 2011c) 95

Figure 45. Drain and gate current of Device H11V05R during voltage step-stress test.. 98

Figure 46. Evolution of I_{Dmax}, I_{DSS}, and I_G of Device H11V05R during voltage step-stress test 99

Figure 47. Evolution of I_{Dmax} and $|I_{Goff}|$ for Device R10C2 during del Alamo's "$V_{DS} = 0$ step-stress experiment" 100

Figure 48. Evolution of I_{Dmax} and $|I_{Goff}|$ for Device R9C2 during V_{DG} step-stress experiment (a modified del Alamo test) 101

Figure 49. Normalized values (to the 1-hour measurements) of I_{Dmax} over time during the 1000-hour test. The top three lines (red) of the legend are Condition 4, the next line (blue) is Condition 5, the next two (green) are Condition 6, and the bottom line is the model with the means of curve-fitting parameters. 103

Figure 50. Fits of Channel 15 normalized I_{Dmax} data to Equation (19) in blue (fit 166) and to the stretched exponential in red (fit 165). 105

Figure 51. Last hours of 1000-hour test showing the similarity of devices' responses to OFF-state stress independent of applied drain voltage. 108

Figure 52. Normalized values (to the 1-hour measurements) of I_{Dmax} over time during the 600-hour test 109

Figure 53. Fits of Channel 26 normalized I_{Dmax} data to Equation (19) in blue (fit 188) and the stretched exponential in red (fit 187). 110

Figure 54. Packaged devices as sent from vendor 124

Figure 55. Packaged devices with lead frames removed 124

Figure 56. Packaged device attached to test module 125

Figure 57. Heater bar for three test modules... 125

Figure 58. Clamps attached above devices and test modules attached to heater bar..... 125

Figure 59. Test module covers and nitrogen tubes attached 126

Figure 60. DC test station 126

Figure 61. Thermal and photoemission imaging system 126

List of Tables

Page

Table 1. Definitions of Experimentally Measured or Derived Parameters (Via, 2010) .. 35

Table 2. Failure Criteria 35

Table 3. Test Conditions for 300-hour, 1000-hour, and 600-hour Tests (Christiansen, 2011a) 52

Table 4. Average Absolute Percentage Changes in Parameters after 300 Hours (Christiansen, 2011b) 60

Table 5. Initial Variation of Parts Tested for 300 Hours (Christiansen, 2011a) 71

Table 6. Parameter Changes by Device and Condition in 300-hour Test (Christiansen, 2011a) 72

Table 7. Arrhenius Acceleration Factors Between Test Conditions (Christiansen, 2011a) 72

Table 8. Slopes of Normalized I_{Dmax} and I_{DSS} Lines for High-power Conditions (Christiansen, 2011a) 75

Table 9. Slopes of Normalized I_{Dmax} and I_{DSS} Lines for High-voltage Conditions (Christiansen, 2011a) 76

Table 10. Initial Measured Parameter Values in 300-hour Test (Christiansen, 2011a)... 77

Table 11. Sensitivity Analysis of Thermal Model R_{th} for Conditions 1, 2, and 3 (Christiansen, 2011a) 82

Table 12. Initial Variation of Parts Tested for 600 Hours (Christiansen, 2011a) 83

Table 13. Parameter Changes by Device and Stress Time Y in 600-hour Test (Christiansen, 2011a) 83

Table 14. Initial Measured Parameter Values in 600-hour Test (Christiansen, 2011a)... 85

Table 15. Parameter Percentage Changes by Channel and Condition in 1000-hour Test (T_{bp} = 245 °C; t = 1 hour vs. t = 1000 hours) 102

Table 16. Model Parameter Solutions and Statistics for Fitting 1000-hour Normalized I_{Dmax} Data to Equation (19) 106

Table 17. Parameter Percentage Changes by Channel and Condition in 1000-hour Test (T_{bp} = 245 °C; t = 0 hours vs. t = 1000 hours)... 106

Table 18. Parameter Percentage Changes by Channel and Condition in 1000-hour Test (T_{bp} = 70 °C; t = 0 hours vs. t = 1000 hours)... 107

Table 19. Parameter Percentage Changes by Channel and Stress Time in 600-hour Test (T_{bp} = 245 °C; t = 1 hour vs. t = Y hours) 109

Table 20. Model Parameter Solutions and Statistics for Fitting 600-hour Normalized I_{Dmax} Data to Equation (19) 111

Table 21. Parameter Percentage Changes by Channel and Stress Time in 600-hour Test (T_{bp} = 245 °C; t = 0 hours vs. t = Y hours)... 111

Table 22. Parameter Percentage Changes by Channel and Stress Time in 600-hour Test (T_{bp} = 70 °C; t = 0 hours vs. t = Y hours).. 112

Table 23. Average I_{Dmax} Degradation in Continuous- and Pulsed-DC, Same-Bias Tests 116

Table 24. Absolute Percentage Changes in Parameters after 300 Hours (see Table 4). 161

Table 25. Parameter Changes by Device and Condition in 300-hour Test (see Table 6) 162

Table 26. Slopes of Normalized I_{Dmax} and I_{DSS} Lines for High-power Conditions (see Table 8) 163

Table 27. Slopes of Normalized I_{Dmax} and I_{DSS} Lines for High-voltage Conditions (see Table 9) 163

Table 28. Parameter Changes by Device and Stress Time Y in 600-hour Test (see Table 13) 164

Table 29. Parameter Percentage Changes by Channel and Condition in 1000-hour Test (T_{bp} = 245 °C; t = 1 hour vs. t = 1000 hours) (see Table 15) 165

Table 30. Parameter Percentage Changes by Channel and Condition in 1000-hour Test (T_{bp} = 245 °C; t = 0 hours vs. t = 1000 hours) (see Table 17) 166

Table 31. Parameter Percentage Changes by Channel and Condition in 1000-hour Test (T_{bp} = 70 °C; t = 0 hours vs. t = 1000 hours) (see Table 18) 167

Table 32. Parameter Percentage Changes by Channel and Stress Time in 600-hour Test (T_{bp} = 245 °C; t = 1 hour vs. t = Y hours) (see Table 19) 168

Table 33. Parameter Percentage Changes by Channel and Stress Time in 600-hour Test (T_{bp} = 245 °C; t = 0 hours vs. t = Y hours) (see Table 21) 169

Table 34. Parameter Percentage Changes by Channel and Stress Time in 600-hour Test (T_{bp} = 70 °C; t = 0 hours vs. t = Y hours) (see Table 22) 170

Table 35. I_{Dmax} Degradation in Continuous- and Pulsed-DC, Same-Bias Tests (see Table 23) 171

List of Abbreviations

2DEG	Two-Dimensional Electron Gas
AFRL	Air Force Research Laboratory
Al	Aluminum
AlGaAs	Aluminum Gallium Arsenide
AlGaN	Aluminum Gallium Nitride
AlN	Aluminum Nitride
Au	Gold
C	Carbon
Cd	Cadmium
CdS	Cadmium Sulfide
CMOS	Complementary Metal Oxide Semiconductor
DC	Direct Current
DoD	Department of Defense
EBL	Electron-Beam Lithography
EDS	Energy-Dispersive X-Ray Spectroscopy
EELS	Electron Energy Loss Spectroscopy
FET	Field-Effect Transistor
Ga	Gallium
GaAs	Gallium Arsenide
GaN	Gallium Nitride
HEMT	High Electron Mobility Transistor
IR	Infrared

MBE	Molecular Beam Epitaxy
MOCVD	Metal-Organic Chemical Vapor Deposition
MURI	Multidisciplinary University Research Initiative
N	Nitrogen
NAVSEA	Naval Surface Warfare Center
Ni	Nickel
NMOSFET	N-channel Metal-Oxide-Semiconductor FET
NPS	Naval Postgraduate School
O	Oxygen
ONR	Office of Naval Research
Pd	Palladium
PCA	Pulsed Condition A
PCB	Pulsed Condition B
PCC	Pulsed Condition C
PE	Photoemission
P-HEMT	Pseudomorphic HEMT
RF	Radio Frequency
RYD	Aerospace Components and Subsystems Division
S	Sulfur
Si	Silicon
SiC	Silicon Carbide
SiN	Silicon Nitride
SEM	Scanning Electron Microscope

SMU	Source/Monitor Unit
TCAD	Technology Computer-Aided Design
TEM	Transmission Electron Microscope
UV	Ultraviolet

INVESTIGATION OF GALLIUM NITRIDE TRANSISTOR RELIABILITY THROUGH ACCELERATED LIFE TESTING AND MODELING

I. Introduction

The material properties of gallium nitride (GaN) enable the production of high electron mobility transistors (HEMT) with characteristics attractive to the United States Department of Defense (DoD) for application in communications and sensing systems. Interest in this technology is demonstrated by the Defense Advanced Research Projects Agency's Wide Bandgap Semiconductor initiative and by the Multidisciplinary University Research Initiatives (MURI) funded by the Office of Naval Research (ONR) and Air Force Office of Scientific Research. Despite the advantages of GaN HEMTs, there is concern that their reliability is low or, in other words, they do not have sufficiently long lifetimes for military systems. This concern has hampered their widespread acceptance and use (Christiansen, 2011b).

Determining GaN HEMT lifetimes is usually accomplished with life testing that is accelerated with temperature, although there may be other stressors that hasten transistor failure. The lifetimes calculated at operating temperatures are estimates since they are extrapolated from the lifetimes at high temperatures. Modeling and simulation of GaN HEMTs is an alternative to life testing for estimating lifetimes.

1.1. Motivation

This section presents several reasons why the knowledge and research of GaN HEMTs is important to the DoD.

1.1.1. Desirable Performance Attributes

The physical attributes of HEMTs result in desirable performance in high-speed, high-temperature, high-voltage, and high-power applications. High speed, usually expressed by a frequency, results from the high electron mobility. The intended use of the first HEMT built (by Mimura *et al.*) was high-speed digital applications at low temperatures (Ali, 1991:91). HEMTs have been used in flip-flop circuits operated at 5.5 GHz and 300 K (Neaman, 2003:608). GaN HEMTs have demonstrated high-frequency operation: 190 GHz for unity current gain cut-off frequency (f_T) and 251 GHz for maximum frequency of oscillation (f_{max}) (Higashiwaki, 2008).

High-temperature operation results from the wide bandgap semiconductor of HEMTs. This high-temperature operation reduces the cooling requirement (Mishra, 2002).

Although gallium arsenide (GaAs) was the wide bandgap material used for the first HEMT, GaN is now being employed in HEMTs for power applications. For a given doping concentration, GaN has a breakdown voltage that is an order of magnitude greater than that of GaAs (Liddle, 2008). GaN also has high current capacity resulting from additional carriers created by spontaneous and piezoelectric polarization effects (Sze, 2007:409). The high breakdown voltage and high current enable high power operation.

With these desirable attributes, HEMTs are beginning to compete with vacuum tubes that have dominated the areas of high RF power at high temperatures and frequencies (Trew, 2005). Compared to vacuum tubes, HEMTs also have a considerable size advantage as depicted in Figure 1.

Figure 1. Relative size comparison of a transistor (left) and a vacuum tube (Nobelprize.org, 2010)

1.1.2. Circuits and Applications

Due to the desirable performance characteristics listed in the previous section, HEMTs can be found in low-noise, wideband, and power amplifiers; oscillators; and frequency multipliers. In addition to the RF circuits listed, HEMTs are employed in high-speed digital integrated circuits (Ali, 1991).

HEMT circuits find application in communications and radar systems. A communications system example is a cellular phone base station, as depicted in Figure 2. For a radar system example (Trew, 2005), Figure 3 shows an X-band radar that is part of the National Missile Defense system.

1.2. Accelerated Testing Research

To better understand and characterize the failure mechanisms of GaN HEMTs, accelerated testing with multiple stressors (temperature, current, and voltage) was conducted on transistors from a commercial vendor. After testing, the devices were analyzed for indicators and causes of failure.

Figure 2. Cell phone base station (Statemaster.com, 2010)

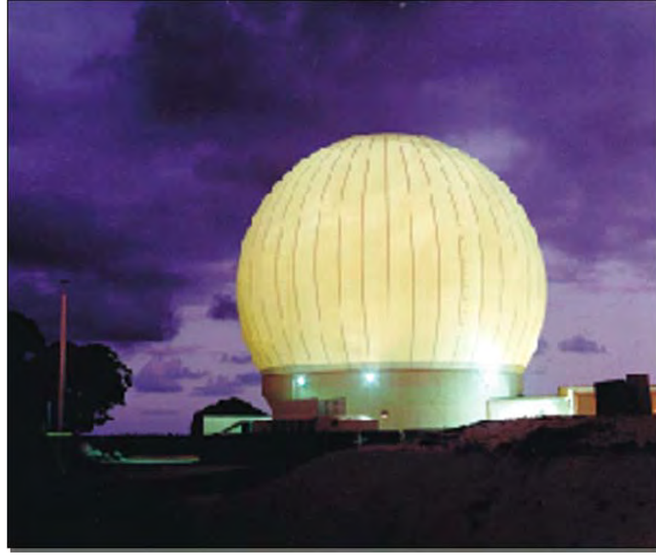

Figure 3. National Missile Defense X-band radar (U.S. DoD, 2010)

1.2.1. Problem Statement

In the literature, competing theories for the cause of failure in GaN HEMTs have been presented. Accelerated life testing has been primarily temperature-accelerated, but some of the failure mechanisms should have other accelerants (stressors) such as electric field and current density. Furthermore, a controlled investigation of multiple stressors on GaN HEMTs is absent from the literature, leaving the stressors' effects unknown (Bozada, 2010a).

1.2.2. Thesis Statement

Conducting a controlled multi-stressor test on GaN HEMTs provides insight into the causes of failure and identifies the stressor or stressors that contribute to device failure.

1.2.3. Contributions

The contributions from the multi-stressor accelerated testing are the:

1. Revelation of different failure mechanisms than are in the literature and that failure mechanisms depend on the test conditions
2. Determination that different stressors cause different lifetimes
3. Determination that voltage can be used as an accelerant
4. Fitting of experimental degradation data to a mathematical model
5. Comparison of continuous-DC test results to pulsed-DC test results.

1.3. Modeling Research

As an alternative to predicting GaN HEMT lifetimes with accelerated testing, modeling and simulation that could be applied to predict GaN HEMT lifetimes was investigated.

1.3.1. Problem Statement

Current industry technology computer-aided design (TCAD) software applications determine electronic device performance based mainly on device characteristics at the time of fabrication. The tools provide few options to predict device degradation over time based on operating conditions. Additionally, the tools do not modify the device model based on the degradation effects of the operating conditions.

1.3.2. Thesis Statement

Creating a framework that considers operating conditions and modifies the device model according to the degradation effects of those conditions enables device lifetime predictions.

1.3.3. Contribution

The contribution from the modeling research is the creation of a framework that modifies a device model during operation and based on operating conditions.

1.4. Publications

The results of this research are published, submitted for publication, or soon to be submitted, in the following papers:

1. Christiansen, B. D., R. A. Coutu, E. R. Heller, B. S. Poling, G. D. Via, R. Vetury, and J. B. Shealy. "Reliability testing of AlGaN/GaN HEMTs under multiple stressors," in *2011 IEEE Int. Rel. Physics Symp. (IRPS)*, Monterey, CA, pp. CD.2.1-CD.2.5.
2. Christiansen, B. D., E. R. Heller, R. A. Coutu, R. Vetury, and J. B. Shealy, "A very robust AlGaN/GaN HEMT technology to high forward gate bias and current," resubmitted to *IEEE Electron Device Lett.*,30 Sep. 2011.
3. Christiansen, B. D., R. A. Coutu, E. R. Heller, C.A. Bozada, B. S. Poling, G. D. Via, J. P. Theimer, and S. E. Tetlak. "Benefits of considering more than temperature acceleration for GaN HEMT life testing," submitted to *Microeletron. Rel.*, 1 Aug. 2011.
4. Christiansen, B. D., A. Acker, R. A. Coutu, T. R. Weatherford, and J. J. Gregory, "Comparison of Pulsed- and Continuous-DC Stressing of AlGaN/GaN HEMTs," in progress.

1.5. Purpose

GaN HEMTs offer gains in increased capability and lower costs due to their ability to operate at high power, high frequencies, and high temperatures (Mishra, 2002). Although extremely attractive for many U.S. Department of Defense applications, insertion of this emerging technology is risky because of the little to no long-term use data that ensures the needed lifetimes are possible (Christiansen, 2011a).

Dr. Charles E. McQueary, former Director, Operational Test and Evaluation, wrote, "Poor reliability not only greatly increases operating and support (O&S) costs, it undermines warrior confidence and adversely impacts our Nation's warfighting capability" (McQueary, 2008). With the knowledge of GaN HEMT failure mechanisms produced by this research, DoD program managers will be empowered to make informed decisions concerning the insertion of GaN HEMT technology into their weapons systems. By selecting the appropriate technology, program managers will reduce costs, increase warfighter confidence, and help to protect our Nation.

1.6. Document Overview

Chapter 2 presents background information concerning GaN HEMTs, accelerated life testing, and modeling. The modeling research is covered in Chapter 3. Chapter 4 discusses the experimental procedures the produced the results for analysis and discussion in the subsequent chapters. Chapter 5 discusses the differences seen in degradation due to the different stresses of the multi-stressor experiment. The validity of Arrhenius temperature-accelerated life testing for GaN HEMTs is analyzed in Chapter 6. Chapter 7 reports the discovery of the tested devices' robustness to high gate voltage and

current. The time-dependence of degradation is examined in Chapter 8. Chapter 9 contains a comparison of continuous- and pulsed-DC testing results. This document concludes with a summary and proposals for future research in Chapter 10.

II. Background

This chapter presents information about GaN HEMTs, accelerated life testing, and modeling to provide an understanding of the completed research.

2.1. Brief History

The following are important steps toward the development of the GaN high electron mobility transistor. In the 1930s, Lilienfeld and Heil were the first to propose a field-effect transistor (Sze, 2007:293). The first transistor, a bipolar transistor, was created by Bardeen and Brattain in 1947 (Sze, 2007:243). In 1960, Kahng and Atalla developed the first metal-oxide-semiconductor field-effect transistor (Sze, 2007:293). For the first time in 1969, Esaki and Tsu contemplated current carrier movement that was in two dimensions, rather than three, and parallel to the layers of a heterostructure superlattice (multiple heterojunctions with overlapping wavefunctions (Sze, 2007:60)). Heterojunctions became more feasible and available following the 1970s development of the molecular beam epitaxy and metal-organic chemical vapor deposition growth processes. Dingle *et al.* were the first to report, in 1978, increased electron mobility in the modulation-doped AlGaAs/GaAs superlattice. In the following year, Stormer *et al.* demonstrated increased electron mobility from only one AlGaAs/GaAs heterojunction (Sze, 2007:401).

Then, in 1980, Mimura *et al.* combined the field effect and increased electron mobility from AlGaAs/GaAs heterojunctions to create the first high electron mobility transistor (Sze, 2007:401). Finally, in 1993, Asif Khan *et al.* created the first HEMT with an AlGaN/GaN heterojunction (Asif Khan, 1993).

2.2. Definitions

The high electron mobility transistor derives its name from the effects of its structure. A HEMT is created by placing a narrower bandgap semiconductor material, such as GaN or GaAs, in contact with a wider bandgap semiconductor material, such as AlGaN or doped AlGaAs. Figure 4 depicts a cross-section of a representative AlGaN/GaN HEMT; the dimensions are not to scale. The source and drain are ohmic contacts, whereas the gate is a Schottky contact. The wide bandgap layer is commonly called the barrier layer and the narrow bandgap layer is commonly called the buffer layer. The junction between the narrow (GaN) and wide (AlGaN) bandgap materials is called a heterojunction because it consists of materials with different bandgaps. In a heterojunction, the electrons flow from the wide bandgap material to the narrow bandgap material to achieve thermal equilibrium. This accumulation of electrons in the narrow bandgap material (buffer layer) is called a two-dimensional electron gas (2DEG). Figure 5 shows the energy band diagram of an AlGaN/GaN heterojunction and highlights the area where the 2DEG forms. The electrons are confined to move parallel to the material layers in the narrow bandgap material (as contemplated by Esaki and Tsu). The electrons in the 2DEG have a high mobility, since the separation of the electrons and their ionized donors minimizes ionized impurity scattering. The HEMT is a field-effect transistor (FET) since the electric field produced by the voltage on the gate terminal determines the concentration of electrons in the 2DEG (Neaman, 2003:602-604, 571).

The HEMT has some aliases. The name heterojunction FET (HFET) results because the HEMT is created with a heterojunction. Due to the 2DEG created in the narrow bandgap material, two-dimensional electron gas FET (TEGFET) is another name.

The name modulation-doped FET (MODFET) arises since the doping of the conduction channel with electrons is varied by the gate voltage, not by permanently implanting or diffusing donor or acceptor ions into the channel.

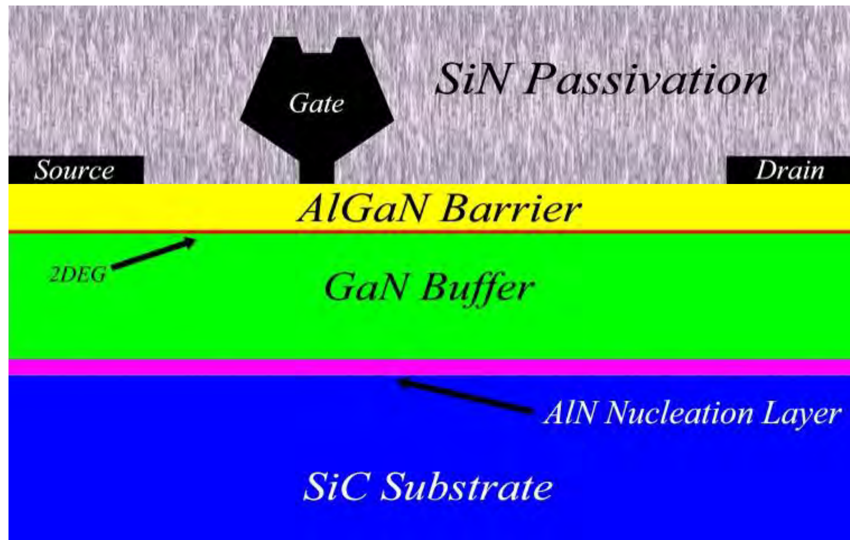

Figure 4. AlGaN/GaN HEMT (after (Liddle, 2008))

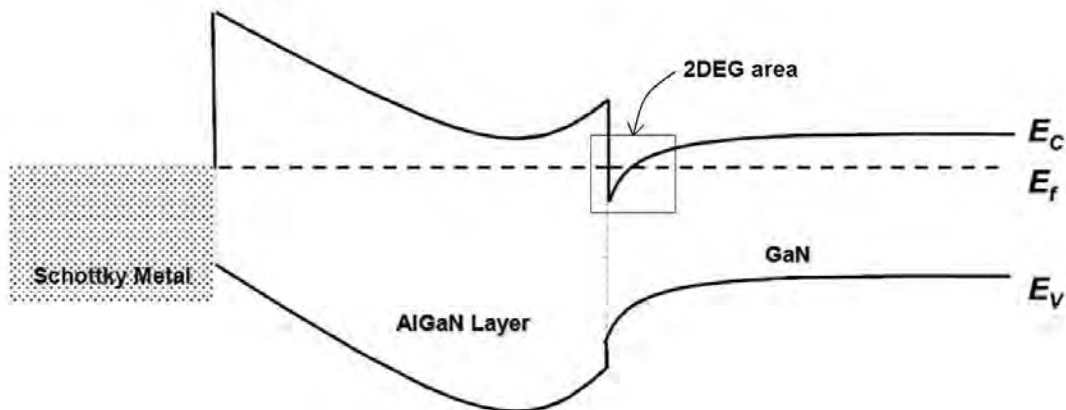

Figure 5. Energy band diagram of AlGaN/GaN hetero-junction with 2DEG area identified (after (McClory, 2008))

In a conventional HEMT, the lattice constants of the two materials match and the epitaxial layer is not strained (see Figure 6(a)). An AlGaAs/GaAs HEMT is a conventional HEMT (Ali, 1991:104). A pseudomorphic HEMT (P-HEMT) is created

when the lattice constants of the two materials do not match (Sze, 2007:408). Lattice mismatch is

$$\Delta \equiv \frac{|a_e - a_s|}{a_e} \quad (1)$$

where a_e is the lattice constant of the epitaxial layer and a_s is the lattice constant of the substrate (Sze, 2007:57). Lattice mismatch is tolerable in P-HEMTs as long as the critical thickness of the epitaxial layer (Sze, 2007:57),

$$t_c \approx \frac{a_e}{2\Delta} = \frac{a_e^{\,2}}{2|a_e - a_s|} \quad (2)$$

is not exceeded and the epitaxial layer remains strained (see Figure 6(b)). If the critical thickness is exceeded, the epitaxial layer will relax and become unstrained or relaxed (see Figure 6(c)). Dislocations in a relaxed epitaxial layer reduce electron mobility (Sze, 2007:409).

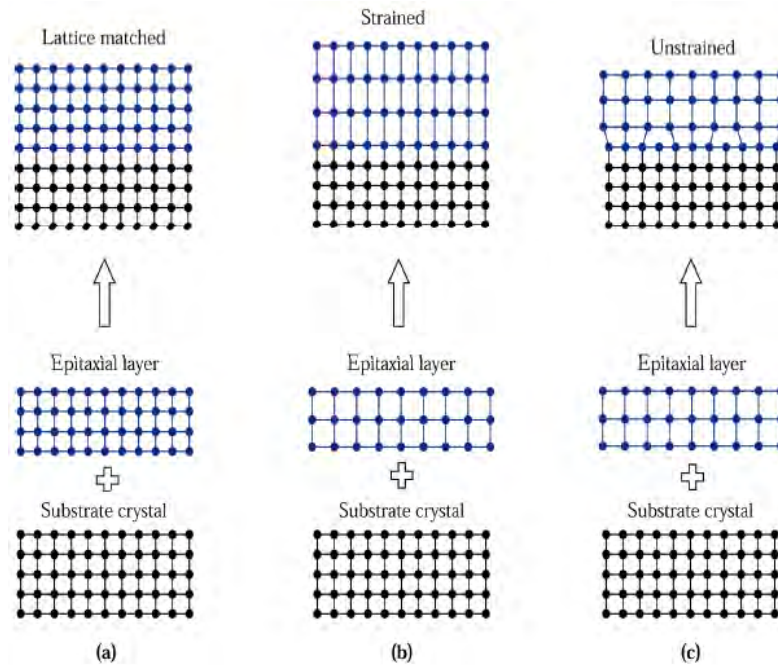

Figure 6. Illustrations of (a) lattice-matched, (b) strained, and (c) unstrained (relaxed) heteroepitxial structures (May, 2004:153)

Although not commonly called a P-HEMT, AlGaN/GaN HEMTs are P-HEMTs (Ambacher, 2002). However, the calculation of lattice mismatch and critical AlGaN thickness is not as straightforward as presented above. Since GaN usually forms in the wurtzite lattice (Vurgaftman, 2001), it has two lattice constants *a* and *c*. Figure 7 shows the CdS wurtzite structure with lattice constants *a* and *c*; in GaN, the Ga atoms are in the Cd locations and the N atoms are in the S locations. When grown on wurtzite GaN, AlGaN assumes the wurtzite structure (McClory, 2008). In Figure 8, calculated lattice constants are shown as a function of aluminum fraction (x) in $Al_xGa_{1-x}N$ alloys; GaN occurs when x is 0 and AlN occurs when x is 1. The fraction of aluminum in AlGaN/GaN HEMTs is usually 0.15 to 0.3 (Schwierz, 2003). For $x = 0.2$ and based on Figure 8, the lattice mismatch in lattice constant *a* is only approximately 0.005 and the lattice mismatch in lattice constant *c* is only approximately 0.009.

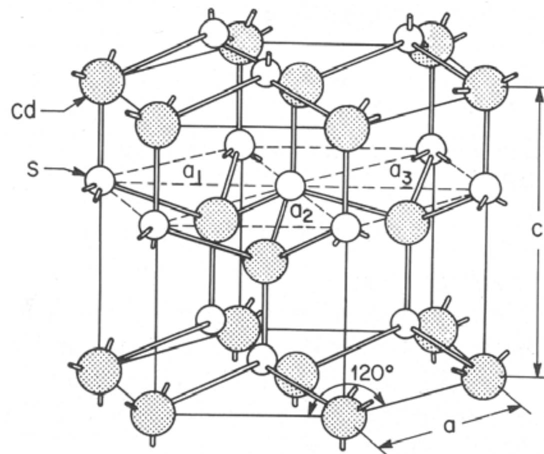

Figure 7. CdS wurtzite structure with lattice constants *a* and *c* (Ullrich, 2010)

Despite the apparently small mismatches, dislocations occur between the GaN and AlGaN lattices. Dislocations also occur at the interface of the nucleation layer and the GaN buffer (see Figure 4). (The purpose of the nucleation layer (AlN in Figure 4) is

to overcome the greater lattice mismatch between the substrate and the GaN (Liddle, 2008).) The dislocations and AlGaN surface atoms are locations where electrons can be trapped, and thus prevented from contributing to conduction. (Surface passivation, such as with SiN in Figure 4, reduces the density of surface traps (Green, 2000).) Drain current degradation due to trapped electrons is reversible (Meneghesso, 2008) with the application of ultraviolet (UV) illumination (Koley, 2003) or rest (Trew, 2009).

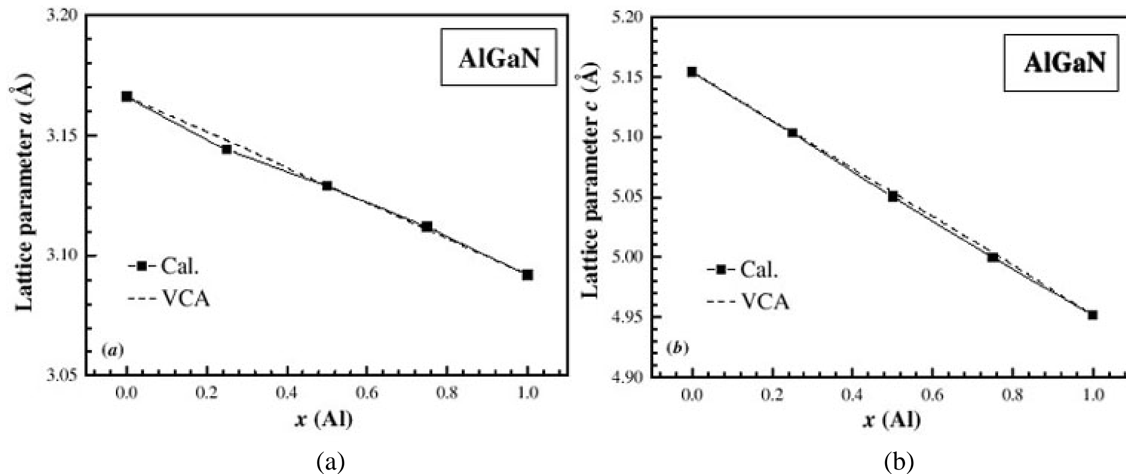

(a) (b)

Figure 8. Calculated (solid line) lattice constant (*a* in (a) and *c* in (b)) dependence on aluminum composition (*x*) in $Al_xGa_{1-x}N$ alloys (Dridi, 2010)

2.3. Fabrication Processes

The epitaxial layers of HEMTs are generally grown by metal-organic chemical vapor deposition (MOCVD) or molecular beam epitaxy (MBE) on semi-insulating substrates (Ali, 1991:79). MOCVD involves the use of gaseous sources to transport elements to the substrate. Figure 9 depicts a MOCVD reactor. Advantages of MOCVD include high throughput and the capability to grow layers on multiple wafers (see Figure 10). Disadvantages of MOCVD include thickness and doping non-uniformities (Ali, 1991:80).

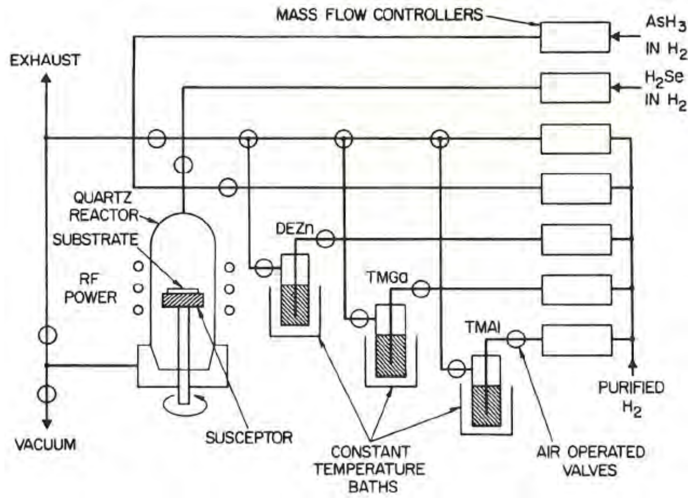

Figure 9. MOCVD reactor (EENG 596, 2008:slide 9)

Figure 10. MOCVD multiwafer processing (EENG 596, 2008:slide 13)

In MBE, elemental sources are evaporated or sublimated, creating molecular beams that strike a heated substrate at very low pressure. An MBE system is shown in Figure 11. The temperatures of the effusion ovens determine the molecular beam fluxes and, thus, the layer composition and doping level. Abrupt changes in doping and composition can be created by moving the shutter at the output of an effusion oven. MBE layer thickness and doping concentration are very uniform (Ali, 1991:79-80).

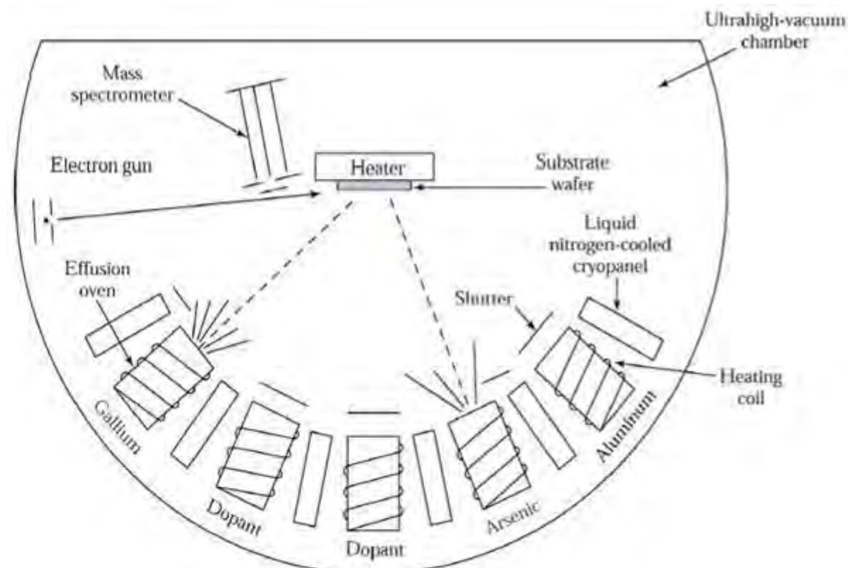

Figure 11. MBE system (May, 2004:149)

Although MBE results in higher growth uniformity than MOCVD, MBE also results in higher dislocation density, which may produce higher gate leakage current (Roy, 2010).

Once the epitaxial layers are deposited, the wafers are ready for device creation. Figure 12 shows typical steps for creating HEMTs. The third step in Figure 12 is gate formation. To create the short gate lengths required (less than 0.5 μm) for high speeds and frequencies, direct-write electron-beam lithography (EBL) is used. In EBL, electron beams pattern gates directly without a mask. Since throughput is low with EBL, a combination of EBL for gates and optical lithography for larger features is employed to improve throughput (Ali, 1991:84). During all fabrication steps, controlling processing temperatures is important when creating P-HEMTs. Temperatures that are too high will relax the pseudomorphic layer, thereby introducing dislocations (Sze, 2007:409).

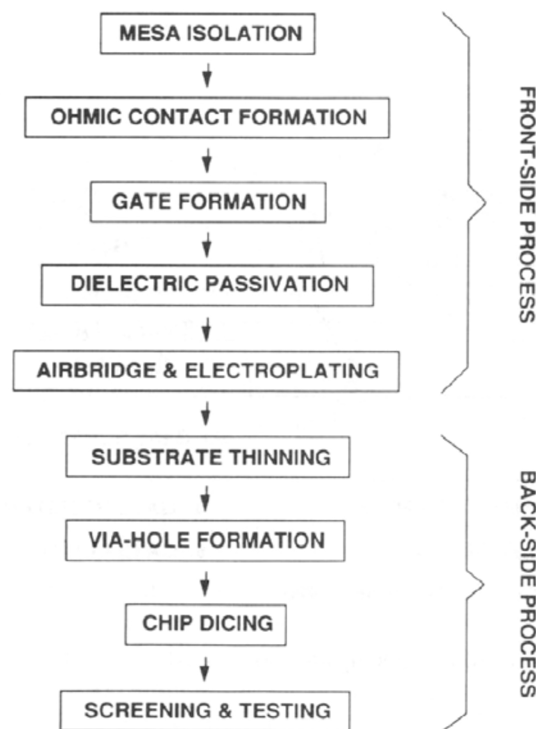

Figure 12. Typical HEMT creation steps (Ali, 1991:85)

2.4. GaN HEMT Structure

HEMTs can be fabricated with various structures that improve device performance. The shape of the gate terminal, the gate-to-drain spacing, and field plates are three device structure considerations.

The T-shaped gate terminal is one possibility for improved HEMT performance. The T-gate is formed from three layers of electron-beam resist and by EBL (Ali, 1991:87). Figure 13 shows a T-gate resist cavity and final product. The T-gate enables a short gate length, which results in increased unity current gain cut-off frequency (f_T) and transconductance (g_m). Gate resistance is reduced and the maximum frequency of oscillation (f_{max}) is increased due to the larger top portion of the T-gate (Sze, 2007:400).

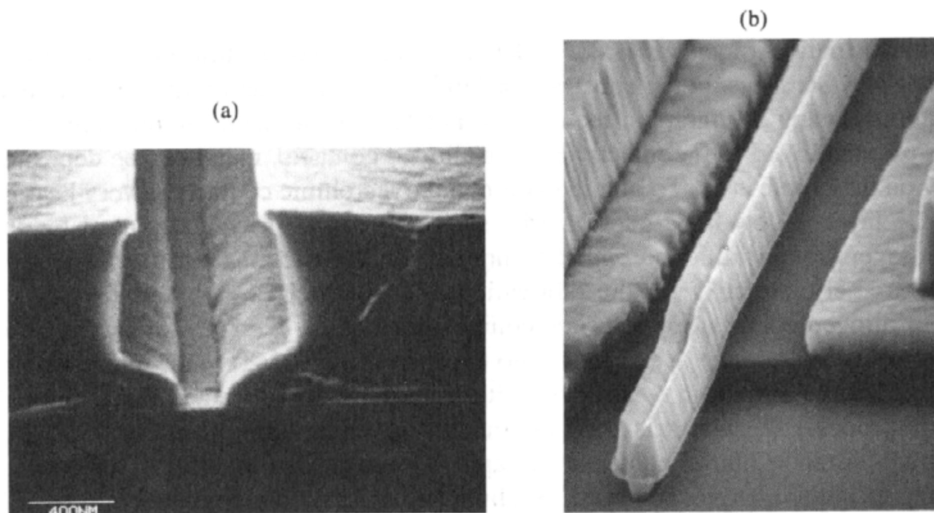

Figure 13. (a) Cross-sectional view of an undercut T-shaped resist cavity with a 0.15-μm bottom opening. Three layers of electron-beam resist are used to form the cavity. (b) Submicron T-gate on the channel of a HEMT after removing the trilayer resist structure shown in (a). (Ali, 1991:88)

Notice the spacing from the T-gate to the other terminals in Figure 13. There is a larger space on the right. Increasing the spacing from the gate to the drain increases the device's breakdown voltage, which in turn enables operation at higher voltages. The

optimum spacing between the gate and drain has been found to be 2.3 times the gate length (Chavarkar, 2003:**8**-8).

Field plates are used to improve the high-voltage and high-power operation of HEMTs. Field plates function to reduce high electric field peaks that cause gate breakdown by smoothing, distributing, and terminating the fields. Without a field plate, electrons can tunnel from the gate metal to the semiconductor on the drain side of the gate due to electric fields that are on the order of 1 MV/cm. With a field plate, the electron tunneling and gate breakdown are suppressed and high drain voltages may be applied (Trew, 2005). Figure 14 is a depiction of a HEMT with a field plate integrated with the gate electrode and another field plate connected to the source electrode. This is the structure of the HEMTs that were investigated in this research. Both field plates extend toward the drain electrode to reduce the electric field in the gate-drain region.

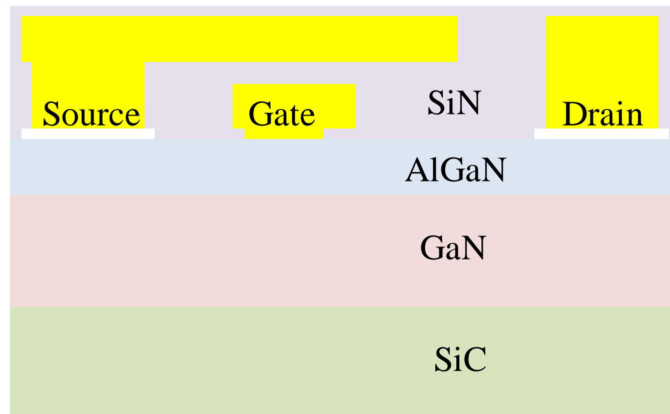

Figure 14. AlGaN/GaN HEMT with gate-integrated and source-connected field plates

2.5. Physics

2.5.1. Basic Operation

HEMTs operate by the field effect. The electric field caused by the voltage on the gate terminal determines the density of electrons in the 2DEG available for conduction between the source and drain terminals. The high mobility of the electrons enables some of the desirable performance attributes described in Chapter 1 (Neaman, 2003:609).

Having the wurtzite structure, GaN and AlGaN exhibit a spontaneous polarization (P_{SP}) (Posternak, 1990). Such spontaneous polarization in group-III nitrides can induce electric fields of up to 3 MV/cm. In addition to spontaneous polarization, strain in the pseudomorphic AlGaN layer produces a piezoelectric polarization (P_{PZ}), which results in a field around 2 MV/cm. The total polarization contributes positively to the formation of the 2DEG by increasing the carrier concentration in the conduction channel (Ambacher, 1999). The charge sheet density induced by this total polarization is given by (Ambacher, 1999)

$$\sigma(x) = P_{SP}(\mathrm{Al}_x\mathrm{Ga}_{1-x}\mathrm{N}) + P_{PZ}(\mathrm{Al}_x\mathrm{Ga}_{1-x}\mathrm{N}) - P_{SP}(\mathrm{GaN}) - P_{PZ}(\mathrm{GaN})\,. \quad (3)$$

Due to the greater thickness of the GaN buffer relative to the AlGaN layer, the GaN buffer may be assumed to be completely relaxed so that P_{PZ} (GaN) ≈ 0 (Rashmi, 2002).

2.5.2. DC Performance

As with any other FET, the threshold voltage of a HEMT is an important characteristic parameter. This voltage is the voltage that must be applied to the gate terminal for conduction to begin in the device (Sze, 2007:404). $\mathrm{Al}_x\mathrm{Ga}_{1-x}\mathrm{N}$/GaN HEMT threshold voltage, as a function of Al fraction (x), is given by

$$V_T(x) = \phi_B(x) - \frac{\Delta E_c(x)}{q} - \frac{qN_d d^2}{2\varepsilon(x)} - \frac{d\sigma(x)}{\varepsilon(x)} \tag{4}$$

where ϕ_B (x) is the Schottky barrier height, $\Delta E_c(x)$ is the conduction band energy difference between the narrow and wide bandgap materials, q is the elemental charge, N_d is the uniform doping concentration, d is the thickness of the wide bandgap layer (AlGaN), σ(x) is total polarization-induced charge sheet density, and $\varepsilon(x)$ is the permittivity of the wide bandgap layer (Rashmi, 2002).

HEMT drain current is a function of sheet carrier density, which is found with

$$n_s(x,y) = \frac{\varepsilon(x)}{q(d+\Delta d)}[V_G - V_T - V(y)] \tag{5}$$

where V_G is the gate voltage, $V(y)$ is the potential along the channel due to the drain voltage V_D (Neaman, 2003:607), and Δd is the channel thickness in the 2DEG (Sze, 2007:404).

Then, the drain current (I_D) can be found as follows:

$$\begin{aligned}
I_D &= qn_s(x,y)Wv(E) = qn_s(x,y)W\mu E = qn_s(x,y)W\mu\frac{dV}{dy} \\
I_D &= q\frac{\varepsilon(x)}{q(d+\Delta d)}[V_G - V_T - V(y)]W\mu\frac{dV}{dy} \\
\int_0^L I_D dy &= \frac{W\mu\varepsilon(x)}{(d+\Delta d)}\int_0^{V_D}[V_G - V_T - V(y)]dV \\
I_D y\,|_{y=0}^{y=L} &= \frac{W\mu\varepsilon(x)}{(d+\Delta d)}[(V_G - V_T)V - \frac{V^2}{2}]\,|_{V=0}^{V=V_D} \\
I_D L &= \frac{W\mu\varepsilon(x)}{(d+\Delta d)}[(V_G - V_T)V_D - \frac{V_D{}^2}{2}] \\
I_D &= \frac{W\mu\varepsilon(x)}{2L(d+\Delta d)}[2(V_G - V_T)V_D - V_D{}^2]
\end{aligned} \tag{6}$$

where W is the gate width, $v(E)$ is the carrier drift velocity, μ is the mobility (assumed constant), E is the electric field in the y direction, and L is the gate length (EENG 717, 2009:slide 6). In the linear region, when $V_D \leq (V_G - V_T)$, the drain current is

$$I_D = \frac{W\mu\varepsilon(x)}{L(d+\Delta d)}(V_G - V_T)V_D. \quad (7)$$

In the saturation region, when $V_D \geq (V_G - V_T)$, the drain current is

$$I_D = \frac{W\mu\varepsilon(x)}{2L(d+\Delta d)}(V_G - V_T)^2. \quad (8)$$

Typical drain current versus drain voltage curves for an n-channel metal-oxide-semiconductor FET (NMOSFET) are shown for several values of gate voltage in Figure 15. Conduction begins at the threshold voltage, denoted V_{GST} in the figure. (Note that the source contact is grounded. Therefore, V_{GS} and V_{DS} are synonymous with V_G and V_D. Lower-case letters may be used in place of subscripted capital letters.) Figure 16 shows the drain current versus drain voltage curves of an AlGaN/GaN HEMT used in this research for several values of gate voltage. Notice that the four upper curves of Figure 16 have begun to decrease toward the right of the graph. This effect is due to self-heating in the HEMT, for which Equation (8) does not account.

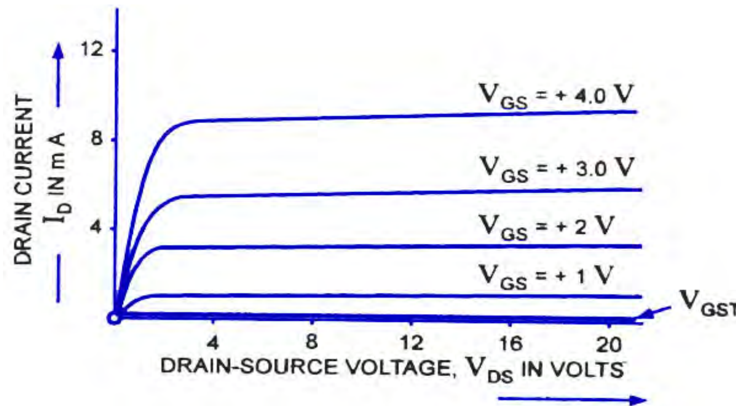

Figure 15. Drain current versus drain voltage at multiple values of gate voltage for an NMOSFET (Circuits Today, 2010)

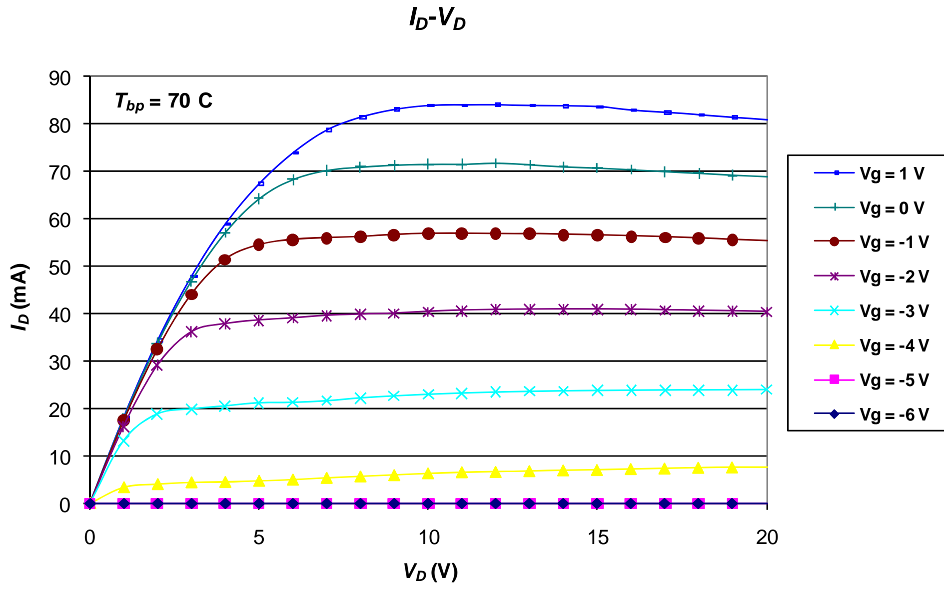

Figure 16. Drain current versus drain voltage at multiple values of gate voltage for a HEMT used in this research

Figure 17 shows the drain current versus gate voltage curve (i.e., transfer curve) at a particular drain voltage for an NMOSFET. This is an "enhancement" device since it is normally off at zero gate voltage and requires an applied positive voltage to "enhance" the channel with electrons for conduction to turn on the device (Sedra, 1991:303). The transfer curve of a HEMT used in this research is shown in Figure 18. This device is normally on with zero volts on the gate contact. The channel must be "depleted" of electrons by the application of negative voltage to turn off the device and, thus, the device is a "depletion" device (Neaman, 2003:511). The threshold voltage for this HEMT is about −4.5 V.

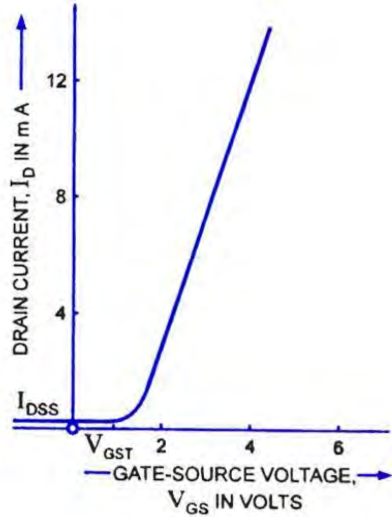

Figure 17. Transfer curve for an NMOSFET (after (Circuits Today, 2010))

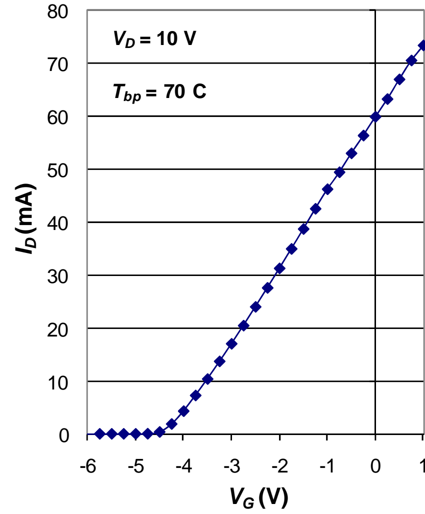

Figure 18. Transfer curve for a HEMT used in this research

A relation for the breakdown voltage is

$$V_{BD} = \frac{\xi_c^2 \varepsilon_s}{2qN} \quad (9)$$

where ξ_c and ε_s are, respectively, the critical field and permittivity of GaN, and N is the background (or unintentional) doping concentration on the semiconductor side of the Schottky gate contact near the drain region (Liddle, 2008). The typical breakdown voltage for the tested devices is greater than 200 V (see Chapter 7).

2.5.3. AC Performance

The AC performance of a HEMT can be described with three figures of merit: transconductance (g_m), unity current gain cut-off frequency (f_T), and maximum frequency of oscillation (f_{max}). Transconductance is defined as the change in drain current caused by a corresponding change in gate voltage, or (Neaman, 2003:498)

$$g_m = \frac{\partial I_D}{\partial V_G} \quad (10)$$

Transconductance can be increased with longer gate width, shorter gate length, and a thinner wide bandgap layer (Liddle, 2008). The transconductance curve of a HEMT used in this research is shown in Figure 19. The maximum value of the curve is used as the figure of merit.

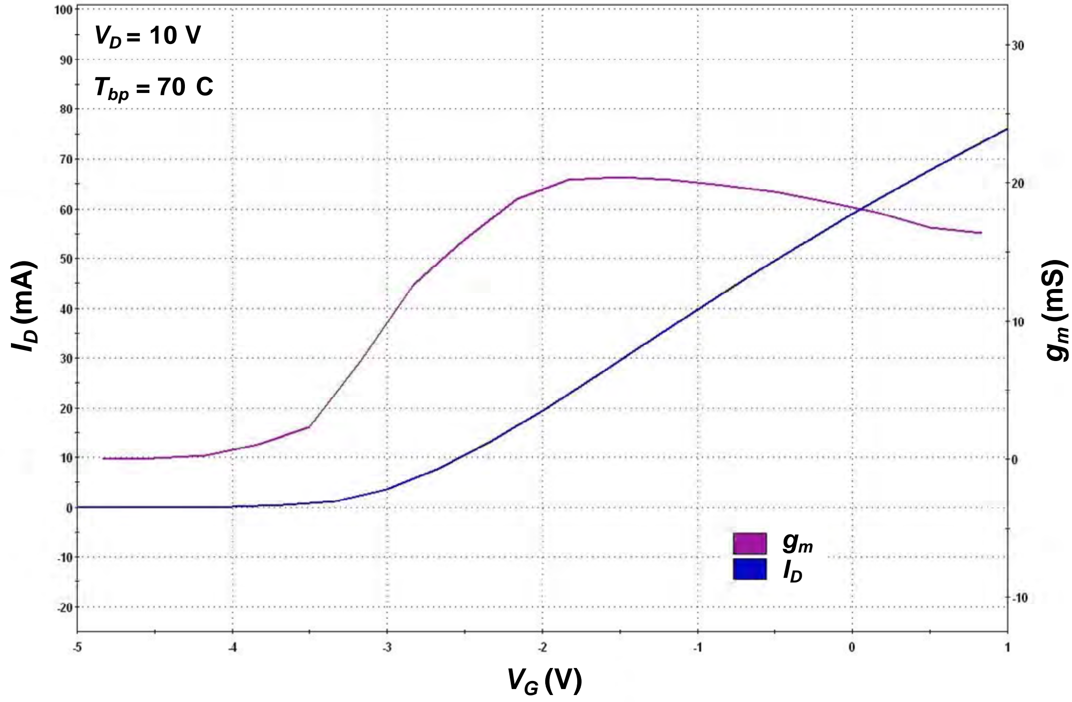

Figure 19. Transfer and transconductance (g_m) curves for a HEMT used in this research

The unity current gain cut-off frequency is

$$f_T = \frac{v_{sat}}{L_{gs} + L_g + L_{gd}} \tag{11}$$

where v_{sat} is the saturation velocity of the narrow bandgap material, and L_{gs}, L_g, and L_{gd} are, respectively, the gate-to-source, gate, and gate-to-drain lengths (Karmalkar, 2001). Using a semiconductor with a high saturation velocity (such as GaN) and reducing gate length (e.g., using a T-gate) generally increase f_T (Liddle, 2008). The other lengths could

also be reduced, but, as mentioned before, the optimum L_{gd} has been found to be 2.3 times the gate length (Chavarkar, 2003:**8**-8).

The maximum frequency of oscillation is

$$f_{\max} = \frac{f_T}{\sqrt{4 g_{ds} R_{in}}} \tag{12}$$

where g_{ds} is the output conductance and R_{in} is the input resistance of the intrinsic device (Chavarkar, 2003:**8**-7). The wider top portion of a T-gate serves to improve f_{max} (Sze, 2007:400). The output conductance can be reduced with a shorter gate (e.g., using a T-gate, as long as the ratio between L_g and barrier thickness is maintained above 5) and a reduced channel thickness (Chavarkar, 2003:**8**-9).

2.6. Accelerated Life Testing

2.6.1. Types of Stress Testing

Several methods for stress-testing GaN HEMTs may be used. GaN HEMTs generally degrade more with higher temperature (Bozada, 2010b). Three or more elevated temperatures are generally employed for accelerated temperature testing. In (Park, 2009), three samples of GaN HEMTs were tested for 1000 hours at base-plate temperatures of 82, 112, and 142 °C with 40 V on the drain and an initial drain current of 250 mA/mm. Using three temperatures enables an estimate of the Arrhenius model activation energy (discussed later) over a wider range of temperatures.

Stresses may also be stepped to cause failure sooner than at lower stress conditions. In (Chou, 2004), the ambient temperature of GaN HEMTs was stepped every 48 hours from 150 °C to 240 °C in steps of 15 °C while V_D was 10 V and I_D was 500 mA/mm. The drain voltage was stepped 5 V every 2 hours in (Glowacki, 2009).

RF stress may also be applied to GaN HEMTs. In (Pavlidis, 2005), with V_D at 10 V, RF power at 5 GHz was applied for one hour under maximum gain conditions. Interestingly, the time to degradation criteria under RF stress was less than an hour, while the time to degradation criteria under DC stress was several hours.

Since the conducting channels of GaN HEMTs increase in temperature during operation, a method to study degradation caused solely by thermal effects is a high-temperature storage test. In this test, no stress voltage is applied to the device (Smith, 2009). (Voltage is applied for brief, periodic characterization measurements.) Smith *et al.* reported that devices tested during a high-temperature storage test failed without the lattice disruptions that occurred in a device from the same wafer but stressed at high-temperature, 28-V DC conditions (Smith, 2009).

2.6.2. Causes of GaN HEMT Failure in the Literature

The following non-thermal failure mechanisms for GaN HEMTs are the most prevalent in the literature. The identified mechanisms may have different names in the literature. Current collapse ("the decrease in the maximum [direct current] current handling capability of a transistor as a result of the application of a large drain-to-source bias" (Katzer, 2006)) is commonly discussed and appears to be caused by the mechanisms identified below. Signatures of the various degradation mechanisms include drain current degradation (itself a result of other signatures such as a decrease in transconductance, shifted threshold voltage, or increased on-resistance), an increase in gate leakage current, and/or reduced RF power output (Christiansen, 2011b).

Two failure mechanisms of concern for GaN HEMTs are identified in (Smith, 2009). High electric fields, "hot" electrons (accelerated by high electric fields to energies

much greater than the thermal-equilibrium value (Neaman, 2003:561)), and high temperatures within a device can form defects in the device. These defects may be electrically active traps of charge. HEMT performance is degraded since charge collects in the traps and is not available for conduction. The second mechanism, structural damage (called lattice disruptions, pits, or cracks), occurs due to high temperatures in combination with electrical stimulus. The authors propose a current and contaminant interaction that creates the lattice disruptions by an etching process (see Figure 20). Device performance is degraded in this case due to a conduction path created in the material beneath the gate (Christiansen, 2011b).

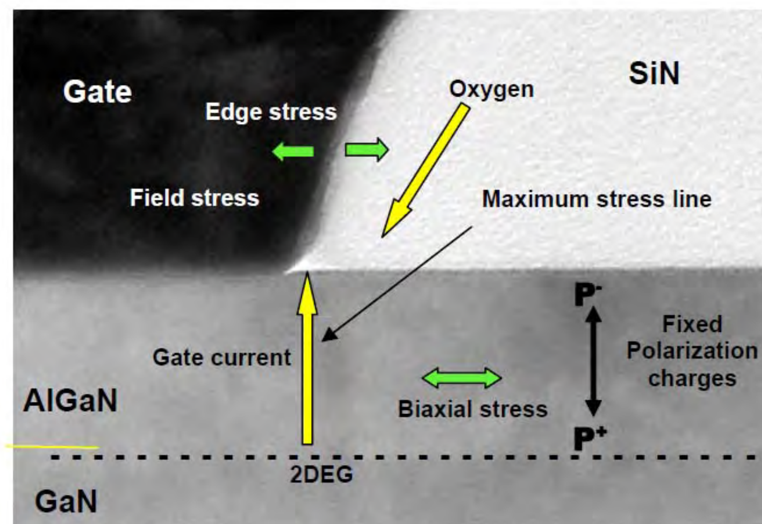

Figure 20. Pictorial representation of lattice disruption creation by an etching process as proposed by Smith *et al.* (Smith, 2009).

Another prominent theory of crack formation has been presented. In (Joh, 2008), (del Alamo, 2009), and (Makaram, 2010), a critical drain-to-gate voltage (V_{DG}), inducing the inverse piezoelectric effect, is claimed to cause the pits and cracks in the AlGaN barrier layer of a GaN HEMT. The theory is that the high electric field on the drain side of the gate causes increased mechanical strain in the piezoelectric materials of the

HEMT. As the electric field is increased in this region, the mechanical stress causes the lattice to crack at a critical voltage. Once this defect is formed, electrons tunnel from the gate to the conduction channel, which degrades the drain current. Gate and drain current degradation reportedly occurs in tests in high-power, OFF, and, most severely, V_{DS}-equals-zero states at respective critical voltages for each condition (see Figure 21). Degradation occurs in minutes as the stress voltage V_{DG} is applied in steps of 1 V per minute (Christiansen, 2011b). Between steps, I_{Dmax} is measured at V_{GS} = 2 V and V_{DS} = 5 V and I_{Goff} is measured at V_{GS} = -5 V and V_{DS} = 0.1 V. Figure 22 shows the cracks and pits theorized to be generated by stress testing in the high-power state.

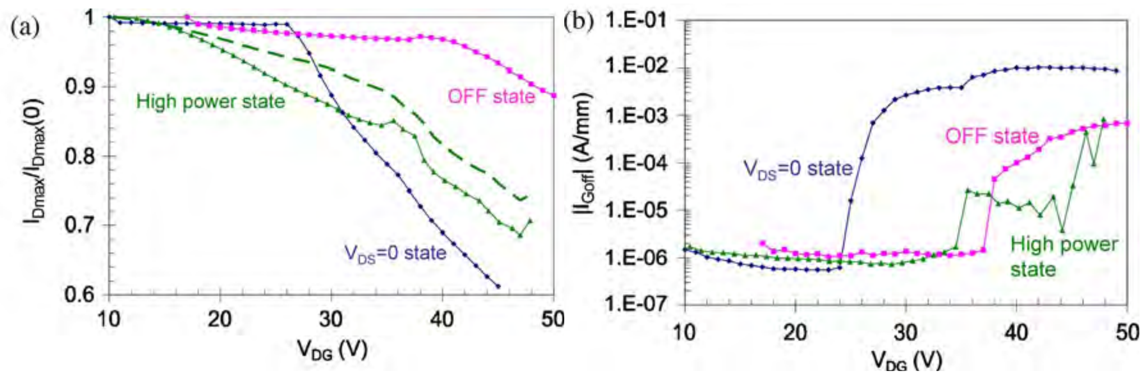

Figure 21. (a) Change in normalized I_{Dmax} in step-stress experiments for three different stress conditions. Dashed line represents the estimated change in I_{Dmax} in the high-power state removing the effect of V_T change. (b) Change in the gate leakage current I_{Goff} (gate current at V_{DS} = 0.1 V and V_{GS} = −5 V) in the same experiment (Joh, 2008).

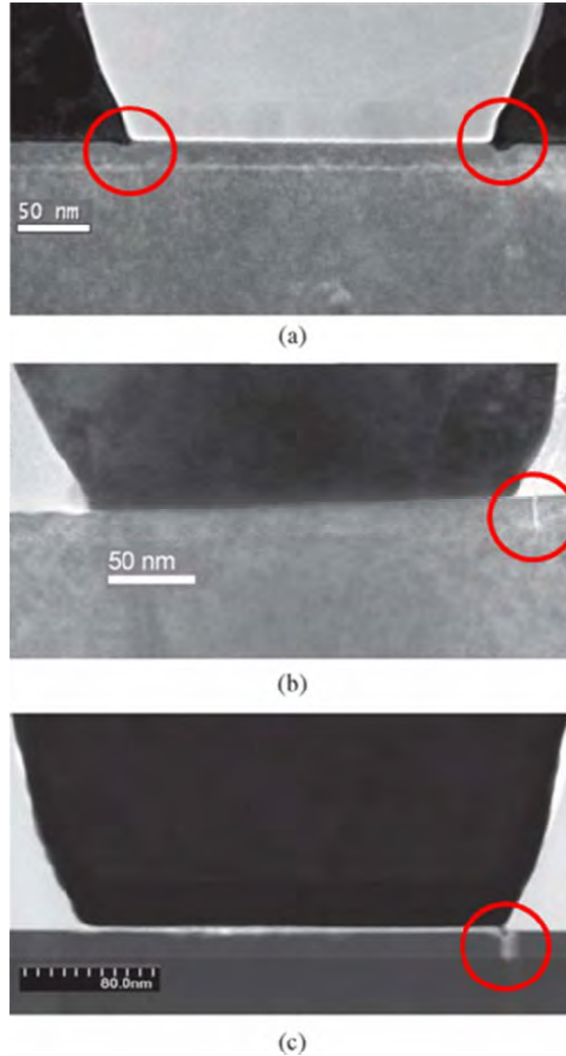

Figure 22. (a) and (b) Cross-sectional HREM and (c) Z-contrast images of three stressed devices. Material below the horizontal interface is semiconductor; the trapezoidal shape defines the gate metal. Right side is toward the drain, and left side is toward the source in all three images. (a) shows the formation of pits on both the source- and drain-side edges of the gate, (b) shows the formation of a crack, and (c) shows a severe case of degradation where the gate metal (Pt) has diffused into the crack formed (Chowdhury, 2008). (b) and (c) have roughly the same scale.

Hot electron degradation is highlighted in (Meneghesso, 2008). Decreases in saturated drain-source current (I_{DSS}) and transconductance (g_m) were caused by hot electrons created by simultaneous high current and high electric field, and not by electric field alone. GaN HEMTs tested for 10 hours in a semi-ON-state condition (V_{DS} = 20 V, V_{GS} = −5.5 V) experienced a 15% decrease in maximum g_m, while the maximum g_m of

devices stressed in an ON-state condition (V_{DS} = 20 V, V_{GS} = 0 V) and OFF-state condition (V_{DS} = 20 V, V_{GS} = −7.7 V) decreased less than 5% (see Figure 23). In addition, devices tested in ON-state conditions exhibited threshold voltage shifts while the same type of devices tested in OFF-state conditions did not (Christiansen, 2011b).

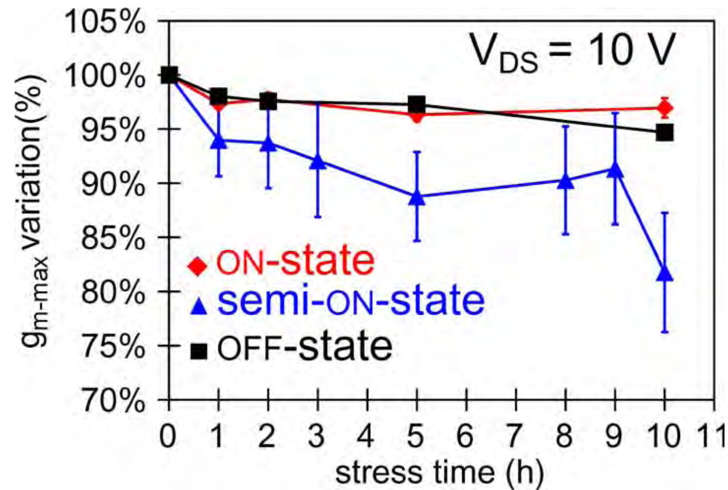

Figure 23. Average percent decrease of the maximum transconductance measured at V_{DS} = 10 V during 10-hour ON-state tests (V_{DS} = 20 V, V_{GS} = 0 V; diamonds), OFF-state tests (V_{DS} = 20 V, V_{GS} = −7.7 V; squares), and semi-ON-state tests (V_{DS} = 20 V, V_{GS} = −5.5 V; triangles) (Meneghesso, 2008)

A proposed physical mechanism that links hot-electron damage to traps is in (Puzyrev, 2010) and (Puzyrev, 2011). During fabrication, GaN HEMTs are exposed to hydrogen either from ammonia (NH_3) as the nitrogen source or from H_2 gas as a carrier for N_2. The hydrogen bonds to intrinsic defects in the GaN, electrically inactivating (i.e., passivating) the hydrogenated defects. Figure 24 depicts the hydrogenation of three defect types. During a stress state of low current and high electric field, hot electrons may remove the hydrogen from the passivated defects. This dehydrogenation causes the defects to become electrically active and behave as traps, degrading device performance (Coutu, 2011).

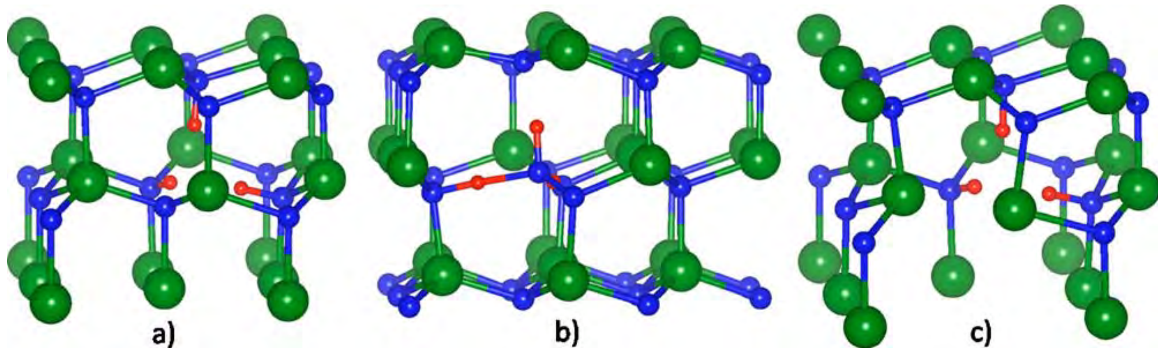

Figure 24. Atomic configurations of triply hydrogenated (a) gallium vacancy,(b) nitrogen antisite, and (c) divacancy. (Puzyrev, 2011)

Gate leakage current due to tunneling electrons is emphasized as a dominant failure mechanism in GaN HEMTs in (Trew, 2009). When a HEMT is under a high drain voltage and driven by a large RF signal, the electric field at the drain side of the gate is sufficient to cause electrons to quantum mechanically tunnel from the gate electrode. These electrons can accumulate on the semiconductor surface, and thus be unavailable for conduction. They can also travel over the surface to the drain or through the AlGaN layer beneath the gate. Conduction from the gate to the drain along the surface is the dominant leakage path. The secondary path is through the AlGaN layer to the channel. See Figure 25. Field plates can be used to reduce RF power degradation by decreasing the electric field at the gate. However, their use is detrimental to X-band and Ka-band devices due to the feedback capacitance the plates create. Surface passivation is a method to reduce the dominate leakage path over the surface (Christiansen, 2011b).

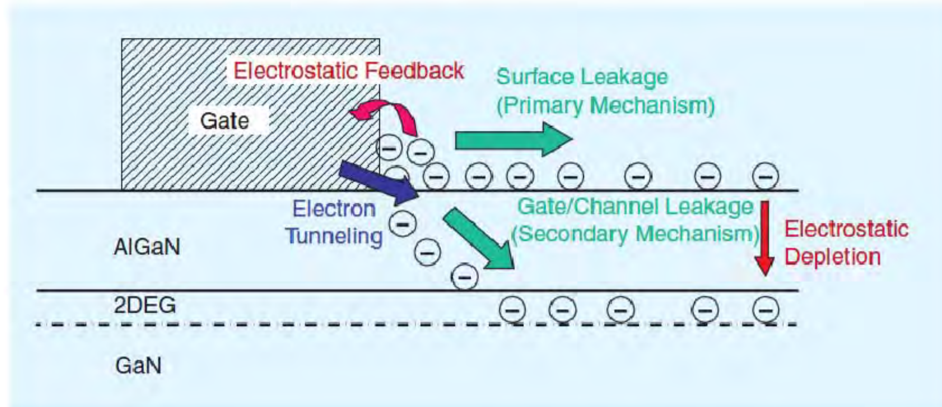

Figure 25. Electron tunneling leakage from the gate electrode and possible current paths (Trew, 2009)

2.6.3. Arrhenius Relationship

The point at which a transistor crosses the threshold of acceptable operation usually occurs after the device's useful life (Trew, 2009). Therefore, a method that accelerates failures is generally employed.

A commonly used method to accelerate failures in microelectronic devices is the use of elevated temperatures and the Arrhenius model of a reaction rate. Most reliability tests of GaN HEMTs are conducted at three or more temperatures above normal operating temperature. Most specimens are operated to failure, which is usually defined as degradation below a certain level of performance (e.g., RF power output, drain current) or above a level of an undesirable characteristic (e.g., gate leakage current). Then, the Arrhenius relationship is used to calculate an acceleration factor with which an estimate of lifetime can be computed at the use temperature. Despite the concerns about the reliability of GaN HEMTs, their lifetimes are extrapolated to more than a million hours (Conway, 2007; Singhal, 2007; Lee, 2008), which is more than 100 years. Many

estimates reported in the literature do not have associated confidence intervals; (Lee, 2008) is an exception.

The Arrhenius model is

$$r(T) = A\exp\left(-\frac{E_A}{kT}\right) \tag{13}$$

where r is the reaction rate, T is temperature in Kelvin (K), A is a constant, E_A is the activation energy in electron-volts (eV), and k is Boltzmann's constant (8.617×10^{-5} eV/K) (Trew, 2009). The activation energy parameter in the Arrhenius model is experimentally determined and denotes the sensitivity of the reaction (degradation, in the case of reliability testing) to temperature (Bozada, 2010b).

An acceleration factor (AF)—in this case, due to the elevated temperatures—is defined as an Arrhenius reaction rate at one temperature divided by an Arrhenius reaction rate at a different temperature. Mathematically, (Ebeling, 2005:327)

$$AF = \frac{r(T_2)}{r(T_1)} = \frac{Ae^{(-E_A/kT_2)}}{Ae^{(-E_A/kT_1)}} = \exp\left[\frac{E_A}{k}\left(\frac{1}{T_1}-\frac{1}{T_2}\right)\right]. \tag{14}$$

With failure time measurements from samples operating at two or more temperatures, the activation energy (E_A) is found from

$$E_A = k\left[\frac{\ln(t_{f1})-\ln(t_{f2})}{\left(1/T_1 - 1/T_2\right)}\right] \tag{15}$$

where t_{f1} is the failure time at temperature T_1 and t_{f2} is the failure time at temperature T_2 (Trew, 2009). Note that t_{f1} and t_{f2} could be the median times to failure (MdTTF) of the sample populations.

Once the activation energy has been computed, an acceleration factor is calculated with Equation (14) using a temperature other than the elevated temperatures, such as operating temperature, as T_1 and one of the elevated temperatures as T_2. An estimate for the time to failure is then this AF multiplied by the time to failure at T_2. Statistical software applications such as JMP® (SAS Institute) provide confidence intervals for the estimated time to failure.

2.6.4. Eyring Model

The Eyring relationship is similar to the Arrhenius model but is based on quantum mechanics and allows the use of multiple accelerated stressors besides temperature. The Arrhenius model was developed empirically (Ebeling, 2005:328). Besides temperature, voltage and/or current could be used as additional stressors for GaN HEMT reliability testing. (Nelson recommends a designed experiment to determine the stressor or stressors that accelerate life (Nelson, 1990:30).) Voltage as an accelerating factor is attractive due to the effect of high electric fields on gate leakage current. Meeker and Escobar state that the Eyring model could lead to better extrapolations at normal operating conditions. They also state that the Arrhenius relationship produces more conservative estimates than the Eyring model (Meeker, 1998:475). Estimates from the Eyring model may be more "practical" (Trew, 2009) than Arrhenius model estimates. Overlapping confidence intervals from both models could lead to more accurate estimates of GaN HEMT lifetimes.

The Eyring model equation is

$$r(T) = AT^{\alpha} \exp\left\{-\frac{E_A}{kT} + \left(B + \frac{C}{T}\right)S_1 + \left(D + \frac{E}{T}\right)S_2\right\} \tag{16}$$

where α, B, C, D, and E are constants determined experimentally, and S_1 and S_2 are functions of relevant non-thermal stressors (NIST, 2010). The Eyring model reduces to the Arrhenius model if α is close to 1 and there are no stressors other than temperature.

2.6.5. Parameter Definitions and Failure Criteria

Table 1 contains definitions that were used in this research for experimentally measured or derived parameters. Some of these definitions are not absolute; the terms may have different meanings for different people.

TABLE 1. DEFINITIONS OF EXPERIMENTALLY MEASURED OR DERIVED PARAMETERS (VIA, 2010)

Parameter	Definition
Maximum drain current (I_{Dmax})	The drain current when $V_G = 1$ V and $V_D = 10$ V
Saturated drain-source current (I_{DSS})	The drain current when $V_G = 0$ V and $V_D = 10$ V
Threshold Voltage (V_T)	The V_G intercept of a tangent line drawn from the peak g_m point on the transfer curve.
Peak transconductance (g_{mp})	The peak value of the curve generated by taking the derivative of the transfer curve.
Breakdown Voltage (V_{BD})	The drain voltage at which $I_D = 1$ mA/mm with V_G at 2 V less than threshold voltage.

The failure criteria used in this research are listed in Table 2. $I_{Dstress}$ is the drain current observed during stress. The other criteria were measured or derived from characterization curves.

TABLE 2. FAILURE CRITERIA

Parameter	Failure Criterion	Priority
Maximum drain current (I_{Dmax})	20% change (Via, 2010)	Primary
Drain current ($I_{Dstress}$)	20% change (Via, 2010)	Secondary
Saturated drain-source current (I_{DSS})	10% change (Lee, 2008)	Secondary
Threshold Voltage (V_T)	15% change (Hafizi, 1994)	Secondary
Peak transconductance (g_{mp})	10% change (Hafizi, 1994)	Secondary
Gate leakage current (I_{Gleak})	100% increase in magnitude (Hafizi, 1994)	Secondary

2.7. Modeling

2.7.1. Recent Examples

The following paragraphs survey recent modeling efforts reported in the literature. Finite-element and lumped-element analyses have been used. Two- and three-dimensional models have been created. Various software tools have been employed.

Li *et al.* used the ABACUS [sic] Standard program (SIMULIA) and finite element analysis to calculate stress and temperature distributions in GaN HEMTs subjected to thermal cycling. They solved Schrödinger's and Poisson's equations to create a charge-control model, including traps, from which they produced the I-V characteristics of the devices. They concluded that the degradation resulting from reliability testing is due to buffer layer traps (Li, 2009).

In (Bertoluzza, 2009), Bertoluzza *et al.* employed a 2-D lumped-element model, which does not include a fitting parameter, coupled with a large-signal model to simulate the temperature characteristics of GaN-based HEMTs. They used the PLECS® toolbox (Plexim) within MATLAB®/Simulink® (MathWorks) to simulate their model. Their model results are in general agreement with a finite-element model simulated in COMSOL Multiphysics® (COMSOL). The authors claim their model can be used for reliability estimation but do not provide such an example.

Heller used ANSYS (ANSYS), a finite element program, to conduct 3-D simulations of AlGaN/GaN HEMT degradation due to temperature. He used power and temperature distributions, rather than averages or peak values, in his model. Using distributions follows the lifetime analysis of a product subjected to non-uniform stress

presented by Nelson (Nelson, 1990:387-392). Heller found that modest error is introduced in model parameters when using only a peak value (Heller, 2008a).

Joh *et al.* (of del Alamo's group at MIT) created a model to investigate their theory that a critical voltage causes cracks in the AlGaN layer of a HEMT through the inverse piezoelectric effect. They used the device simulator ATLAS from Silvaco (Silvaco) to determine the electric fields in two dimensions. Using this field distribution, they calculated the stress and strain at every point in the device model. Finally, they computed the elastic energy density throughout the device. The critical voltage is the bias at which the elastic energy density exceeds a critical value. The authors claim that their first-order model produces critical elastic energy density predictions—when their experimentally determined critical voltage is applied—that "match" others' observations of critical elastic energy (Joh, 2009).

2.7.2. Current Industry Software – Synopsys TCAD

The technology computer-aided design (TCAD) suite in use at AFIT is the Sentaurus suite by Synopsys (Synopsys). Sentaurus Process is the modeling environment for fabrication process simulation. A device model can also be created in Sentaurus Structure Editor by specifying the device's dimensions and doping concentrations. After being created in either Sentaurus Process or Sentaurus Structure Editor, a semiconductor device's electrical and thermal characteristics can be simulated in Sentaurus Device (Coutu, 2011).

Within Sentaurus Device is the capability to simulate degradation by trap formation or hydrogen transport in complementary metal oxide semiconductor (CMOS) designs (Synopsys, 2010). To perform a degradation simulation, an initial

characterization is run in Sentaurus Device, followed by application of the desired stress bias conditions. Then, the degradation model is executed and a post-degradation characterization is completed for comparison to the initial performance (Synopsys, 2008). (Coutu, 2011)

Currently, there is not a specific degradation model in Sentaurus Device for GaN HEMTs. However, Sentaurus Device's multistate configuration (MSC)-hydrogen transport degradation model may possibly be used to model the dehydrogenation of hydrogenated GaN defects as discussed above (Heller, 2011a). (Coutu, 2011) The MSC-hydrogen transport degradation model does not modify the device model.

2.8. Chapter Summary

This chapter described GaN HEMT structure and operation. GaN HEMT degradation mechanisms that are prominent in the literature were reviewed. Accelerated life testing and lifetime prediction models were discussed. Recent modeling examples from the literature were presented, and Synopsys TCAD was introduced.

III. Modeling Research

3.1. Introduction

This chapter presents the AFIT results of a joint research project with the Naval Postgraduate School (NPS), Monterey, California.

Currently, there is a not a commercial TCAD software suite that is able to modify an electronic device model due to the simulated operating conditions. An ideal situation would be for the device simulator output to be coupled with the fabrication process simulator to achieve the desired modification of the device model. The modeling and simulation capabilities of the Synopsys TCAD software suite were investigated. A seamless integration of device simulator output and fabrication process simulator, as currently coded, was not possible. However, a workaround was created in which device simulator output was iteratively used, through Unix and MATLAB scripts, to modify the device model in the suite's structure editor (Coutu, 2011).

3.2. General Motivation for Modeling Microelectronic Devices

There is no industry TCAD tool to predict device lifetime via electrical and thermal simulation of operating conditions. The industry judges itself by yields and profits, but it no longer has an interest in end-of-life estimates because the marketplace doesn't require such estimates. A TCAD tool that predicts microelectronic device lifetime would enable the creation of longer-living systems for the Department of Defense through design optimization. Such a tool would also reduce the time and cost to acquire and test new systems (Coutu, 2011).

Many failures in microelectronics are related to mass movement (e.g., electromigration, corrosion, creep) of lattice atoms at high current densities, thermal gradients, or electric fields. Movement of particles other than lattice atoms can cause other problems (e.g., negative bias temperature instability, hot carriers). To predict the movement-of-mass failures, a capability to change a device's physical structure during or between electrical and thermal simulations is required. This capability does not exist. Current commercial simulation applications that examine device degradation assume "perfect" structures at yield, not a compromised device due to aging (Coutu, 2011).

The basis of many electronic device failures is related to the creation of defects from energy gradients. Small defects migrate and create larger defects. Large defects create device failures. This is the correlation between integrated circuit yield and end-of-life failures (Kuo, 1999). Yield is limited by larger defects from the manufacturing process. End-of-life failures are caused by small defects becoming larger at a later time. Energy gradients such as electrical, thermal, and mechanical forces are required to move mass, either in fabrication or operation. Presently, defects are modeled only electrically in device TCAD codes by energy density and rates of carrier generation or removal. Present TCAD tools cannot predict the movement of mass within the crystal lattice during device operation. However, present process simulation tools can deposit, diffuse, and implant mass by virtually growing the device structure (Coutu, 2011).

Present semiconductor industry design tools have considerable knowledge of fabrication processes. The tools use this knowledge to predict mass movement during fabrication simulation. Even though present-day tools employ highly developed physics-based modeling, they can only determine electrical performance at the time of yield

following fabrication, assuming a perfect non-changing component. Currently, commercial software applications do not integrate the results of device simulation with fabrication process simulation to modify devices based on use conditions (Coutu, 2011).

3.3. Approach

The approach to modeling was to use existing commercial TCAD software from Synopsys (NPS is using TCAD software from Silvaco) and investigate the interfaces required to integrate the output of the device simulation with the input of the process simulation (Coutu, 2011).

To achieve the objective of developing a tool that will predict the reliability of microelectronic devices, the output of a device simulator needs to become the input to the software that modifies the device model. The basic technique is to run linked electrical, mechanical, and thermal simulations to automatically determine the locations and magnitudes of the electrical, mechanical, and thermal energy gradients. After locating the energy gradients, the model structure is automatically changed based on these simulated operating characteristics. The cycle of locating energy gradients and changing the device model accordingly is repeated at intervals (e.g., days, months, or years). The electrical degradation of the electronic device model is tracked until the failure criterion of the chosen failure mechanism is met. Then, device lifetime could be estimated automatically with the simulated elapsed time achieved by the device model before failure. Figure 26 shows the envisioned process flow of the approach (Coutu, 2011).

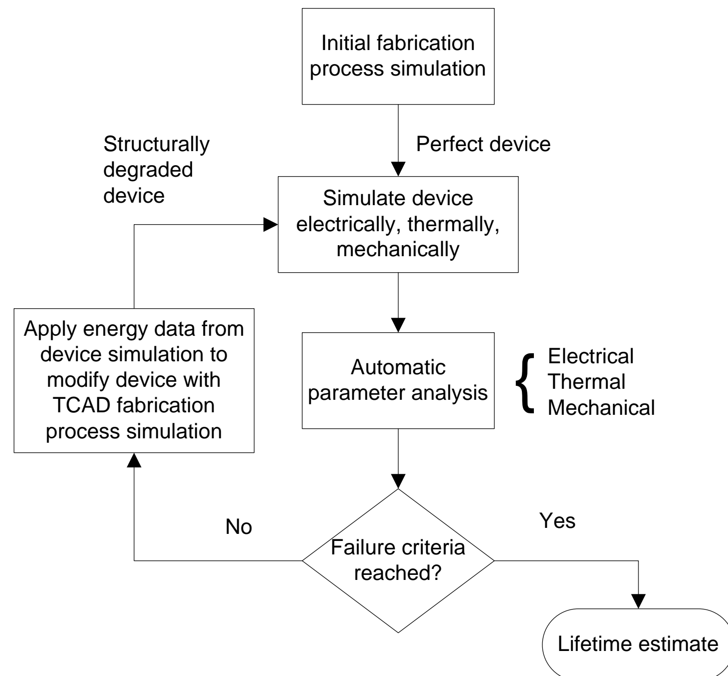

Figure 26. Flow chart for automated device modification. (Coutu, 2011)

The ONR MURI mentioned in Chapter 1 has an objective similar to the objective of this joint research project. The objective of the ONR MURI is to create a predictive failure model based on the physics and chemistry of the GaN HEMT failure mechanisms. The University of California, Santa Barbara, leads the team that includes the Massachusetts Institute of Technology, the University of Michigan, Vanderbilt University, The Ohio State University, and others. Significant time and effort has been applied in pursuit of the MURI's objective, which has not been achieved yet. The experience of the ONR MURI illustrates the difficulty of creating a model that incorporates physical mechanisms to predict microelectronic device failure (Coutu, 2011).

3.4. Modeling at AFIT

To begin the modeling efforts, a manual version of the Figure-26 process was investigated as a means of modifying a device model in accordance with simulated device operating conditions. Then, the manual device modification concept was demonstrated with an electromigration example. Electromigration is a dominant failure mechanism in silicon-based microelectronic devices. It is simpler than many gallium nitride failure mechanisms, and thus, provides a means to prove the manual and automated device modification concepts (Coutu, 2011).

A metal line was constructed in Sentaurus Structure editor. Then, device simulation was performed in Sentaurus Device. All other tasks of Figure 26 were performed manually (a lifetime estimate was not calculated). Figure 27 depicts the progression by electromigration of a pre-made divot in the metal line as a voltage was applied across the line and illustrates the manual device modification concept. In the region of highest current density, the metal was manually moved to a region of low current density until the void completely separated the metal line into two segments (Coutu, 2011).

The next step in the modeling efforts was to automate the manual electromigration example. A seamless method in Sentaurus Process, as currently coded, to modify the device model (e.g., through etching or diffusion) based on parameter values in the Sentaurus Device output was not possible. Such a method would be ideal for the process of Figure 26. To create the metal wire for the automated electromigration example, Sentaurus Structure Editor files, similar to the ones created for the manual

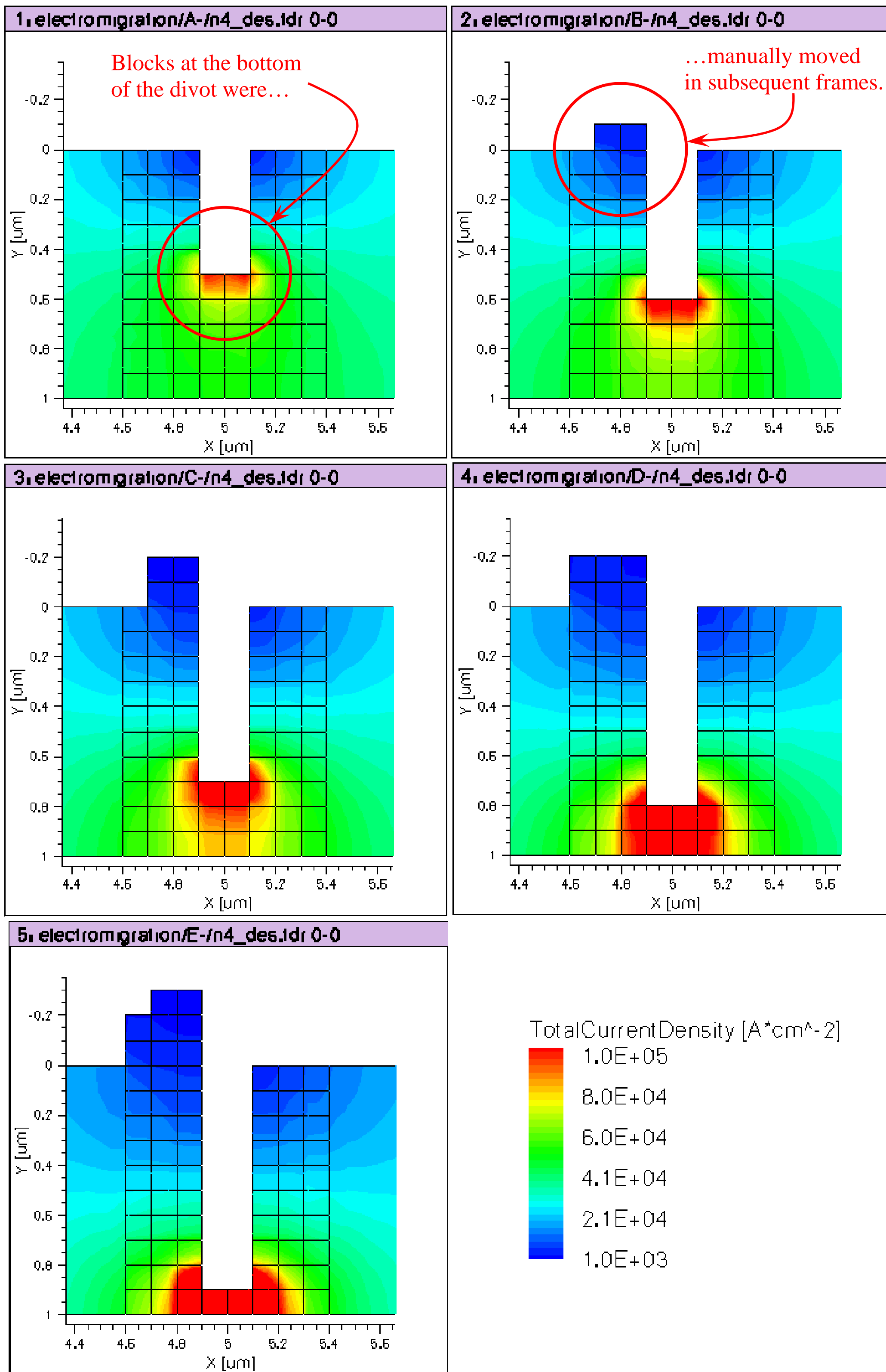

Figure 27. Manual electromigration example. Current densities range from 1 kA/cm^2 (and less) in blue to 100 kA/cm^2 (and greater) in red. The last frame (not shown) is a complete void.

example, were used. Then, with Unix and MATLAB[1] scripts, the process of Figure 26 was automated to create the device model in Sentaurus Structure Editor, simulate device operation in Sentaurus Device, modify the device model in Sentaurus Structure Editor based on current density obtained from Sentaurus Device output, and repeat. Appendix B contains the Unix and MATLAB scripts and Sentaurus files used in the automated process. If a block had an electrical current density greater than 100 kA/cm^2 (Weatherford, 2010), the scripts deleted that entire block. A refinement would be to create smaller blocks. The failure criterion was the complete separation of the wire into two segments (as in the manual example, a lifetime estimate was not calculated) (Coutu, 2011).

Figure 28 shows the progression of electromigration of the pre-made divot in the metal line and illustrates the automated device modification concept. Notice the difference in progression between Figures 27 and 28, aside from the difference of moving the high-current-density blocks in Figure 27 and the deletion of such blocks in Figure 28. The automated process selected the appropriate blocks to modify, whereas the manual process did not modify blocks that should have been modified, and the divot grew faster and larger in the automated example than in the manual example (Coutu, 2011).

Upon further investigation of electromigration, there are additional and more complex factors affecting electromigration than solely a threshold of current density. Stress and concentration gradients and temperature affect electromigration. Additionally, there are multiple diffusion paths through the lattice and across interfaces and grain boundaries. Cacho *et al.* (Cacho, 2008) considered these additional factors along with

[1] MATLAB scripts were modified versions of scripts originally created by Martha Gallivan in July 2006.

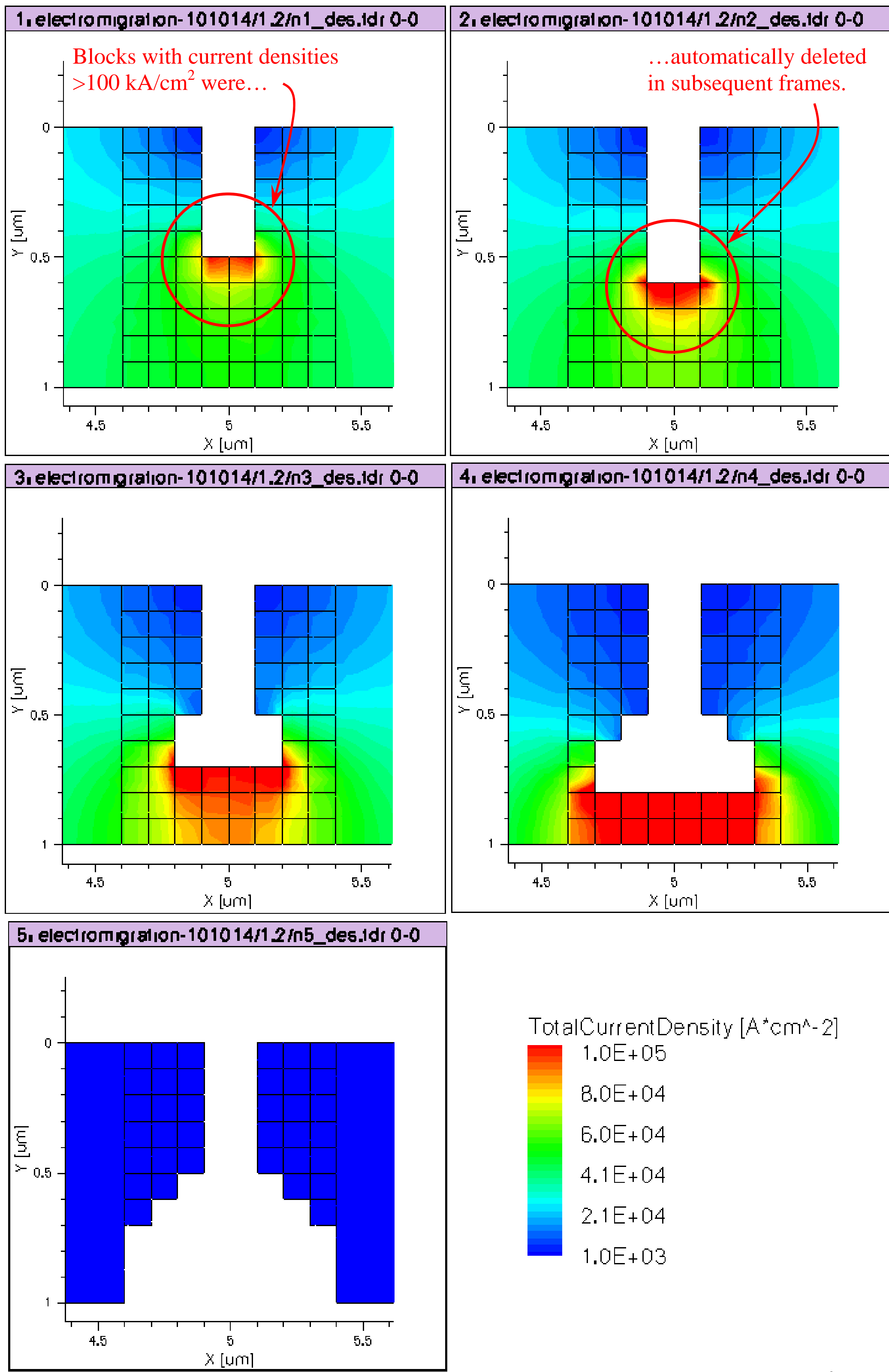

Figure 28. Automated electromigration example. Current densities range from 1 kA/cm^2 (and less) in blue to 100 kA/cm^2 (and greater) in red.

electrical current in their implementation of a multiphysics model to investigate interconnect failure due to electromigration. Their model exhibited reasonable agreement with the time evolution of resistance measurements (Coutu, 2011).

3.5. Future Work

To continue on to modeling GaN HEMT degradation, a model describing the time-dependence of degradation is needed (Coutu, 2011). Prominent GaN degradation mechanisms in the literature were discussed in Section 2.6.2. Empirical evidence could also be used to create the time-dependent degradation model. Both AFIT and NPS have collected independent measurements on the same device family, with NPS conducting pulsed direct current (DC) testing and AFIT conducting life testing with accelerated test methods (Coutu, 2011). (A joint paper is forthcoming that compares the NPS test results to the AFIT test results.)

Pits were observed in physical devices that were tested under the sponsorship of the Air Force Research Laboratory (AFRL). Both AFIT and NPS have tested devices from the device family in which the pits were observed and under similar bias conditions after which the pits were seen (Coutu, 2011). Figure 34(b) in Section 5.3 is a transmission electron microscope (TEM) image of a device after being stressed in a high-power state (Christiansen, 2011b).

From the research sponsored by AFRL, the following model was obtained by fitting to Equation (19) of Section 8.3.2 the data from devices tested at conditions similar to those under which the device of Figure 34(b) was tested:

$$I_{Dnormalized} = 0.05171 \cdot \exp(-0.03459 \cdot t) + 0.94525 \cdot \exp(2.94\text{E-}05 \cdot t). \quad (17)$$

$I_{Dnormalized}$ is the drain current normalized to the drain current at time $t = 0$ hours. Time t is in hours. With this mathematical model, the size of the pit may be changed over time in a device model and device degradation due to the pit may be tracked (Coutu, 2011).

3.6. Chapter Summary

The use of the Synopsys TCAD suite for degradation modeling was investigated. The Synopsys device simulator contains models for CMOS device degradation by traps or hydrogen transport. There is not a specific model for GaN HEMT degradation, but the hydrogen transport model may possibly be used for GaN HEMTs (Heller, 2011a). (Coutu, 2011)

The use of the Synopsys TCAD suite was investigated to create an automated process whereby a device model can be modified based on the simulated operating characteristics (Coutu, 2011). The ONR MURI experience demonstrates the difficulty of creating a predictive failure model for microelectronic devices. Using the Synopsys device simulator output in the fabrication process simulator to modify the device model was not possible; Synopsys will need to modify the software to make this feature available. However, an automated process using the device editor tool was created, and a demonstration was performed that showed the device simulator output can be used to alter the device structure (Coutu, 2011).

IV. Experimental Procedures

4.1. Introduction

This chapter presents the experimental procedures used in this research. The two subsequent paragraphs contain information that applies to all tests. The sections that follow describe specific test procedures.

The devices used in this research were selected from two wafers of the same lot from a commercial foundry. The AlGaN/GaN HEMT structure consisted of a SiC substrate, a gate-integrated field plate, and a source-connected field plate. Gate length was 0.5 μm (by design rules) and periphery was 2×50 μm. The distance between the gate and drain was greater than the distance between the gate and source (Christiansen, 2011c). See Figure 14 for a schematic diagram of the tested devices.

The devices tested in the voltage step-stress tests were on a wafer. Devices packaged in Stratedge 580274 packages were used in the other tests. No burn-in was performed prior to testing.

Appendix B contains the Unix and MATLAB scripts used to process the collected data.

4.2. Voltage Step-Stress

To determine if there was a drain bias alone that caused these devices to fail and to determine their voltage limits, voltage step-stress was applied in a probe station to four on-wafer devices. The thermal stage temperature was maintained at 70 °C. The transistors were in deep pinch-off with the gate at −10 V. Drain voltage stress began at 50 V and was increased by 10 V after each 1 hour of stress. Two devices were taken to

150 V and the other two were taken to 200 V. Transfer curves were collected before and after each step at $V_D = 10$ V and V_G was swept from −6 V to 1 V in 0.25-V steps. Drain and gate voltages and currents during the stress steps and characterizations were measured with Agilent power supply models E5280A High Power Source/Monitor Unit (SMU) Module (for the drain) and E5281A Medium Power SMU module (for the gate) in a model E5273A 2 Channel SMU. A representative Excel macro that controlled the Agilent power supplies is in Appendix B.

Step-stress tests similar to those conducted by J. A. del Alamo's group at MIT were conducted on the devices studied in this research. Two on-wafer devices were tested in a probe station at a base-plate temperature of 25 °C, since del Alamo's group tested at room temperature (del Alamo, 2009).

One device, R10C2, was stressed at $V_D = V_S = 0$ V with V_G being stepped from −10 to −50 V in −1-V steps for 1 minute each. This is del Alamo's "$V_{DS} = 0$ step-stress experiment" (del Alamo, 2009). I_{Dmax} was measured at $V_D = 10$ V and $V_G = 1$ V in this research. del Alamo's group used $V_D = 5$ V and $V_G = 2$ V (del Alamo, 2009). For the devices in this research, the drain current has already begun to saturate at $V_G < 2$ V (when $V_D = 10$ V). Additionally, the drain current was not near a maximum when $V_D = 5$ V (and $V_G = 1$ V), as seen in Figure 16. I_{Goff} was measured at $V_D = 0.1$ V and $V_G = -5$ V, which were the biases del Alamo's group used (del Alamo, 2009).

Another device, R9C2, was tested at the same values of V_{DG}, and in the same order, as R10C2. However, the method to obtain V_{DG} was different. In this test, V_G was held at 0 V, as was V_S, while V_D was stepped from 10 to 50 V in 1-V steps for 1 minute each. I_{Dmax} and I_{Goff} were measured at the same conditions used for R10C2.

4.3. 300-hour Test

For 300-, 1000-, and 600-hour tests, two different sets of test conditions were used: one was high DC drain voltage (V_{DS} = 60, 80, and 100 V) and low current with the gate pinched off ($V_{GS} = -10$ V) and the other was high DC power dissipation (≥11 W/mm). These conditions may occur during the RF sweep of device operation (Christiansen, 2011a). The test conditions, determined from preliminary overstress tests, are listed in Table 3. The rationale for selecting Conditions 1, 2, and 3 was to map the boundaries of life for the tested devices with increasing voltages. Conditions 2 and 3 were to have the same power dissipation (P_{diss}), and Condition 1 half that power. Conditions 1 and 2 were to have the same drain current (I_D). The base-plate temperatures (T_{bp}) of the power test Conditions 1, 2, and 3 were selected so that the devices had similar estimated peak channel temperatures (T_{ch}), while the high-voltage test Conditions 4, 5, and 6 would also have similar peak channel temperatures and were chosen to investigate the effects of high voltage. All peak channel temperature estimates are based on bias-dependent electrothermal modeling of the full device (Heller, 2008a). In all cases, testing was conducted in the dark under dry nitrogen in an Accel-RF DC test station, P/N 96100-01 (Christiansen, 2011a). See Appendix A for a pictorial presentation of the test preparation and setup. Appendix B contains the Accel-RF test sequence and configuration files for Condition 7.

For the 300-hour test, three devices were placed on test at each of Conditions 1, 2, 3, 4, and 6. For high-power Conditions 1, 2, and 3, the drain voltage (V_{DS}) was set and the gate voltage (V_{GS}) was adjusted until the target drain current (I_D) was reached (within the capabilities of the test station). After the initial setting of V_{GS}, V_{GS} was maintained for

the duration of the test. The expected values of V_{GS} for Conditions 1, 2, and 3 were based on previous testing and were not anticipated to cause forward gate current based on previous testing of parts from the same family at $V_{GS} = 2$ V. For the high-voltage Conditions 4 and 6, both V_{DS} and V_{GS} were set, and the expected I_D is based on values seen during step-stress testing of four on-wafer devices in a probe station. The range of T_{ch} estimates for Condition 6 is based on the range of I_D values seen during the step-stress testing (Christiansen, 2011a).

TABLE 3. TEST CONDITIONS FOR 300-HOUR, 1000-HOUR, AND 600-HOUR TESTS (CHRISTIANSEN, 2011A)

Condition	**T_{bp} (°C)**	**V_{DS} (V)**	**Target I_D (mA/mm)**	**P_{diss} (W/mm)**	**Expected V_{GS} (V)**	**T_{ch} (°C) estimate**
1	245	20.0	550	11.0	~2	394
2	133	40.0	550	22.0	< 2	392
3	130	60.0	367	22.0	< 0.5	391
			Expected I_D (mA/mm)		**Set V_{GS} (V)**	
7	245	17.5	690	12.1	3	405
			Approx. I_D (mA/mm)	**Approx. P_{diss} (W/mm)**	**Set V_{GS} (V)**	
4	245	60.0	< 0.026	< 0.00156	-10	245
5	245	80.0	< 0.076	< 0.00608	−10	245
6	245	100.0	< 2.0	< 0.2	-10	246-248

The intended test sequence for the power test conditions was an initial characterization, followed by stress until $I_{Dstress}$ (measured by the test station) degraded to a pre-determined failure criterion, and ending with a post-failure characterization. However, it was found that test station drain current measurement was not sufficiently precise (±1.5 mA, equivalently ±15 mA/mm) and drift (as much as 15 mA/100 hr with 3mA typical) was too great to track I_D during stress, and the test was ended at 300 hours

to conduct a characterization (Christiansen, 2011a). The test station has since been upgraded to measure I_D with more precision and less drift (Christiansen, 2011b).

Since drain current was expected to be small in the devices in the high-voltage set, these devices were periodically characterized. Their degradation was tracked with I_{DSS} and I_{Dmax}, rather than with the stress drain current. One hundred hours was arbitrarily chosen for the time between characterizations (Christiansen, 2011a).

The automated characterization is supported by the test stand (the sample did not leave the test module), and consisted of transfer curves collected at T_{bp} = 70 °C with Agilent power supplies (model E5280B Precision High Power SMU modules in a model E5270B 8-Slot Precision Measurement Mainframe). The Agilent power supplies are not subject to the measurement imprecision and drift mentioned two paragraphs above. The transfer curve was conducted at V_{DS} = 10 V with V_{GS} being swept from −5 to 1 V. The characterization was shown to be benign in on-wafer testing. I_{DSS} was measured at V_{DS} = 10 V and V_{GS} = 0 V. I_{Dmax} was measured at V_{DS} = 10 V and V_{GS} = 1 V (Christiansen, 2011a).

To investigate whether the changes seen after 300 hours of testing would recover with rest, an additional period of testing was begun after more than 48 hours of rest at room temperature in the dark under dry nitrogen. Most devices did not complete the intended additional period of testing for various reasons. The main reason was system glitches that appear to have been caused by building power fluctuations, which also knocked offline a chiller for the cleanroom in the same building (Christiansen, 2011b).

After testing, several devices were selected for analysis by thermal and photoemission imaging in a Quantum Focus Instruments InfraScope™ to find apparent

weak spots. In addition, select devices were imaged by scanning electron microscope (SEM) and transmission electron microscope (TEM) to reveal physical degradation (Christiansen, 2011b). One stressed device was mapped by energy-dispersive X-ray spectroscopy (EDS) and electron energy loss spectroscopy (EELS) for elemental analysis. To reveal the effects of stressing, a pristine device was also imaged by TEM and mapped by EDS and EELS for comparison to the stressed device.

4.4. 1000-hour Test

For the 1000-hour test, three devices were placed on test at each of Conditions 4, 5, and 6. For this testing, V_{DS}, V_{GS}, and I_D were as in the 300-hour test. These parts experienced three stress periods for a total of over 1000 hours of stress with rests occurring at approximately 450 and 800 hours of stress. The transfer curve characterizations occurred at T_{bp} = 70 °C before and after each stress period. Additionally, transfer curves were collected every hour at the stress temperature of T_{bp} = 245 °C.

4.5. 600-hour Test

A test similar to the 300-hour, high-power, Condition-1 test was conducted for 600 total stress hours on three devices. The differences were the conditions (Condition 7 in Table 3), rest periods at 200 and 400 stress hours, and hourly characterizations at the stress base-plate temperature of T_{bp} = 245 °C. In addition, and similar to the 300-hour test, transfer curve characterizations occurred at T_{bp} = 70 °C before and after each stress period (Christiansen, 2011a).

Prior to conducting this 600-hour test, three packaged devices were tested in a probe station to determine bias conditions at which very little (< 1 mA/mm) forward gate current would flow. With the thermal stage at 245 °C, the voltages of Condition 7 were observed to cause very little forward gate current. The average drain current at these biases was 690 mA/mm (Christiansen, 2011a).

4.6. Gate Bias Test

Three AlGaN/GaN HEMTs were stressed on a Peltier thermal baseplate in air. The power supplies used were Agilent models E5280A High Power Source/Monitor Unit (SMU) Module (for the drain) and E5281A Medium Power SMU Module (for the gate) in a model E5273A 2 Channel SMU (Christiansen, 2011c).

The devices were stressed to define a safe operating area. An initially tested part (not shown) was stressed at a gate current of approximately 260 mA/mm and a baseplate temperature of T_{bp} = 35 °C without any discernable degradation which provided the reference and motivation for this study. A second device (also not shown) was stressed at T_{bp} = 45 °C for 24 hours at I_G > 1.70 A/mm with qualitatively similar results as presented here. A test issue (likely a loose contact) caused a question of the validity of those observations and, hence, those results are not described here. Based on these observations of extremely robust devices, a detailed study of gate robustness was conducted as described next. For this third device, the source and drain were wire-bonded and the gate was contacted by a needle probe. The following sequence was used at T_{bp} = 45 °C. The voltage-sweep and transfer-curve voltage ranges were divided into 201 linear, ~35-ms-dwell steps (~7 seconds total sweep time) (Christiansen, 2011c).

1. Initially characterize with a transfer curve (V_G = −6 V to 1 V and V_D = 10 V).
2. Sweep V_G from 0 V to +2.5 V with $V_S = V_D = 0$ V.
3. Characterize with a transfer curve using Step-1 biases.
4. Repeat steps 2 and 3 two more times each.
5. Sweep V_G from 0 V to +2.5 V with $V_S = V_D = 0$ V and hold V_G at +2.5 V for 1 minute.
6. Characterize with a transfer curve using Step-1 biases.
7. Repeat steps 5 and 6 three more times each.
8. Sweep V_G from 0 V to +3.0 V with $V_S = V_D = 0$ V and hold V_G at +3.0 V for 1 minute.
9. Characterize with a transfer curve using Step-1 biases.
10. Repeat steps 8 and 9 at +0.5-V increments to V_G = +6.5 V (I_G = 1.89 A/mm).
11. Sweep V_G from 0 V to +6.0 V with $V_S = V_D = 0$ V and hold V_G at +6.0 V for 30 minutes.
12. Characterize with a transfer curve using Step-1 biases.
13. Repeat steps 11 and 12 with 30-minute, 150-minute, 120-minute, and >12-hour holding times, respectively, at V_G = +6.0 V ($I_G \approx$ 1.82 A/mm). After the last hold, the device was in a small-bias state ($I_G \approx$ 300 μA/mm, $V_S = V_D = 0$ V) for two days due to the gate contact needle probe coming loose.

In summary, this third device experienced more than 17.5 hours at V_G = +6.0 V in addition to 1 minute at V_G = +6.5 V (Christiansen, 2011c).

4.7. Chapter Summary

This chapter presented the test procedures used in this research. The following chapters refer to these test procedures.

V. Reliability Testing of AlGaN/GaN HEMTs under Multiple Stressors

5.1. Introduction

Various stressors are claimed in the literature to cause degradation in GaN HEMTs. Stressor examples include high electric fields, high temperature with electrical stimulus, current with high electric field, and high drain bias with large RF drive. These stressors may result in various degradation mechanisms identified by signatures such as drain current degradation (itself a result of other signatures such as a decrease in transconductance, shifted threshold voltage, or increased on-resistance), an increase in gate leakage current, and/or reduced RF power output (Christiansen, 2011b).

The various stressors and failure mechanisms in the literature were reviewed in Section 2.6.2.

With so many proposed stressors, degradation mechanisms, and degradation signatures, it is important to differentiate which stressors cause which effects. Due to this variety of stressors, mechanisms, and signatures, GaN HEMTs were tested under multiple stressors to discover the relevant stressor or stressors, degradation mechanisms, and signatures. Knowing the limitations of a component in terms of potential parameter degradation is important to a circuit designer (Christiansen, 2011b).

Two objectives of this study were to investigate the effects of different stressors and, specifically, to investigate whether high electric fields alone cause significant degradation (Christiansen, 2011b).

5.2. Experiment Description

The test procedures that pertain to this chapter are in Sections 4.1 and 4.3.

5.3. Results and Discussion

The results of thirteen of the fifteen devices placed on test are compared. Of the two devices that are not included in the comparison, one device tested at Condition 4 apparently suffered infant mortality before 100 hours. Another device tested at Condition 3 reached the pre-determined failure criteria for I_D at 133 hours. Two devices that are included in the comparison did not achieve 300 hours. One device tested at Condition 3 reached the pre-determined failure criteria for I_D during stress at 253 hours due to the test station's I_D measurement drift; this device is included in the comparison because other devices (not included in this study) tested at similar conditions showed no significant changes in transfer curves at 200 at 400 hours. The other device was tested at Condition 6 and reached only 263 hours also due to the test station's I_D measurement drift; this device is included because it showed less than 2% change in transfer curves from 263 to 1017 hours in subsequent testing (Christiansen, 2011b).

A summary of the results of the thirteen devices is in Table 4. The percentages are average absolute changes from the pre-stress to the post-stress characterizations since two high-voltage-tested devices were exceptions to the general trends in changes to the selected parameters. One device at Condition 4 and one device at Condition 6 exhibited increases in I_{DSS} and negative threshold voltage (V_T) shifts. The same device at Condition 6 also exhibited an increase I_{Dmax} (see Figure 30). All devices experienced decreases in peak transconductance (g_{mp}) and increases in on resistance (R_{on}). The other general trends were positive threshold voltage shifts and decreases in I_{Dmax} and I_{DSS} (Christiansen, 2011b).

TABLE 4. AVERAGE ABSOLUTE PERCENTAGE CHANGES IN PARAMETERS AFTER 300 HOURS (CHRISTIANSEN, 2011B)

Condition	g_{mp}	V_T	I_{Dmax}	I_{DSS}	R_{on}
1	1.68%	10.8%	8.80%	11.8%	8.06%
2	1.98%	10.9%	10.9%	13.2%	12.2%
3	3.53%	19.4%	15.7%	21.5%	15.4%
4	3.45%	5.95%	4.51%	5.09%	3.78%
6	4.53%	6.05%	5.15%	7.08%	5.21%

Figure 29 shows the transfer and transconductance curves of a typical (meaning, following the general trends in I_{Dmax}, I_{DSS}, V_T, and g_{mp}) high-voltage-tested device. Figure 30 shows the transfer and transconductance curves of one of the two exceptional high-voltage-tested devices. Figures 29 and 30 illustrate the variability in the performance of the tested HEMTs. Although discovering the cause of the negative threshold voltage shift in Figure 30 was not an objective of this study, a possible explanation is a trapping phenomenon near the gate (Rao, 2010; Fang, 2009). The transfer and transconductance curves of Figure 31 are representative of the power-tested devices. Figures 30 and 31 contain the transfer and transconductance curves from testing subsequent to the initial 300 hours; these curves show little change after 300 hours (Christiansen, 2011b).

Comparing the two sets—high voltage and high power—since estimated peak channel temperatures were similar for the respective sets, the devices tested at high power changed more significantly than the devices tested at high voltages and low current, except in g_{mp}. The high-power-tested devices changed more in V_T (13.0%), I_{Dmax} (11.3%), I_{DSS} (14.8%), and R_{on} (11.5%) than the devices tested at high voltage (6.01%, 4.89%, 6.28%, and 4.64%, respectively). Unlike (Meneghesso, 2008), threshold voltage shifts were seen from both ON- and OFF-state conditions. Peak transconductance (g_{mp})

changed more for the devices tested at high voltage (4.10%) than for the devices tested at high power (2.25%). Similar to (Meneghesso, 2008), the decrease in g_{mp} of devices tested in ON-state and OFF-state was less than 5%. The different degradation signatures in the two sets indicate different degradation mechanisms (Christiansen, 2011b).

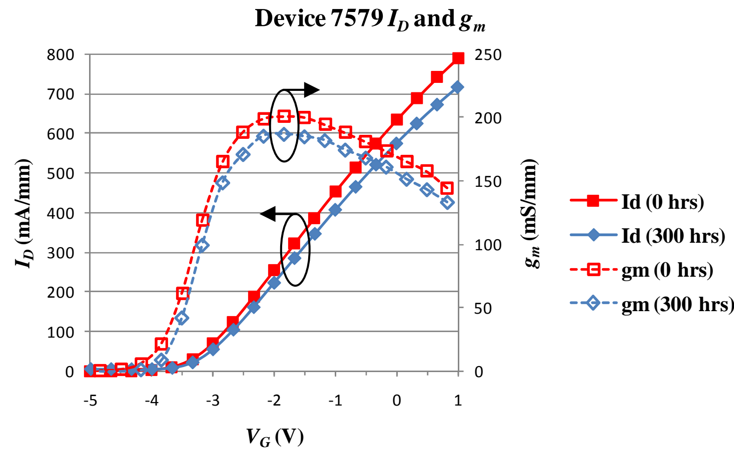

Figure 29. Transfer and transconductance curves at 0 and 300 hours of typical high-voltage-tested device. Device 7579 was tested at Condition 6. (Christiansen, 2011b)

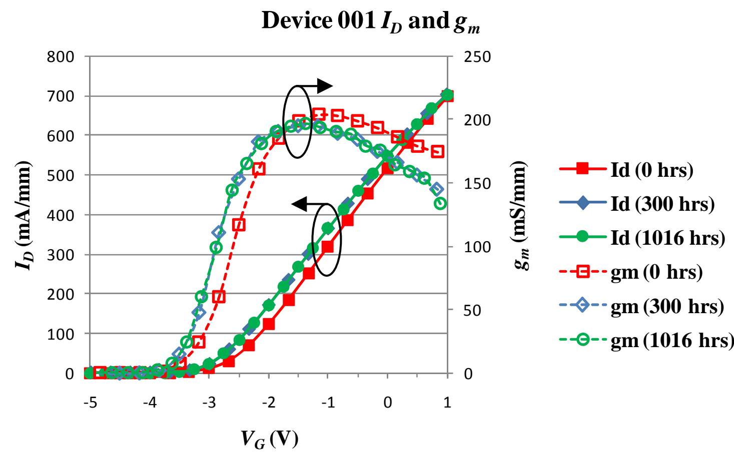

Figure 30. Transfer and transconductance curves at 0, 300, and 1016 hours of exceptional high-voltage-tested device. Device 001 was tested at Condition 6. (Christiansen, 2011b)

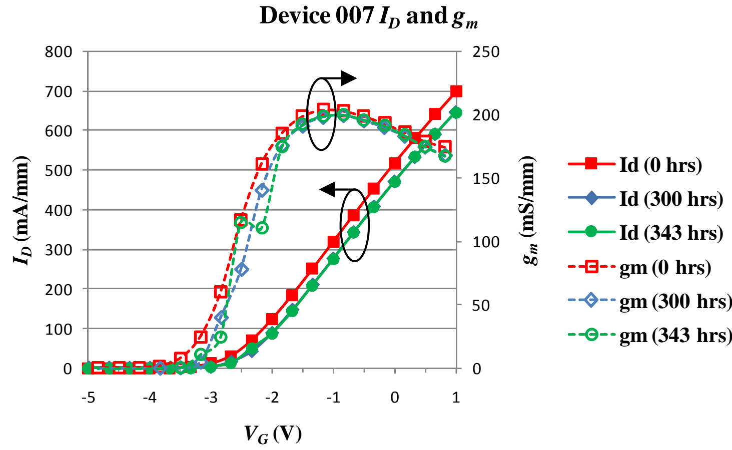

Figure 31. Representative transfer and transconductance curves at 0, 300, and 343 hours of high-power-tested device. Device 007 was tested at Condition 1. (Christiansen, 2011b)

There appears to be a correlation between higher drain biases and greater degradation. Although the estimated peak channel temperatures were similar for Conditions 1, 2, and 3 and separately for Conditions 4 and 6, the average absolute change for the four parameters increased with drain voltage (see Table 4). Despite that apparent drain bias and degradation correlation, significant drain current degradation (> 10%) caused by high biases alone was not seen. Comparing Conditions 4 and 6 with other published OFF-state conditions (del Alamo, 2009; Joh, 2008), the biases of Conditions 4 and 6 were at least 10 V higher. Yet, the significant degradation seen at the lower voltages after minutes of stress in the other studies was not seen at the higher voltages after hours of stress in this study (Christiansen, 2011b).

The changes that occurred in the devices during stress seem to be unrecoverable with rest. The average change in I_{Dmax} between the value measured at 300 hours of stress and the value measured after rest was 0.01% with a maximum of 2.3% and a minimum of −2.37%. For I_{DSS}, the average change was 0.12% with a maximum of 2.26% and a

minimum of −2.29%. Both maximums were measured on one device and both minimums were measured on another. All other percent changes were less than 1% in absolute value. In addition to the changes in I_{Dmax} and I_{DSS} before and after rest, four of six power-tested devices that began the additional testing period required greater gate voltages to attain the target drain current—an indication of permanent degradation (Christiansen, 2011b).

After stress testing, the four select devices were investigated by thermal and photoemission imaging in a Quantum Focus Instruments InfraScope™. In three of the four devices, hot spots corresponded with bright spots. These four devices were delivered to NanoTEM, Inc., for transmission electron microscope (TEM) imaging at the hot and bright spots. Although Device 001 was exceptional (with a negative V_T shift and increases in I_{Dmax} and I_{DSS}), its transfer and transconductance curves and its infrared (IR), photoemission (PE), and TEM images are shown since it had notable IR and PE images, whereas the other imaged high-voltage-tested device did not. Figure 32 contains IR (radiance) and PE images for the high-voltage-tested Device 001 whose transfer and transconductance curves are in Figure 30. (An insufficient number of samples were imaged by IR and PE to determine whether the features of Figure 32 correlate to the negative threshold voltage shift of Figure 30.) The IR (radiance) and PE images in Figure 33 are those of the power-tested Device 007 whose transfer and transconductance curves are in Figure 31 (Christiansen, 2011b).

The TEM images of Devices 001 and 007 are in Figure 34. As in the TEM image of Device 001 (stressed at Condition 6), the other high-voltage-tested part that was imaged by TEM, Device 7632 (stressed at Condition 4 and not shown), does not exhibit a

crack or pit at the drain edge of the gate. This is contrary to the findings reported in (Makaram, 2010). However, in the TEM images of the two high-power-tested devices, Devices 007 and 008 (not shown), that were both stressed at Condition 1, small pits have formed at the drain edge of the gate. Thus, current appears necessary to create the pits in the AlGaN layer (Christiansen, 2011b).

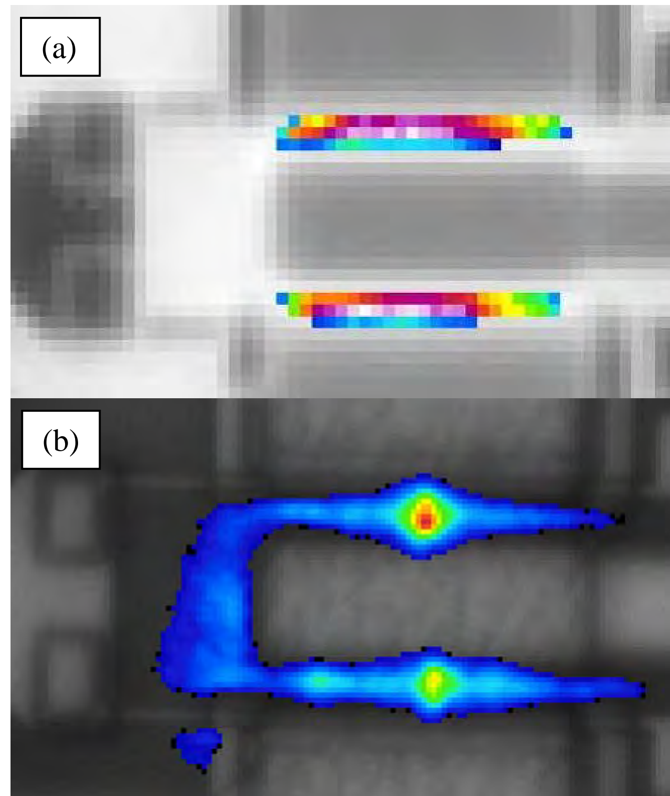

Figure 32. Device 001 (high-voltage-tested) at a baseplate of 85 °C. The upper middle spot was targeted for TEM imaging. (a) IR (radiance) image at 15X magnification. V_{DS} = 40 V, I_D = 10 mA, V_{GS} = −2.42 V, I_G = −5 μA. (b) PE image at 20X magnification. V_{DS} = 100 V, I_D = 11 μA, V_{GS} = −10 V, I_G = −12 μA. (Christiansen, 2011b)

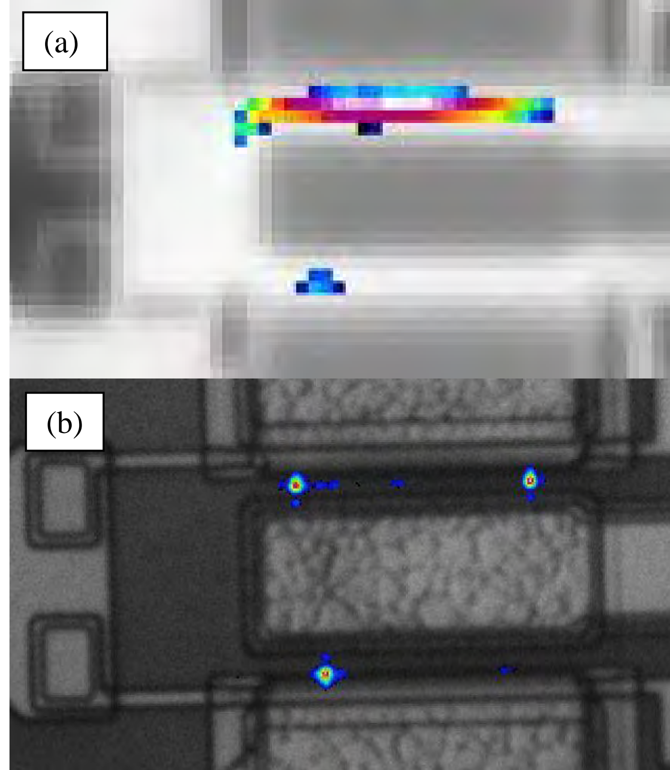

Figure 33. Device 007 (high-power-tested) at a baseplate of 85 °C. The lower left spot was targeted for TEM imaging. (a) IR (radiance) image at 15X magnification. V_{DS} = 28 V, I_D = 10 mA, V_{GS} = −1.69 V, I_G = −3.3 μA. (b) PE image at 50X magnification. V_{DS} = 10 V, I_D = 3.2 mA, V_{GS} = −1 V, I_G in nA range. (Christiansen, 2011b)

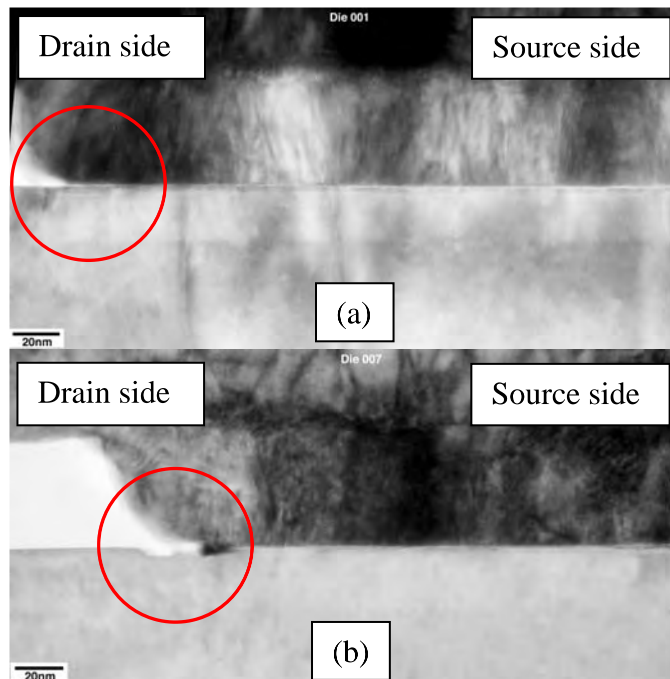

Figure 34. TEM images of (a) Device 001 (high-voltage-tested) and (b) Device 007 (high-power-tested). Notice absence of a pit or crack in Device 001 and the presence of a pit in Device 007. (Christiansen, 2011b)

5.4. Conclusion

The degradation of AlGaN/GaN HEMTs subjected to the conditions of high DC power and high voltage with the gate pinched off was studied. More degradation was generally observed due to the high-power conditions than to the high-voltage conditions. The degradation seen appears to be unrecoverable with rest. Severe drain current degradation due to high drain biases was not observed as has been reported elsewhere. Pits in the AlGaN layer on the drain side of the gate were observed in the high-power-tested devices. However, pits or cracks were not seen in the high-voltage-tested devices, which is contrary to published reports. Thus, electric field alone does not appear to cause significant degradation and current in conjunction with high electric fields seems to be required for pit or crack formation. Possible reasons for the differences between these and others' observations include material quality, fabrication processes, device structure, and bias conditions. The AlGaN/GaN HEMT structure studied herein is robust to high drain biases (Christiansen, 2011b).

VI. Benefits of Considering More Than Temperature Acceleration for GaN HEMT Life Testing

6.1. Introduction

GaN HEMTs offer gains in increased capability and lower costs due to their ability to operate at high power, high frequencies, and high temperatures (Mishra, 2002). Although GaN HEMTs are extremely attractive for many U.S. Department of Defense applications, insertion of this emerging technology is risky because of the little to no long-term use data that ensures the needed lifetimes are possible. Most estimates of GaN HEMT lifetimes have used conventional temperature-accelerated DC operational-life test predictions. The Arrhenius extrapolations reported in the literature (Conway, 2007; Singhal, 2007; Lee, 2008) have extremely long predicted median times to failure. While encouraging, the long estimates and high activation energies may not be indicative of the actual lifetimes at use conditions (Christiansen, 2011a).

The GaN HEMT is a complex electrothermomechanical system that will be used at high channel temperatures, extreme bias, and high RF drive. Is the conventional temperature-accelerated Arrhenius extrapolation sufficient to describe the long-term behavior of the system? Are these extrapolations adequate to compare one generation of GaN HEMTs from a single vendor to another generation, or to compare GaN HEMTs from multiple vendors? (Christiansen, 2011a).

In using the Arrhenius model to estimate lifetimes, several assumptions are made that were investigated. Using the Arrhenius model assumes a dominant failure mechanism exists and is accelerated by temperature. In other words, the high

temperatures cannot “turn on” different and more temperature-sensitive mechanisms or mask unknown lower-temperature mechanisms. Other assumptions of this Arrhenius technique, such as the existence of one unique temperature (i.e., T_1) that describes the device at a specific bias condition, are known issues (Heller, 2008a) but will not be investigated in detail here. (Leach, 2010) questioned whether surface, channel, or hot electron temperature should be used as the critical temperature for analysis. The estimation of the temperature at the site of degradation/failure is critical. Direct measurement of the actual temperature in the area of interest is difficult because the area is sub-micron in size in at least two of three dimensions (Heller, 2008b) and is buried within the structure of the device, usually under a metal stack that cannot be removed without affecting the temperature to be measured. Therefore, current approaches to temperature estimation rely on modeling and indirect measurements. Other important sources of error in thermal estimation are that the degrading region of a power device is not at a single uniform temperature during operation (Heller, 2008a) and that the thermal resistance estimates usually only consider the total power dissipated within the device. These thermal resistance estimates do not account for the way that different bias conditions cause different temperature distributions within a device (Heller, 2008b). Finally, the value of the thermal resistance between the GaN buffer and the substrate appears to vary greatly from vendor to vendor (Kuball, 2010). (Christiansen, 2011a).

In addition to the query of the critical temperature for analysis in (Leach, 2010), the authors explored the validity of the assumption that the failure mechanisms in GaN HEMTs follow the Arrhenius model. Furthermore, (Marcon, 2011) reported that gate degradation in GaN HEMTs depends strongly on electric field but weakly on

temperature. The authors of (Marcon, 2011) concluded that this weak temperature dependence can lead to optimistic lifetime estimates if conventional high-temperature acceleration is used and that voltage-accelerated tests are needed (Christiansen, 2011a).

The Arrhenius model is $r(T) = A \cdot \exp(-E_A/kT)$, where r is the reaction rate, T is temperature in Kelvin (K) at the site of failure in the device (typically attributed to the channel), A is a constant, E_A is the activation energy in electron-volts (eV), and k is Boltzmann's constant (8.617×10^{-5} eV/K) (Trew, 2009). The activation energy parameter in the Arrhenius model is experimentally determined and denotes the sensitivity of the reaction (degradation, in the case of reliability testing) to temperature (Christiansen, 2011a).

An acceleration factor (AF)—in this case, due to the elevated temperatures—relates an Arrhenius reaction rate at one temperature to an Arrhenius reaction rate at a different temperature (Christiansen, 2011a). The acceleration factor is defined mathematically as (Ebeling, 2005:327)

$$AF = \frac{r(T_2)}{r(T_1)} = \frac{Ae^{(-E_A/kT_2)}}{Ae^{(-E_A/kT_1)}} = \exp\left(\frac{E_A}{k}\left(\frac{1}{T_1} - \frac{1}{T_2}\right)\right). \tag{18}$$

With failure time measurements from samples operating at two or more temperatures, the activation energy (E_A) can be found. Once the activation energy has been computed, an acceleration factor is calculated with Equation (18) using a temperature other than the elevated temperatures, such as operating temperature, as T_1 and one of the elevated temperatures as T_2. An estimate for the time to failure at T_1 is then this AF multiplied by the time to failure at T_2 (Christiansen, 2011a).

6.2. Experiment Description

The test procedures that pertain to this chapter are in Sections 4.1, 4.3, and 4.5.

6.3. Results and Discussion

6.3.1. 300-hour Test

The devices showed a very apparent burn-in effect, with a rapid change in electrical characteristics followed by slow and more consistent (part-to-part) change. Due to this apparent burn-in effect, some of the following comparisons will treat the first post-stress characterization for the high-voltage-tested parts as the "initial" values; doing so is sufficient to remove the burn-in effect for all parts. Since the first post-stress characterization for the high-power-tested parts is also the last characterization for these devices, the pre-stress characterization will be treated as the initial values for the high-power-tested devices (Christiansen, 2011a).

Two high-voltage-tested parts did not reach 300 hours due to infant mortality and instrumentation issues; this data is excluded from the data set and discussion. In contrast, two high-power-tested devices were depowered due to instrumentation issues before 300 hours but after sufficient time that the data collected from these parts are useful and so will be included (Christiansen, 2011a).

To show that the devices were nominally the same initially, the initial variation of the parts tested for 300 hours is shown in Table 5. The table lists the averages and standard deviations of peak transconductance (g_{mp}),threshold voltage (V_T), I_{Dmax}, and I_{DSS} for each condition, both sets of conditions, and for all devices in the 300-hour test. The 0-hour characterizations for the high-voltage-tested parts are used for the comparison.

The devices were within family; the standard deviations are small compared to the averages (Christiansen, 2011a).

TABLE 5. INITIAL VARIATION OF PARTS TESTED FOR 300 HOURS (CHRISTIANSEN, 2011A)

Conditions	Number of devices	g_{mp} (mS/mm) Avg	g_{mp} (mS/mm) Stdev	V_T (V) Avg	V_T (V) Stdev	I_{Dmax} (mA/mm) Avg	I_{Dmax} (mA/mm) Stdev	I_{DSS} (mA/mm) Avg	I_{DSS} (mA/mm) Stdev
1	3	200.0	1.4	-2.89	0.17	742	30	573	33
2	3	202.0	1.4	-2.74	0.19	726	31	551	35
3	3	201.6	0.9	-2.80	0.19	733	30	561	34
1, 2, and 3	9	201.2	1.4	-2.81	0.17	734	27	562	31
4	2	202.0	0.08	-3.06	0.15	771	16	608	25
6	2	200.3	1.7	-2.92	0.49	743	65	576	81
4 and 6	4	201.2	1.4	-2.99	0.31	757	42	592	53
1, 2, 3, 4, 6	13	201.2	1.4	-2.86	0.22	741	32	571	39

Table 6 contains the changes at the end of the test period for each device. Most changes are listed as percentages, but the V_T change is absolute. The initial values for the high-voltage-tested parts are from the 100-hour characterization to remove the burn-in effect, as explained above. All devices trended as indicated by the signs in Table 6. All devices exhibited a positive threshold voltage shift. The high-power stress caused more change than the high-voltage stress. Note that two devices at Condition 3 did not reach 300 hours of stress as did the other devices (Christiansen, 2011a).

Based on averages of the parameter data presented in Table 6, there appears to be a correlation between higher drain biases (when power dissipation and channel temperature are held constant) and greater degradation. Although the estimated channel temperatures were similar for Conditions 1, 2, and 3 and separately for Conditions 4 and 6, the average change for the four parameters generally increased in magnitude with drain voltage. For high-power Condition 3, the degradation was more than for the other two

high-power conditions even though two parts at Condition 3 did not reach the full 300 hours of stress (Christiansen, 2011a).

TABLE 6. PARAMETER CHANGES BY DEVICE AND CONDITION IN 300-HOUR TEST (CHRISTIANSEN, 2011A)

Condition	Device	g_{mp}	ΔV_T (mV)	I_{Dmax}	I_{DSS}
1	55	-2.37%	253	-7.9%	-10.1%
	56	-1.20%	310	-8.6%	-11.9%
	57	-2.57%	365	-10.0%	-13.6%
2	58	-2.29%	316	-11.6%	-14.2%
	59	-3.50%	312	-12.1%	-14.1%
	60	-1.64%	263	-9.0%	-11.2%
3	28	-5.37%	603	-18.3%	-24.6%
	29	-2.03%	356	-10.7%	-14.9%
	30	-2.72%	514	-13.0%	-18.3%
4	31	0.04%	49.6	-1.3%	-1.7%
	33	-0.14%	31.7	-0.7%	-1.4%
6	25	0.01%	71.4	-1.7%	-2.4%
	27	-1.02%	12.3	-1.2%	-1.2%

Using the average of the activation energies presented in (Conway, 2007), (Singhal, 2007), and (Lee, 2008)—2.09 eV—the acceleration factors from Equation (18) between the test conditions are listed in Table 7. The two lines for Condition 6 account for the T_{ch} estimate variation shown in Table 3 (Christiansen, 2011a).

TABLE 7. ARRHENIUS ACCELERATION FACTORS BETWEEN TEST CONDITIONS (CHRISTIANSEN, 2011A)

Condition	T_{ch} (°C) estimate		Condition	T_{ch} (°C) estimate	Acceleration Factor
1	394	to	2	392	1.12
1	394	to	3	391	1.18
2	392	to	3	391	1.06
6	248	to	4	245	1.31
6	246	to	4	245	1.09
7	405	to	1	394	1.80

The acceleration factors suggest that the devices tested at Condition 1 should have, based on the *AF* alone, degraded slightly more than the Condition-2 devices, and

Condition 2 slightly more than Condition 3. However, one can see in Table 6 that Condition 3 degraded the fastest as would be expected for a positive degradation correlation with drain voltage. To be fair, Conditions 2 and 3 are more comparable to each other than to Condition 1 since Conditions 2 and 3 experienced the same power dissipation; error in the estimate of the thermal resistance of the sub-micron sized channel region will affect Conditions 2 and 3 in about the same way and still leave them comparable to each other. Still, one can observe that the degradation caused by the high-power electrical conditions overshadows the degradation that may be caused by temperature for Condition 3 (Christiansen, 2011a).

On the other hand, high-voltage Condition 6 may have had a channel temperature between 246 and 248 °C versus 245 °C for the baseplate temperature and the other high-voltage conditions. This implies $1.09 < AF < 1.31$ for Condition 6 versus Condition 4. As such, for the changes shown in Table 6 for Conditions 4 and 6, agreement with the expectations of the Arrhenius model is not ruled out (Christiansen, 2011a).

Figure 35 shows the pre- and post-stress values of I_{Dmax} and I_{DSS}, respectively, normalized to the pre-stress values for the high-power conditions. The plots of the Condition-1 and -2 drain currents overlap, indicating that these conditions had similar responses to their stresses, despite different drain voltage and power dissipation levels. The plots of the Condition-3 drain currents are distinctly separate from those of Conditions 1 and 2, despite the similar T_{ch} estimates for all three conditions and the same power dissipation as Condition 2. The slopes for each device are listed in Table 8. Condition 3 shows a marked difference to Conditions 1 and 2. In fact, ±15% ranges around Condition-1 and -2 slope averages overlap each other, while the ±15% range

around the Condition-3 average does not overlap the ±15% ranges of either Condition-1 or -2 averages. Fifteen percent was chosen since the part-to-part variation (the standard deviation divided by the average) of I_{Dmax} and I_{DSS} in Table 5 is less than 10% and the variation in initial measured I_D in Table 10 (shown later) is less than 5% (Christiansen, 2011a).

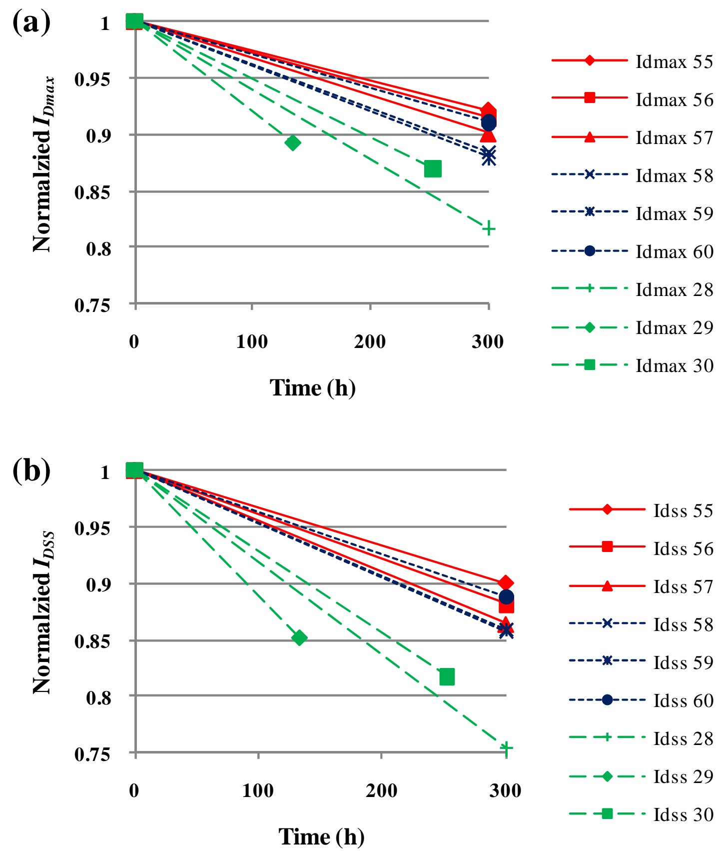

Figure 35. Normalized pre- and post-stress values of (a) I_{Dmax} and (b) I_{DSS} for high-power conditions. The top three lines (red) of the legend are Condition 1, the middle three (blue) Condition 2, and the bottom three (green) Condition 3. (Christiansen, 2011a)

TABLE 8. SLOPES OF NORMALIZED I_{DMAX} AND I_{DSS} LINES FOR HIGH-POWER CONDITIONS (CHRISTIANSEN, 2011A)

Condition	Device	I_{Dmax} slope (normalized fraction/hr)	I_{DSS} slope (normalized fraction/hr)
1	55	-2.6E-04	-3.4E-04
	56	-2.9E-04	-4.0E-04
	57	-3.3E-04	-4.5E-04
2	58	-3.9E-04	-4.7E-04
	59	-4.0E-04	-4.7E-04
	60	-3.0E-04	-3.7E-04
3	28	-6.1E-04	-8.2E-04
	29	-8.0E-04	-1.1E-03
	30	-5.2E-04	-7.2E-04

A similar analysis of the slopes of the I_{Dmax} and I_{DSS} lines can be performed for the high-voltage conditions. Figure 36 shows the pre- and post-stress values of I_{Dmax} and I_{DSS}, respectively, normalized to the 100-hour values. The plots of I_{Dmax} overlap, and the Condition-6 I_{DSS} lines encompass the Condition-4 I_{DSS} lines, indicating that both conditions had similar responses to their stresses, despite different drain voltages. The slopes of linear fits for each device are listed in Table 9. Ranges of ±15% around the Condition-4 and -6 I_{DSS} slope averages overlap, but ±15% ranges around the I_{Dmax} slope averages do not. Although the slope averages increase with drain voltage and the ±15% I_{Dmax} slope average ranges do not overlap, the overlapping I_{Dmax} and I_{DSS} plots indicate similar behavior for Conditions 4 and 6 (Christiansen, 2011a).

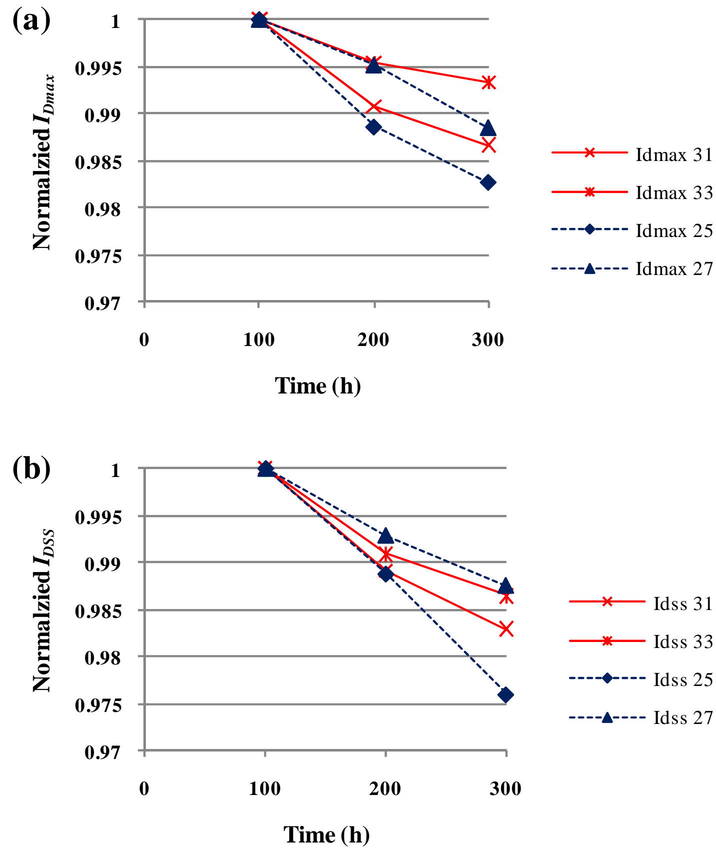

Figure 36. Normalized pre- and post-stress values of (a) I_{Dmax} and (b) I_{DSS} for high-voltage conditions. The top two lines (red) of the legend are Condition 4 and the bottom two (blue) Condition 6. (Christiansen, 2011a)

TABLE 9. SLOPES OF NORMALIZED I_{DMAX} AND I_{DSS} LINES FOR HIGH-VOLTAGE CONDITIONS (CHRISTIANSEN, 2011A)

Condition	Device	I_{Dmax} slope (normalized fraction/hr)	I_{DSS} slope (normalized fraction/hr)
4	31	-6.7E-05	-8.5E-05
	33	-3.3E-05	-6.8E-05
6	25	-8.7E-05	-1.2E-04
	27	-5.8E-05	-6.2E-05

The following is an analysis of the sensitivity of Conditions 1, 2, and 3 to various sources of variation. To examine the effect of the test station on device degradation measurements, first the initial parameter measurements were recorded. Table 10 contains

the values of parameters of interest at time 0 of the stress period as measured by the test station while at the stress base-plate temperature. As can be seen, there is significant variation from the channel temperature estimates of Table 3 for the high-power conditions. There are multiple sources of measurement variation within the test station: ±2 °C for base-plate temperature, ±50 mV for drain voltage, and ±1.5 mA (equivalently 15 mA/mm) for drain current. In addition to the measurement variation, the settability accuracy for drain current is 1.5 mA and for base-plate temperature is ±2 °C. The drain current measurements (and calculated power dissipations) are the largest sources of variation in the channel temperature estimates in Table 10 for the high-power conditions (Christiansen, 2011a).

TABLE 10. INITIAL MEASURED PARAMETER VALUES IN 300-HOUR TEST (CHRISTIANSEN, 2011A)

Condition	Device	Measured T_{bp} (°C)	Measured V_{DS} (V)	Measured I_D (mA/mm)	Measured V_{GS} (V)	Calculated P_{diss} (W/mm)	T_{ch} (°C) estimate
1	55	245.2	20.011	568.9	2.011	11.4	399
	56	245.2	19.994	547.9	2.004	11.0	393
	57	245.2	20.000	532.8	2.017	10.7	389
2	58	133.0	40.012	552.8	2.016	22.1	393
	59	133.2	40.010	576.8	1.806	23.1	406
	60	133.2	40.012	571.9	1.708	22.9	404
3	28	130.3	60.005	380.8	0.3028	22.8	403
	29	130.3	60.015	349.4	0.4022	21.0	378
	30	130.2	60.018	366.7	0.25	22.0	391
				Approx. I_D (mA/mm)			
4	31	245.0	60.005	< 0.026	-10.002	< 0.00156	245
	33	245.1	59.996	< 0.026	-9.992	< 0.00156	245
6	25	245.1	99.995	< 2.0	-9.996	< 0.19999	246-248
	27	245.1	100.005	< 2.0	-9.999	< 0.20001	246-248

Assuming the initial measured values had persisted throughout the test, a correlation between the channel temperature estimates of Table 10 and the degradation for each device (Table 6) for the high-power conditions can be investigated. For

comparison purposes, the high-power-tested device values are compared to nominal values of T_{ch} = 395 °C (the average of the T_{ch} estimates in Table 10), −2% g_{mp}, a ΔV_T of +300 mV, −10% I_{Dmax}, and −10% I_{DSS}. With the nominal T_{ch} value as T_1 in Equation (18), acceleration factors are calculated to compare each high-power-tested device to the nominal values. Figure 37 shows this comparison as a plot of the natural logarithms of the acceleration factors and degradation ratios (meaning ratio of observed degradation to the nominal value). If a correlation existed between the acceleration factors and observed degradation, the points for the respective parameters would form lines similar to the reference Arrhenius slope line (but with slope proportional to the activation energy). As is evident, there is <u>no correlation</u> between the acceleration factors and the observed degradation, which means the observed degradation was not caused by the variation in initial measured parameter values (Christiansen, 2011a).

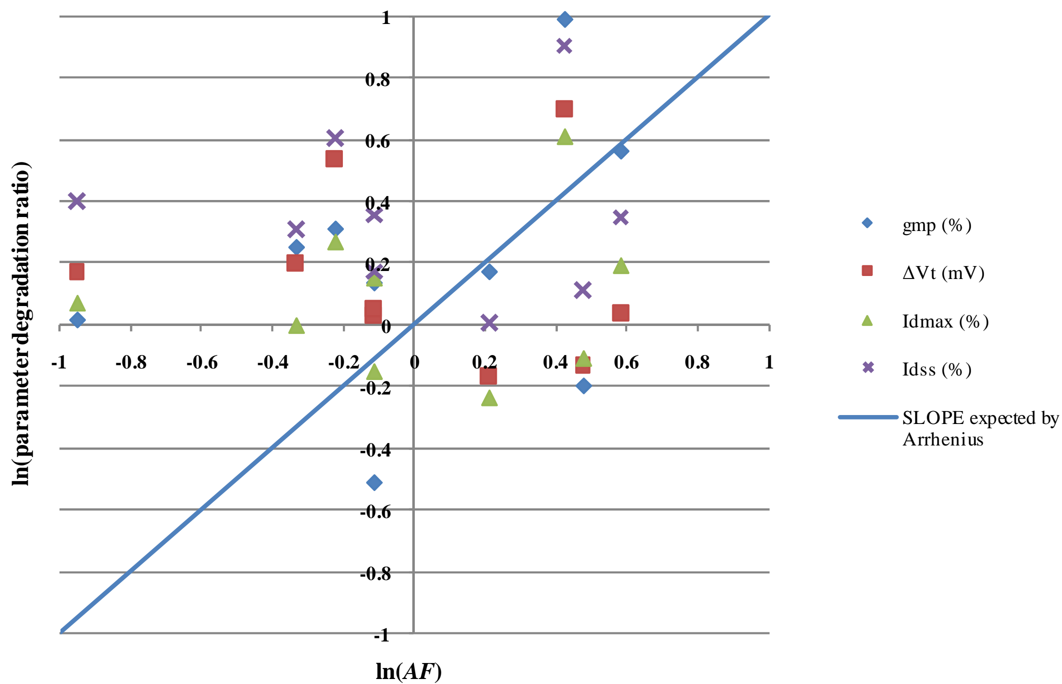

Figure 37. Comparing acceleration factors based on initial T_{ch} estimates and observed degradation. The reference slope line assumes an activation energy of 2.09 eV. (Christiansen, 2011a)

The following analysis investigates the initial T_{ch} estimates of Table 10 and the measurement error from the Agilent power supplies during initial and final characterizations. Based on the Agilent specifications (Agilent, 2004), the drain current measurement error depends on the measured current value and the output voltage, which also has a measurement error dependent on the measured output voltage. The drain voltage measured 10 V and the error was ±7 mV. For the high-power-tested devices, the maximum drain current error for the initial characterizations was 0.108 mA, and for the final characterizations was 0.102 mA. The maximum drain current error for the initial and final characterizations of the high-voltage-tested devices was 0.107 mA. Degradation rates (the slopes from Tables 8 and 9) are calculated from the initial and final I_{Dmax} characterizations and times. Finally, the magnitudes of the degradation rates are plotted against the temperatures ($1/kT$) in Figure 38. The center points are the average T_{ch} estimates and the average rates in a condition. The endpoints are the minimum and maximum rates along the line of average temperature and the minimum and maximum T_{ch} estimates along the line of average rate in a condition. Conditions 4 and 6 have greater rate ranges since there was little difference between the initial and final drain current values, which resulted in the same maximum error of 0.107 mA. Also included in Figure 38 are reference lines that pass through the center point of Condition 1 and assume activation energies of 2.09 (used previously in this paper), 1.6, and 2.47 eV (the range of values surveyed in (Leach, 2010) that resulted from DC testing) (Christiansen, 2011a).

As can be seen from Figure 38, Conditions 1 and 2, and separately 4 and 6, have overlapping ranges and are similar. Notice that the reference lines through Condition 1

do not approach Conditions 4 and 6. Conditions 4 and 6 appear related to each other by the Arrhenius model, yet, they are not related to the high-power conditions by the Arrhenius model. Since Conditions 1, 2, and 3 are clustered closely in Figure 38, the portion of the graph containing these conditions is magnified in Figure 39 (Christiansen, 2011a).

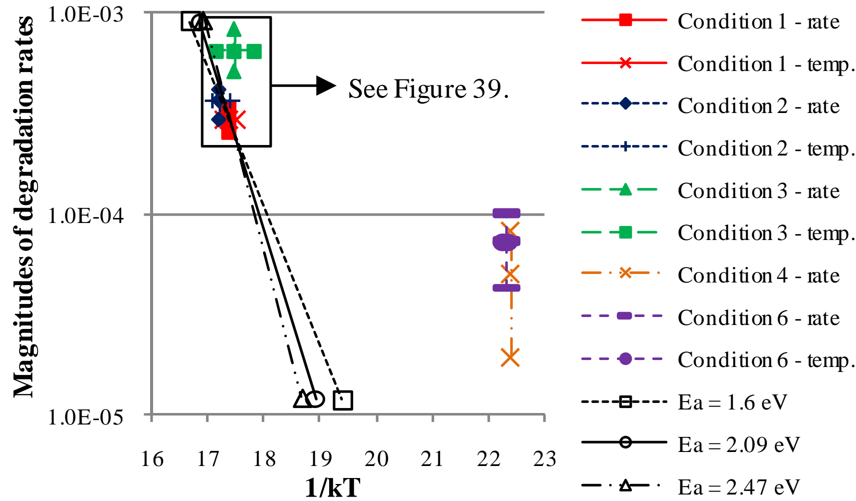

Figure 38. Comparing Agilent power supply measurement error and initial T_{ch} estimates in 300-hour test. (Christiansen, 2011a)

In Figure 39, the error bars are replaced with error boxes, and individual device data are plotted. As seen in Figure 39, the ranges of Condition 3 do not overlap those of Conditions 1 and 2, which suggests that Condition 3's behavior may not have been caused by temperature, even with measurement error and the variation of initial biases. However, the reference lines could be shifted to the right such that the lines intersect all three boxes, suggesting an Arrhenius relationship between the conditions. The inconsistency, though, is that Condition 3's box is up and to the right of Condition 1, when it should be down and to the right for its lower average initial T_{ch} estimate (see Table 10) (Christiansen, 2011a).

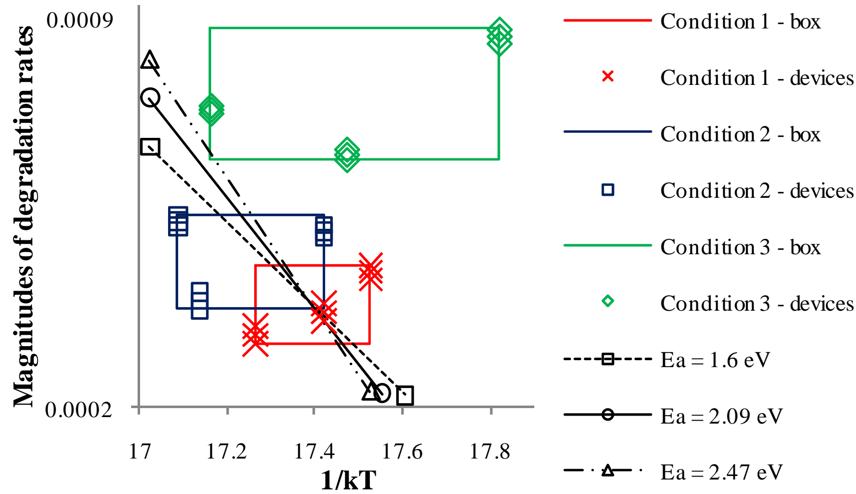

Figure 39. Magnified portion of Figure 38 but on different scales. (Christiansen, 2011a)

Finally, an analysis of the sensitivity of Conditions 1, 2, and 3 to thermal resistance (R_{th}) changes in the thermal model is investigated. The accuracy of any thermal resistance estimate for these devices is subject to significant error (Heller, 2008a; Heller, 2008b; Kim, 2005) and it is an under-appreciated fact that the sensitivity of conclusions drawn in an accelerated life test to the thermal resistance assumed should be considered (Heller, 2008b). The analysis computes new T_{ch} estimates with $[(T_{ch} - T_{bp}) \times (\pm 20\%)] + T_{bp}$ for a ±20% change in thermal resistance. Then, acceleration factors between test conditions are calculated, as in Table 7, with the new T_{ch} estimates. Table 11 lists the new T_{ch} estimates and acceleration factors (*AF*), as well as the original T_{ch} estimates and acceleration factors from Table 7. The new *AF*s generally indicate the same behavior as the original *AF*s for Conditions 2 vs. 3: Conditions 2 and 3 are about the same with, if anything, Condition 2 degrading slightly more. Depending on the error, though, Condition 1 may degrade much more or less than Conditions 2 and 3 based on

the *AF*s. Recall that the observed behavior was not what was indicated by the Arrhenius model—Condition 2 and 3 were not similar (Christiansen, 2011a).

TABLE 11. SENSITIVITY ANALYSIS OF THERMAL MODEL R_{TH} FOR CONDITIONS 1, 2, AND 3 (CHRISTIANSEN, 2011A)

Condition	**T_{ch} (°C) estimate (−20% R_{th})**	**T_{ch} (°C) estimate (Model R_{th})**	**T_{ch} (°C) estimate (+20% R_{th})**	**Comparison**	**AF (−20% R_{th})**	**AF (Model R_{th})**	**AF (+20% R_{th})**
1	364	394	424	1 to 2	4.44	1.12	0.379
2	340	392	444	1 to 3	4.73	1.18	0.397
3	339	391	443	2 to 3	1.07	1.06	1.05

Based on the foregoing data, the evidence indicates that temperature was not the cause of degradation in the high-power-tested devices. Especially, there are significant differences in the responses of Conditions 2 and 3. From the sensitivity analysis, the variation of the test station bias setting and measurement in initial measured parameter values, the characterization measurement error, and the thermal resistance error in the thermal model are not sufficient to discount the differences in degradation or the conclusion that temperature did not cause the degradation. In contrast, for the high-voltage-tested parts, there is sufficient similarity and overlap in degradation values and plots to indicate that the observed changes may have been caused by temperature. Therefore, the Arrhenius model may be valid for some bias conditions, but not for others (Christiansen, 2011a). Although the temperature-accelerated Arrhenius model may not be valid for all conditions, the average degradation rates of all the test conditions exhibit a positive correlation to drain voltage. Additionally, other acceleration models may be useful in testing GaN HEMTs (two possible models are cited in Section 6.3.3).

6.3.2. 600-hour High-Power Test

Similar to the increasing transfer curve at the first post-stress characterization exhibited by the high-voltage-tested parts above, the devices of the 600-hour test showed a more rapid decrease in the first hour of stress than in subsequent hours. Consequently, the 1-hour characterizations at 245 °C are considered to be the "initial" data points for the hourly characterizations. The 0-hour, 70-°C characterizations are the "initial" data points for the pre- and post-stress characterizations (Christiansen, 2011a).

One of the three test channels used in this test became unusable after the first 200 hours. Hence, only 200 hours of Device 27-026 will be shown (Christiansen, 2011a).

The initial variation of the parts tested for 600 hours is shown in Table 12. The 0-hour, 70-°C characterizations are used for the comparison. The devices are from the same family of devices used for the 300-hour test (compare to Table 5) (Christiansen, 2011a).

TABLE 12. INITIAL VARIATION OF PARTS TESTED FOR 600 HOURS (CHRISTIANSEN, 2011A)

	Number	g_{mp} (mS/mm)		V_T (V)		I_{Dmax} (mA/mm)		I_{DSS} (mA/mm)	
Condition	**of devices**	**Avg**	**Stdev**	**Avg**	**Stdev**	**Avg**	**Stdev**	**Avg**	**Stdev**
7	3	202.1	3.3	-2.96	0.06	760	15	591	17

Table 13 contains the changes at the end of 200 and 600 hours for each device. All devices trended as indicated by the signs in the table (Christiansen, 2011a).

TABLE 13. PARAMETER CHANGES BY DEVICE AND STRESS TIME Y IN 600-HOUR TEST (CHRISTIANSEN, 2011A)

Y (hours)	Device	g_{mp}	ΔV_T (mV)	I_{Dmax}	I_{DSS}
200	25-024	-4.1%	311	-10.4%	-13.5%
	26-025	-3.2%	248	-8.1%	-10.6%
	27-026	-2.4%	243	-7.1%	-9.7%
600	25-024	-3.2%	246	-8.3%	-10.9%
	26-025	-2.4%	172	-5.8%	-7.3%

For illustration purposes and comparison to the 70-°C measurements to be shown later, Figure 40 shows the normalized values (to the 1-hour, 245-°C measurements) of I_{Dmax} over time for the devices in the 600-hour test. Interestingly, after initially degrading, the devices began to recover during stress. This recovery is evident in decreased magnitudes of averages, from 200 to 600 hours, of the parameter data in Table 13 (Christiansen, 2011a).

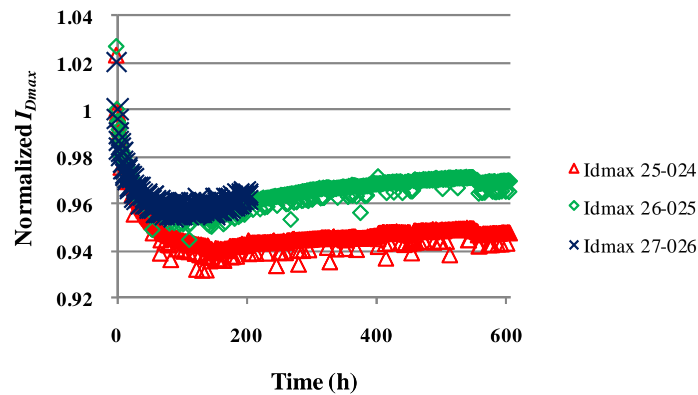

Figure 40. Normalized values (to the 1-hour, 245-°C measurements) of I_{Dmax} over time during the 600-hour test. (Christiansen, 2011a)

As with Conditions 2 and 3 of the 300-hour test, Condition 1 of the 300-hour test and Condition 7 of the 600-hour test are comparable since they experienced similar power dissipation. However, the T_{ch} estimate for Condition 7 is 405 °C, and the acceleration factor between Conditions 7 and 1 is 1.80, indicating that Condition 7 should be different than the other conditions. Therefore, Condition 7 was expected to degrade more than Condition 1. Figure 41 contains plots of the 70-°C characterization data for the 300-hour and 600-hour tests. As in Figure 40, the drain current recovers in the 600-hour test devices. Interpolating the 600-hour test data at 300 hours reveals that

Condition 7, in fact, did not degrade more than Condition 1, contrary to Arrhenius expectations (Christiansen, 2011a).

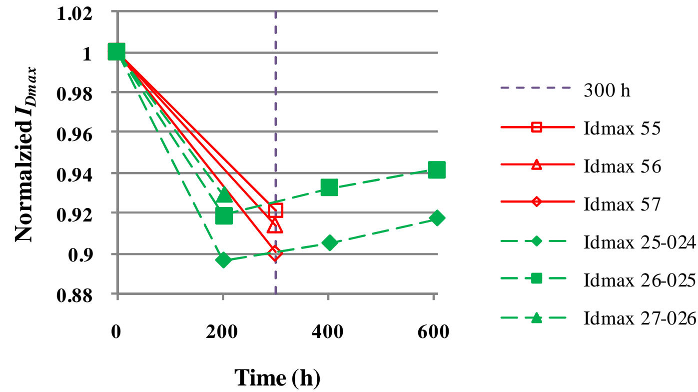

Figure 41. Normalized values (to the 0-hour, 70-°C measurements) of I_{Dmax} over time during the 300-hour, Condition-1 (lines 2-4 in the legend, in red) and 600-hour, Condition-7 (lines 5-7 in the legend, in green) tests. (Christiansen, 2011a)

The following is a brief analysis of the sensitivity of Conditions 1 and 7 to the initial measured parameter values. To begin, the initial measured parameter values of Condition 7 are listed. Table 14 contains the values of parameters of interest at time 0 of the stress period as measured by the test station while at the stress base-plate temperature. As can be seen, there is a difference from the channel temperature estimates of Table 3 for Condition 7. The difference is due to the lower-than-expected drain current values (Christiansen, 2011a).

TABLE 14. INITIAL MEASURED PARAMETER VALUES IN 600-HOUR TEST (CHRISTIANSEN, 2011A)

Condition	Device	Measured T_{bp} (°C)	Measured V_{DS} (V)	Measured I_D (mA/mm)	Measured V_{GS} (V)	Calculated P_{diss} (W/mm)	T_{ch} (°C) estimate
7	25-024	245.2	17.494	655.3	3.033	11.5	397
	26-025	245.3	17.509	658.9	3.034	11.5	399
	27-026	245.3	17.507	658.5	3.028	11.5	398

Now, the initial T_{ch} estimates for Conditions 1 and 7 in Tables 10 and 14 and the measurement error from the Agilent power supplies during initial and 300-hour characterizations are analyzed in direct analogy to the analysis of Figures 38 and 39. Linear interpolations of the 200-hour and 400-hour characterizations of Devices 25-024 and 26-025 are used to obtain 300-hour characterization estimates for these devices. A 300-hour characterization estimate is extrapolated for Device 27-026 from its 200-hour characterization using the average of the slopes calculated for the linear interpolations of Devices 25-024 and 26-025. Based on the Agilent specifications (Agilent, 2004), the error for the measured drain voltage of 10 V is ±7 mV. For Condition 1, the maximum drain current error for the initial characterizations is 0.108 mA, and for the 300-hour characterizations is 0.102 mA. For Condition 7, the maximum drain current error for the initial characterizations is 0.109 mA, and for the 300-hour characterization estimates is 0.103 mA. Degradation rates are calculated from the initial and 300-hour I_{Dmax} characterizations and times. Finally, the magnitudes of the degradation rates are plotted against the temperatures ($1/kT$) in Figure 42. The center points are the average T_{ch} estimates and the average rates in a condition. The endpoints are the minimum and maximum rates along the line of average temperature and the minimum and maximum T_{ch} estimates along the line of average rate in a condition (Christiansen, 2011a).

As can be seen in Figure 42, Conditions 1 and 7 have overlapping ranges and the reference lines could be moved left to intersect both boxes, indicating similar behavior. The initial T_{ch} estimates for Condition 7 are generally higher than those of Condition 1, yet the degradation rates are generally similar. The average initial T_{ch} estimate for Condition 7 is 398 °C, and the average initial T_{ch} estimate for Condition 1 is 394 °C. The

Arrhenius acceleration factor between these average temperatures is 1.24. The inconsistency here with the Arrhenius model is that the Condition 7 box is down and to the left of the Condition 1 box, when it should be up and to the left for its higher average initial T_{ch} estimate (Christiansen, 2011a).

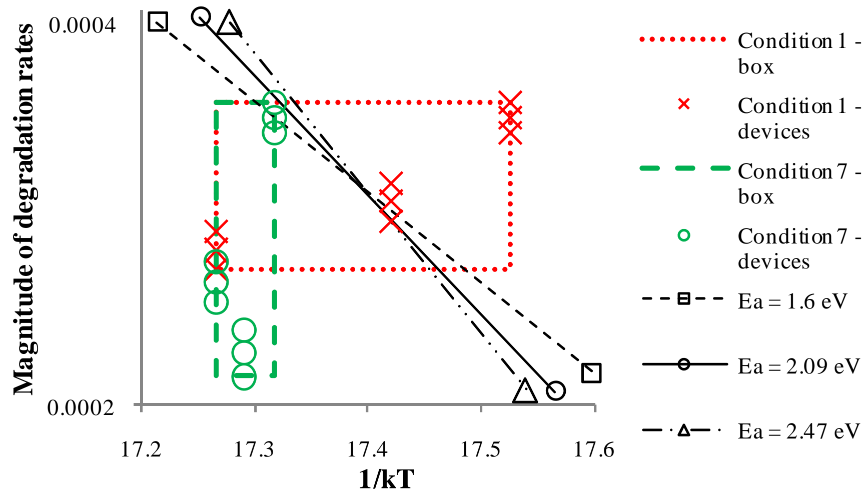

Figure 42. Comparing Agilent power supply measurement error and initial T_{ch} estimates in Conditions 1 and 7. (Christiansen, 2011a)

6.3.3. Discussion

In the data presented, there are two instances where the Arrhenius model seems reasonable. These instances occur when GaN HEMTs were tested at similar channel temperature estimates. These instances are between Conditions 1 and 2 and between Conditions 4 and 6 (although the average degradation for these conditions has a positive correlation to drain voltage) (Christiansen, 2011a).

Conversely, there are two instances of inconsistency with the Arrhenius model. Both instances occur when the test conditions are similar. One instance—between Conditions 2 and 3—occurs when similar degradation was expected, but the two conditions exhibited different degradation. The other instance—between Conditions 1

and 7—occurs when different behavior was expected, but similar behavior was observed. In addition, the error boxes of Conditions 3 and 7 are not where they are expected to be based on the Arrhenius relation. See Figures 39 and 42 (Christiansen, 2011a).

Another instance of inconsistency is between the high-voltage conditions and the high-power conditions. Reference lines assuming activation energies do not intersect the error regions of the two different sets of conditions. See Figure 38. This inconsistency indicates that GaN HEMT degradation depends on the test conditions (Christiansen, 2011a).

The average points of all the test conditions follow a positive correlation to drain bias. For the high-voltage conditions, the average degradation rate is higher for Condition 6 (V_{DS} = 100 V) than for Condition 4 (V_{DS} = 60 V). For the high-power conditions, the progression from lowest to highest average degradation rate is Condition 7 (V_{DS} = 17.5 V), Condition 1 (V_{DS} = 20 V), Condition 2 (V_{DS} = 40 V), and Condition 3 (V_{DS} = 60 V). See Figures 38, 39, and 42 (Christiansen, 2011a).

Reliability evaluation of AlGaN/GaN HEMTs will benefit from considering other accelerants besides temperature. Based on the observations from this study, drain bias showed a positive correlation to degradation in a high-power test condition. Voltage acceleration would be a primary additional accelerant to pursue. To adequately consider other accelerants, the design of experiments methodology (Montgomery, 2009) could be applied to create the multi-variable tests. Then, multi-stress models could be used in place of the single-stress Arrhenius model to analyze the data. Possible multi-stress models to use include the Generalized Eyring model (Ebeling, 2005:328), General Log-

Linear relationship, and the Proportional Hazards model (ReliaSoft, 2011). Each model allows more than two stressors to be applied as accelerants (Christiansen, 2011a).

Reliability assessments that employ more and different accelerants than temperature will result in more accurate lifetime estimates of AlGaN/GaN HEMTs since they will account for the failure mechanisms of the electrothermomechanical system that are not primarily thermally activated. For example, if a temperature-accelerated life test was conducted near Conditions 1 and 2, but device operation occurred near Condition 3, the Arrhenius extrapolations would be optimistic (Christiansen, 2011a).

Based on this study and that in (Marcon, 2011), the need for different accelerants in GaN reliability testing spans at least two fabricators. Marcon, Kauerauf, and Decoutere probably used devices fabricated by imec, a European research institution in Belgium, and not by the vendor of the devices used in this study. The devices used in this study were not fabricated by imec (Christiansen, 2011a).

6.4. Conclusion

Studied in this report was the degradation of AlGaN/GaN HEMTs subjected to the conditions of high DC power and high voltage with the gate pinched off, conditions which may occur during device operation. A discovery was made that degradation in the devices stressed by DC does not fit to the temperature-accelerated model. The experimental data show that single-DC-stress, temperature-accelerated life testing does not account for the critical degradation in a GaN HEMT. Further studies are required to understand the stress effects of RF operation, to assess whether or not DC-only accelerated-life tests can identify the dominant end-of-life degradation mechanism, and to

assess whether or not temperature-accelerated life tests provide the appropriate end-of-life estimation (Christiansen, 2011a).

VII. A Very Robust AlGaN/GaN HEMT Technology to High Forward Gate Bias and Current

7.1. Introduction

There are recent reports that high negative gate bias causes the gates of GaN HEMTs to degrade. The signature of this degradation mechanism is an increase in gate leakage current (Joh, 2008; del Alamo, 2009; Marcon, 2010). (Christiansen, 2011c)

Other reports state that forward gate current limits the survival times of GaN HEMTs, especially during RF operation (Joshin, 2006; Bettidi, 2009). GaN HEMTs in (Xu, 2004) reached about 400 mA/mm forward gate current before burning out (Christiansen, 2011c).

(Joh, 2007) specifically considered the effects of high positive gate bias (up to +6 V) on GaN HEMTs with integrated field plates. By stepping V_G from +0.5 V to +6 V in 0.5-V steps for 30 minutes per step, a reduction in V_{Gon} (V_G at a normalized gate current of 1 mA/mm) after 360 minutes was observed, accompanied by about a 10^4 increase in gate leakage current and strong Ohmic gate behavior. The authors of (Joh, 2007) concluded that the large forward gate current and high temperature degraded the Schottky contact. Despite the reduction in V_{Gon}, (Joh, 2007) showed there was little degradation in drain and source resistances and maximum drain current (Christiansen, 2011c).

Shown are the results of stressing GaN HEMTs at extremely high gate current densities but for longer times and with more positive results. Despite the extremely high biases, the tested devices survived well past the current density in (Xu, 2004) and were

less conductive and with less V_{Gon} degradation than those in (Joh, 2007). Remarkably, it is noted that the tested devices survived the stresses with very little degradation in device drain current and voltage capability (Christiansen, 2011c).

7.2. Experiment Description

The test procedures that pertain to this chapter are in Sections 4.1 and 4.6.

7.3. Results

Results from the third device are described below. In summary, the device survived for >17.5 hours the stress of biasing at $V_G = +6.0$ V and $I_G \geq 1820$ mA/mm forward gate current (see Figure 44), which is a current density of >360 kA/cm^2 and >10.9 W/mm power *through the gate*. I_{Dmax} (defined as drain current at $V_G = 1$ V and $V_D = 10$ V) degraded slightly and saturated over stress duration (see Figure 43(a)). After 210 minutes of stress, degradation in the ideality of I_G-V_G was observed at low currents (see the upper left inset of Figure 44), although it is noted that this ideality degradation did not significantly impact the current handling capability and breakdown voltage capability of the device (Christiansen, 2011c).

The forward gate current values from the tested devices were far more than the value of 400 mA/mm (57 kA/cm^2) reported in (Xu, 2004) that destroyed the particular GaN HEMTs tested in that report. The devices tested in this report were also less conductive at high gate bias (1.63 A/mm, 326 kA/cm^2 at $V_G = +5$ V) compared to those of (Joh, 2007) wherein the forward gate current was reported to be 2 A/mm (800 kA/cm^2) at $V_G = +5$ V. It is noted that these comparisons are to devices with different gate lengths, contact and sheet resistances, and source-to-gate-to-drain gaps, although the

point made strictly regards the robustness of the Schottky gate which is less sensitive to these differences. Technology maturity, gate metal stack differences, and device structure (e.g., source-connected field plate) are possible reasons for the observed improvements over (Xu, 2004) and (Joh, 2007). (Christiansen, 2011c)

Figure 43 shows the transfer curves (a), and associated gate current in absolute value (b) and transconductance (c) of the third device throughout stressing. Black lines show Step 1 and the last repeat of Step 4; red lines show the last repeat of Step 7 and the result of Step 10; finally, green lines show Steps 12-13. Initial slight improvement in gate current (trapping or burn-in behavior likely) gives way to degradation. The transfer curves exhibit a degradation trend with a *saturation* apparent after the first 30-minute holding time, much like a transient burn-in effect. Two separate causes—resulting in quick degradation in the short term and slow degradation in the long term—appear responsible for the electrical changes observed during exposure to bias. The gate current increases in a different fashion, with a decreased rate of change—leading to possible saturation—after the first several hours of stress. There was little drain current degradation at the tested current density—a 6.1% reduction, comparing the pre-stress I_{Dmax} of 787 mA/mm to the post-stress I_{Dmax} of 739 mA/mm. In addition, there was only a 0.1-V positive shift in threshold voltage (Christiansen, 2011c).

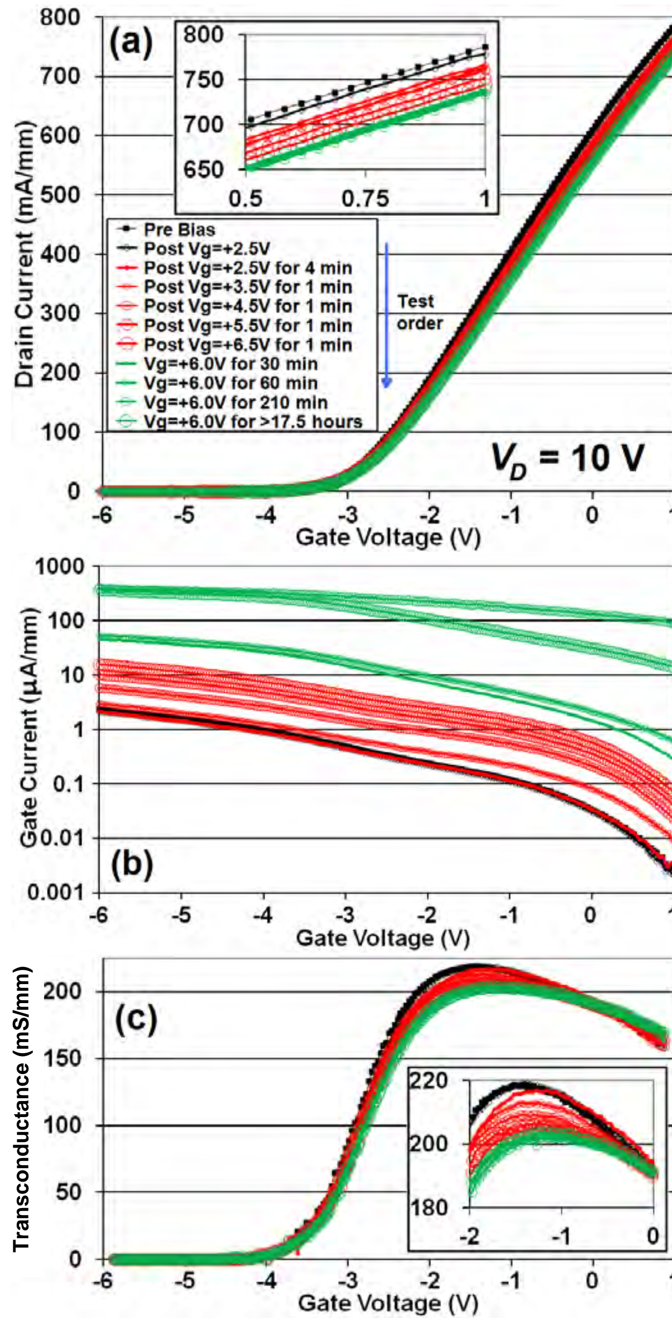

Figure 43. Transfer curves (a), and associated gate current in absolute value (b) and transconductance (c) of the device as measured during characterizations between gate stressing events. Insets show detail at regions of interest in the same data sets. Extra gate current is seen in (b) above $V_G \approx -3.5$ V after 210 minutes stress (top curve) that is not seen after longer stress time (second-to-top curve). It is not known if there was a temporary test issue or if that is indeed real.

Figure 44 shows the device's gate diode curves during the stress sweeps from V_G = 0 V to +2.5 V ≤ V_G ≤ +6.5 V (Steps 2, 4, 7, 10, 11, and 13). During the first few

sweeps, the gate current improved. After this, excess leakage at low gate bias appeared (see upper left inset), then the gate current increased with stress time and saturated. Despite the ideality degradation, the breakdown voltage remained above 200 V (based on satisfying the nominal 1-mA/mm industry criterion for breakdown). If there is any change in V_{Gon} it is slight and masked by other effects. In contrast, (Joh, 2007) observed a noticeable change in V_{Gon} of ~0.5 V in significantly shorter stress time (Christiansen, 2011c).

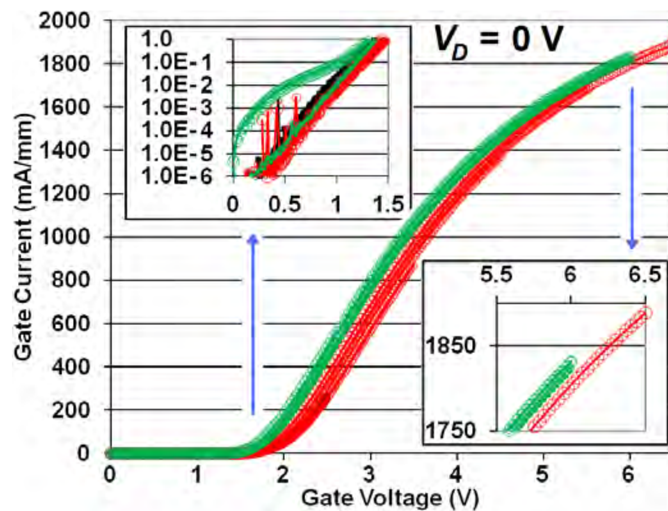

Figure 44. Gate diode curves during the stressing. Insets show additional detail for regions of interest of the same curves as the main plot and share the same units (i.e., mA/mm and V) as the main figure. The data was collected at stress times represented in Figure 43. Black curves represent the initial Vg = +2.5 V gate stresses. Red curves represent the gate voltage stress ramps of increasing magnitude collected just prior to the red curves of Figure 43. Green curves are gate voltage stress ramps collected just after the total stress times represented by the green curves of Figure 43. (Christiansen, 2011c)

7.4. Conclusion

The mere survival of the device tested at $I_G \geq +1.8$ A/mm and $V_G \geq +6.0$ V for >17.5 hours is remarkable, in addition to the modest degradation in drain current that appears to saturate over stress time. The results observed indicate that the GaN HEMTs tested are extremely robust to high forward gate bias and current. Devices based on the

tested structure show the potential to withstand the rigors of forward gate bias and current during RF operation, and the high I_G tolerance seen may allow extra latitude to circuit designers (Christiansen, 2011c).

The results of this chapter illustrate that the tested GaN HEMTs can survive extremely high DC gate bias (+6.0 V) and low DC stress drain current at a low baseplate temperature (45 °C) for tens of hours with only minor drain current degradation. Only minor drain current degradation was also seen in the results of Section 6.3.2 that demonstrate that the tested GaN HEMTs can survive high DC gate bias (+3.0 V) and high DC stress drain current at a high baseplate temperature (245 °C) for hundreds of hours. From these two tests, forward gate voltage and current are observed to be insignificant contributors to drain current degradation in the tested GaN HEMTs.

VIII. Time-dependent Electrical Degradation of AlGaN/GaN HEMTs Subjected to High DC Power and High Drain Bias

8.1. Introduction

The DoD seeks perceptivity of the degradation mechanisms of GaN HEMTs. In addition, having a correlation between DC tests and RF performance is desirable. Characterizing GaN HEMTs over time during testing is important to gaining that perceptivity. Understanding the time-dependence of DC degradation is necessary to be able to correlate DC to RF stress. Having the time dependence of degradation is also useful for creating models from which further insight can be obtained.

Various models have been presented to describe drain current degradation in GaN HEMTs. The authors of (Vetury, 2001) fit the drain current under RF operation to a stretched exponential. In (Coffie, 2007), a power law was used to fit the drain current under RF drive. DC drain current data was fitted to a logarithmic relationship in (Singhal, 2007).

In this work are presented several aspects of GaN HEMT degradation due to multiple DC stress conditions. The DC data are fit to an exponential model.

8.2. Experiment Description

The test procedures that pertain to this chapter are in Sections 4.1, 4.2, 4.4, and 4.5.

8.3. Results and Discussion

8.3.1. Voltage Step-Stress Test

Drain and gate currents during the voltage step-stress test for one device are shown in Figure 45, which shows the most gate current change seen of the four devices during the step-stress test. I_{Dmax} and I_{DSS}, and I_G from pre- and post-stress characterizations are shown in Figure 46. I_G was measured at $V_{DS} = 0$ V and $V_{GS} = -10$ V. Despite the changes seen during stress, I_{Dmax} changed only $+1.59\%$ from pre-stress to the end of the test and I_{DSS} changed only -0.65%. I_G changed -186% from endpoint to endpoint. A possible reason for this difference is the relative magnitudes of the drain current during stress and during the transfer curve sweep—two orders of magnitude different.

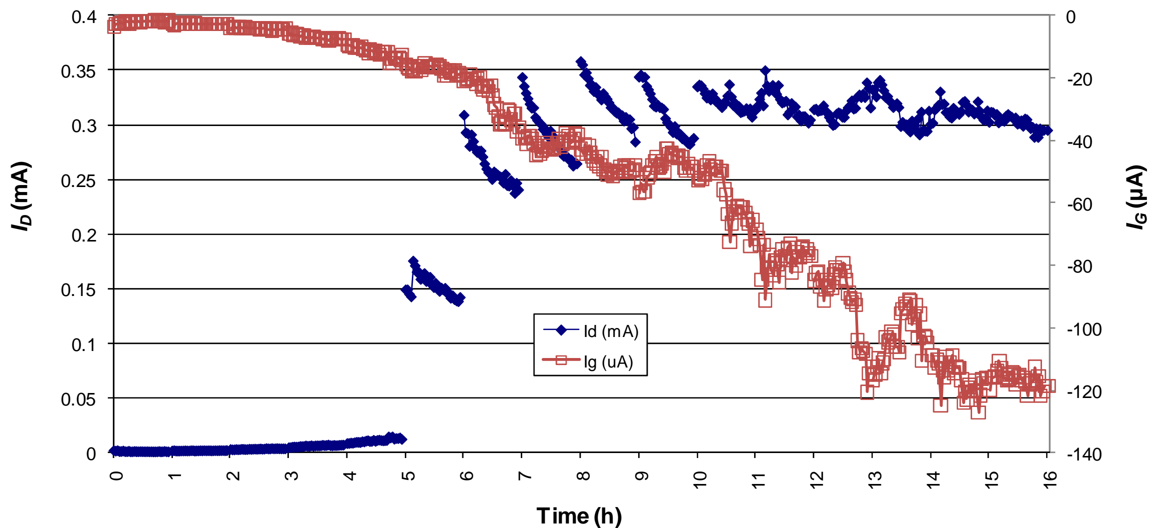

Figure 45. Drain and gate current of Device H11V05R during voltage step-stress test.

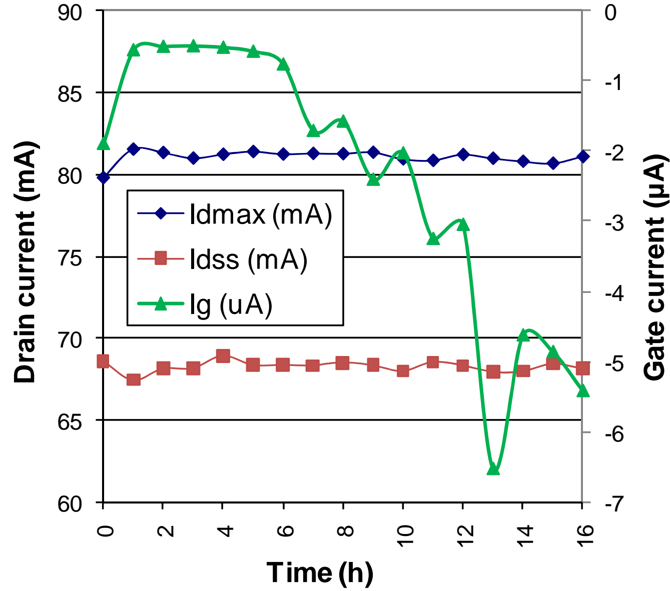

Figure 46. Evolution of I_{Dmax}, I_{DSS}, and I_G of Device H11V05R during voltage step-stress test

The other three devices exhibited similar responses to the voltage step-stress. The voltage step-stress test demonstrated that these devices could withstand the maximum drain voltage of 100 V of the Accel-RF test station. The insignificant changes in these devices and their survival up to 150 and 200 V is remarkable, considering other reports of significant degradation within minutes at significantly lower voltages (Joh, 2008; del Alamo, 2009; Makaram, 2010) and at room temperature (Joh, 2008; del Alamo, 2009).

The results of the voltage step-stress tests similar to those conducted by J. A. del Alamo's group at MIT are described next. The plots of I_{Dmax} and $|I_{Goff}|$ for Device R10C2 are in Figure 47. The first points are pre-stress measurements. Comparing these plots to those in Figure 21, there is no apparent critical voltage for Device R10C2. The drain current of Device R10C2 generally decreases linearly with increasing stress. In addition, the gate current actually improves with increasing stress by decreasing in magnitude.

The lack of a voltage at which the currents degrade and the improving gate current are counter to the observations of the del Alamo group.

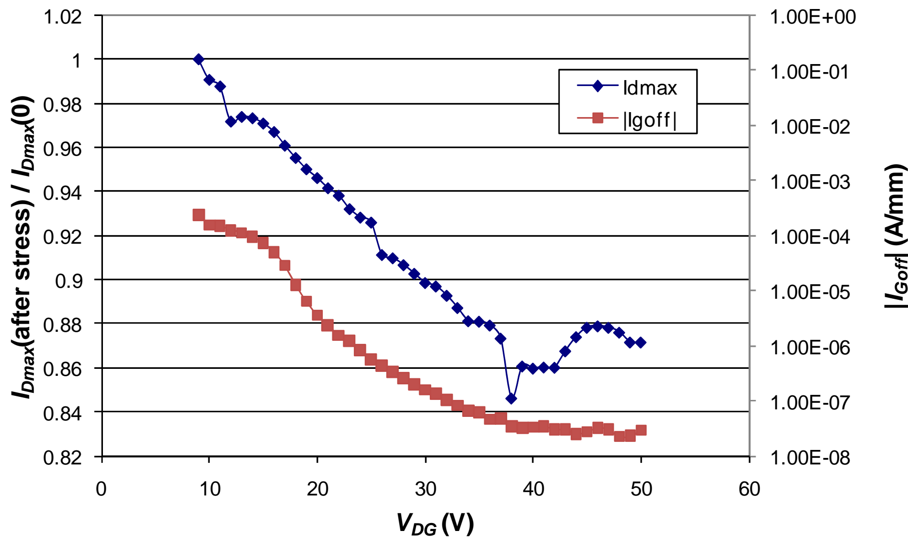

Figure 47. Evolution of I_{Dmax} and $|I_{Goff}|$ for Device R10C2 during del Alamo's "V_{DS} = 0 step-stress experiment"

The plots of I_{Dmax} and $|I_{Goff}|$ for Device R9C2 are in Figure 48. The first points are pre-stress measurements. Comparing these plots to those in Figure 21, there is no apparent critical voltage for Device R9C2. The plot of I_{Dmax} versus V_{DG} has the appearance of an I-V curve. The gate current exhibits an overall improvement, or reduction in magnitude, and only shows increases at six of the last nine stress voltages. The gate current slope for R9C2 is also less than that of R10C2. The difference in the device responses is due to the different methods of obtaining V_{DG}, with stepping the gate voltage being more stressful on the gate contact.

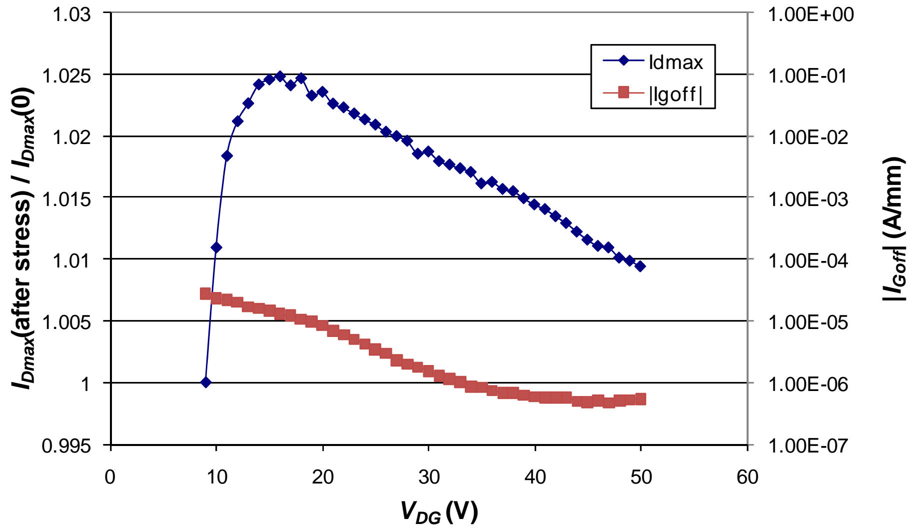

Figure 48. Evolution of I_{Dmax} and $|I_{Goff}|$ for Device R9C2 during V_{DG} step-stress experiment (a modified del Alamo test)

The difference in device responses demonstrates that using V_{DG} as the critical voltage (V_{crit}) is not a valid degradation criterion, since different methods to obtain V_{DG} produce different characteristics. The differences between the present testing and that of del Alamo's group may be explained by different device structures from different vendors.

There are several noteworthy observations obtained from this voltage step-stress experiments. First, there is no apparent critical voltage at which the drain current degrades significantly, as seen in Figures 46 and 47. Second, drain current degradation does not follow gate current degradation, as seen in Figures 45, 46, and 47. Finally, all V_{DG} are not the same, as seen in Figures 47 and 48.

8.3.2. 1000-hour Test

Eight of the nine devices originally placed on test for the 1000-hour test exhibited a burn-in effect—a negative threshold shift and increased transfer curve at the first post-

stress characterization (after 1 hour of stress), then followed by degradation. This trend of negative threshold voltage shift is typical when testing GaN HEMTs in the OFF state (Joh, 2011). Due to this apparent burn-in effect, some comparisons that follow will treat the first post-stress characterizations as the "initial" values for these parts.

Three devices at each of Conditions 4, 5, and 6 were intended to be stressed for 1000 hours. However, the programming from previous testing was not cleared for two channels for which Condition 5 was intended. The data from these two channels will not be presented. In addition, a device at Condition 6 failed catastrophically at 1.36 hours of stress.

The percentage changes between the characterizations at 1 hour and 1000 hours for each individual channel and the average for each condition are listed in Table 15. The changes in I_{Dmax} and I_{DSS} shown in Table 15 exhibit a general decrease in degradation magnitude with increasing voltage and channel temperature estimate. However, the ranges of degradation magnitudes for the conditions overlap, indicating similar behavior.

TABLE 15. PARAMETER PERCENTAGE CHANGES BY CHANNEL AND CONDITION IN 1000-HOUR TEST (T_{BP} = 245 °C; T = 1 HOUR VS. T = 1000 HOURS)

Condition	Channel	g_{mp}	V_T	I_{Dmax}	I_{DSS}
4	13	-4.13%	3.62%	-5.37%	-7.42%
	14	-3.91%	3.41%	-5.59%	-6.70%
	15	-2.94%	3.20%	-4.93%	-6.27%
	Average	-3.66%	3.41%	-5.29%	-6.80%
5	19	-3.29%	3.41%	-4.94%	-6.76%
6	23	-3.92%	2.16%	-4.44%	-6.20%
	24	-4.63%	2.23%	-5.24%	-6.84%
	Average	-4.27%	2.19%	-4.84%	-6.52%

Figure 49 shows the normalized values (to the 1-hour measurements) of I_{Dmax} for the devices of the 1000-hour test. Also shown is a curve based on the model to be

described shortly. The model parameters used for the "Mean" curve are the means of the model parameters of the six devices. Two points that illustrate the burn-in effect for these devices are visible in Figure 49. The time-0 values of normalized drain current for Channels 13 (diamonds) and 14 (squares) at about 0.975 and 0.965, respectively.

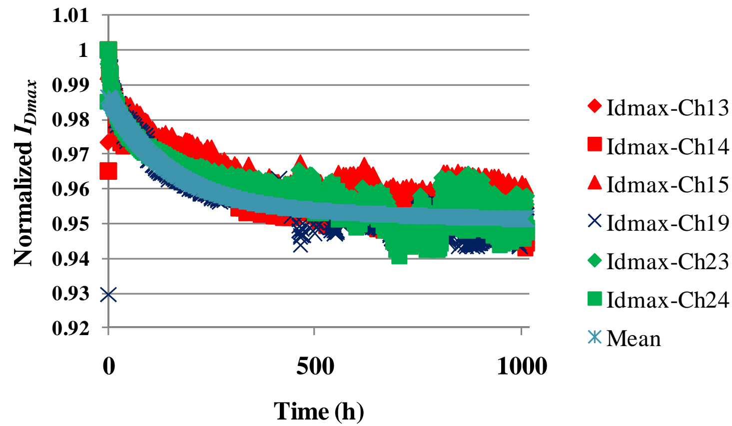

Figure 49. Normalized values (to the 1-hour measurements) of I_{Dmax} over time during the 1000-hour test. The top three lines (red) of the legend are Condition 4, the next line (blue) is Condition 5, the next two (green) are Condition 6, and the bottom line is the model with the means of curve-fitting parameters.

The normalized data were fitted to the following model, which is available as a pre-defined model in the Curve Fitting Tool of MATLAB, and with which AFRL has had success in describing the initial sharp decrease followed by the gradual decrease exhibited in Figure 49:

$$I_D = Ae^{Bt} + Ce^{Dt} \tag{19}$$

where A, B, C, and D are model parameters, and t is time. Note that $(A + C)$ is the maximum drain current at time 0. The physical significance of Equation (19) is that two mechanisms contribute to the drain current degradation—one for the initial steep decline and another for the long-term gradual descent.

The stretched-exponential model used in (Vetury, 2001) was

$$I_D = I_0 + I_1 e^{-(t/\tau)^\beta} \qquad (20)$$

where I_0 is the steady state current, I_1 is an indication of the extent of current collapse, τ is the time constant associated with the degradation process, and β, the stretching parameter ($0 < \beta < 1$), is a measure of the deviation from the exponential. Note that ($I_0 + I_1$) is the maximum drain current at time 0. The physical significance of Equation (20) is that the rate of degradation changes with time—a lower value of β indicates that the rate of decay diminishes as the current degradation progresses (Vetury, 2001).

The stretched-exponential model in Equation (20) generally had higher *R*-squared values than fits to Equation (19) for the 1000-hour test data. However, the fit to Equation (19) generally fit better qualitatively. Figure 50 is an example of the stretched exponential having a slightly higher *R*-squared value, but the fit to Equation (19) looks better; the red fit line (stretched exponential) does not follow the data at the left as well as the blue fit line. The *R*-squared value of the stretched exponential was 0.8982 and that from Equation (19) was 0.89. In addition to AFRL's previous success with the model above, when fitting the data of the 600-hour test (discussed next in Section 8.3.3), Equation (19) had higher *R*-squared values than the stretched-exponential, logarithmic, and power-law models. To fit Equation (19) and the stretched exponential, the timestamps of the data were adjusted so that 1 hour measured time became 0 hours for the fit, 2 hours measured time because 1 hour for the fit, and so forth. This adjustment removed the burn-in effect discussed in Section 6.3.1 and allowed the models to equal 1 at time 0.

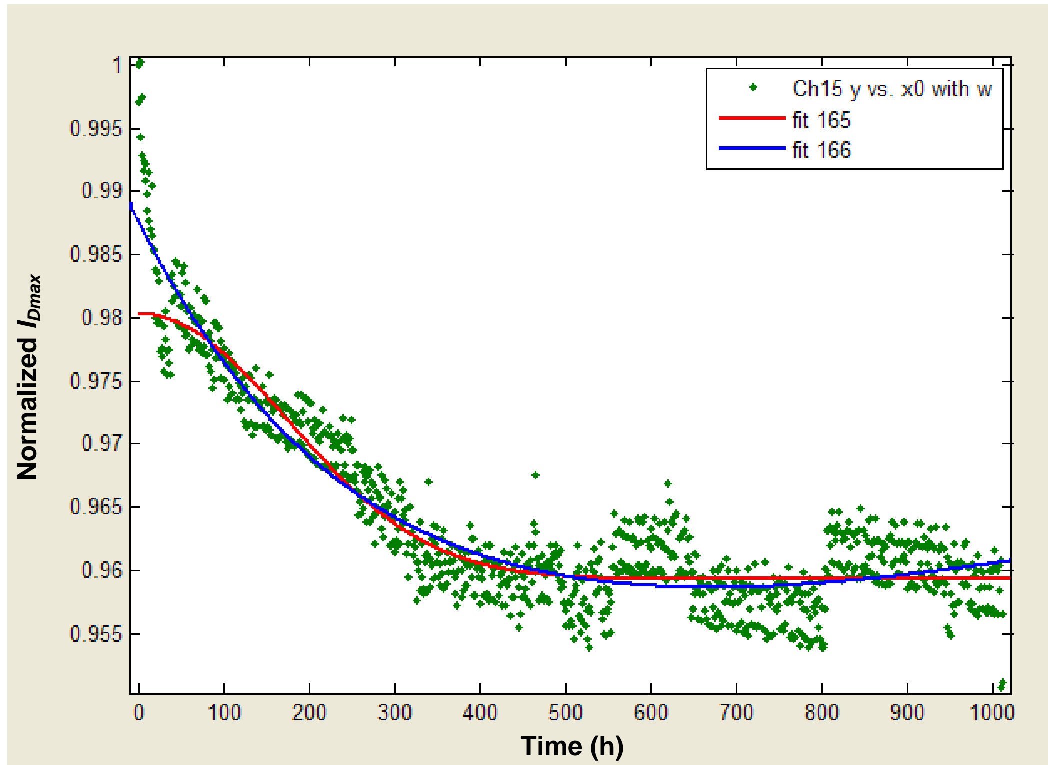

Figure 50. Fits of Channel 15 normalized I_{Dmax} data to Equation (19) in blue (fit 166) and to the stretched exponential in red (fit 165).

The solutions computed by the Curve Fitting Tool of MATLAB for each channel are listed in Table 16 for I_{Dmax}. In addition, the minimum, maximum, mean, and median model parameter values are included in the table. The parameter values in the "Mean" row of Table 16 were used in Equation (19) for the "Mean" curve in Figure 49.

The temperature at which characterizations are made may make a difference when deciding whether a device has reached a degradation limit that is pre-defined as failure. The percentage changes between the characterizations conducted at 245 °C at 0 and 1000 hours for each individual channel and the average for each condition are listed in Table 17. (The 0-hour characterizations are to enable a comparison to the characterizations conducted at 70 °C.) The percentage changes between the characterizations conducted at 70 °C at 0 and 1000 hours for each individual channel and

the average for each condition are listed in Table 18. The values highlighted in yellow are those for which the 245-°C parameter value is greater than 10% different than the 70-°C parameter value. Using one of these values may lead to a different failure time than the other value would produce.

TABLE 16. MODEL PARAMETER SOLUTIONS AND STATISTICS FOR FITTING 1000-HOUR NORMALIZED I_{DMAX} DATA TO EQUATION (19)

		Parameter	Parameter	Parameter	Parameter
Condition	**Channel**	**A**	**B**	**C**	**D**
4	13	0.03809	-0.00343	0.9469	4.53E-06
	14	0.03966	-0.00339	0.9440	4.59E-06
	15	0.04287	-0.00349	0.9450	1.50E-05
5	19	0.02969	-0.01334	0.9633	-1.80E-05
6	23	0.02205	-0.00702	0.9612	-6.09E-06
	24	0.02161	-0.01105	0.9653	-1.86E-05
	Min	0.02161	-0.01334	0.9440	-1.86E-05
	Max	0.04287	-0.00339	0.9653	1.50E-05
	Mean	0.03233	-0.00695	0.9543	-3.10E-06
	Median	0.03389	-0.00525	0.9541	-7.76E-07

TABLE 17. PARAMETER PERCENTAGE CHANGES BY CHANNEL AND CONDITION IN 1000-HOUR TEST (T_{BP} = 245 °C; T = 0 HOURS VS. T = 1000 HOURS)

Condition	Channel	g_{mp}	V_T	I_{Dmax}	I_{DSS}
4	13	-4.388%	-5.828%	-2.795%	0.943%
	14	-3.355%	-5.059%	-2.181%	1.699%
	15	-2.028%	1.196%	-4.295%	-3.676%
	Average	-3.257%	-3.230%	-3.091%	-0.345%
5	19	-3.107%	-12.14%	2.252%	8.680%
6	23	-4.505%	-3.598%	-3.795%	-0.824%
	24	-4.740%	-6.224%	-3.674%	0.507%
	Average	-4.623%	-4.911%	-3.734%	-0.158%

TABLE 18. PARAMETER PERCENTAGE CHANGES BY CHANNEL AND CONDITION IN 1000-HOUR TEST (T_{BP} = 70 °C; T = 0 HOURS VS. T = 1000 HOURS)

Condition	Channel	g_{mp}	V_T	I_{Dmax}	I_{DSS}
4	13	-4.316%	-7.271%	-2.032%	0.845%
	14	-3.049%	-8.814%	-0.704%	2.879%
	15	-3.119%	-0.709%	-3.784%	-3.143%
	Average	-3.495%	-5.598%	-2.173%	0.194%
5	19	-4.196%	-16.67%	2.590%	9.035%
6	23	-4.630%	-3.845%	-4.375%	-2.480%
	24	-5.020%	-6.613%	-3.082%	-0.035%
	Average	-4.825%	-5.229%	-3.728%	-1.257%

The relatively small changes in these devices and their survival for 1000 hours are noteworthy, considering other reports of significant degradation within minutes at lower voltages (Joh, 2008; del Alamo, 2009; Makaram, 2010).

Although the changes in I_{Dmax} and I_{DSS} shown in Table 15 exhibit a general decrease in degradation magnitude with increasing voltage and channel temperature estimate, the degradation in the OFF state is similar at any of the voltages tested. Figure 51 shows the last hours of the 1000-hour test and includes the two channels whose programming was not cleared before starting the test. Notice that there is little difference between the "mistake" channels and the channels that were stressed as intended. Also notice that the responses of the channels tested as intended are overlapping and similar, confirming the overlapping ranges of Table 15. Note that $V_G = -6.5$ V was applied to Channel 21, instead of $V_G = -10$ V as was applied to the other channels. With the threshold voltage being on the order of −3 V for these devices, Channel 21 was pinched off, though not as deeply as the others.

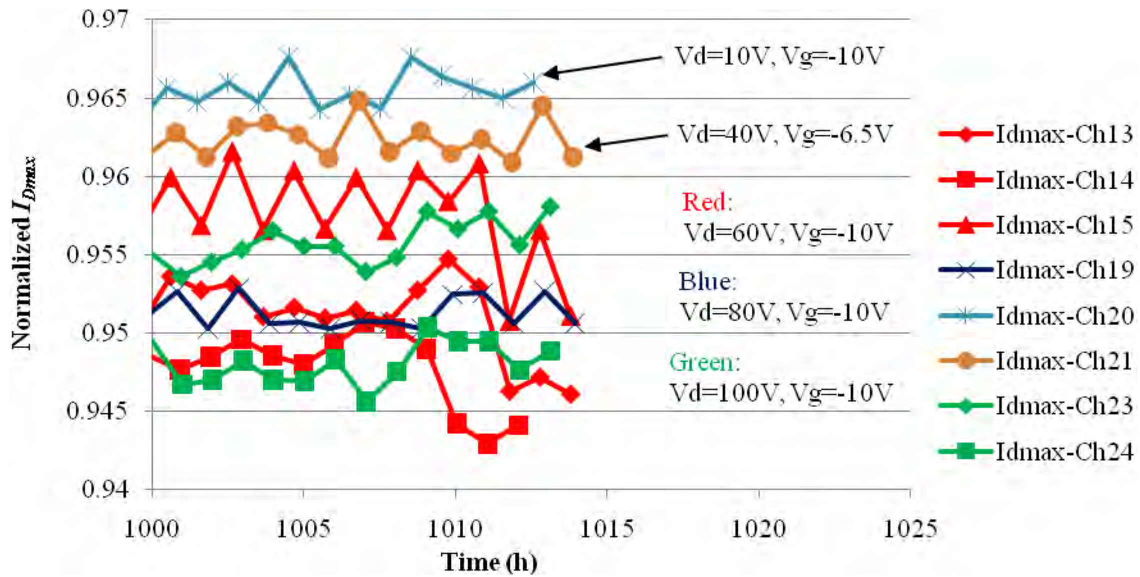

Figure 51. Last hours of 1000-hour test showing the similarity of devices' responses to OFF-state stress independent of applied drain voltage.

8.3.3. 600-hour Test

Similar to the increasing transfer curve at the first post-stress characterization exhibited by the high-voltage-tested parts above, the devices of the 600-hour test showed a more rapid decrease in the first hour of stress than in subsequent hours. Consequently, the 1-hour characterizations are considered to be the "initial" data points for some comparisons that follow.

The percentage changes between the characterizations at 1 hour and Y hours for each individual channel and the average for the condition are listed in Table 19. The changes are calculated from 1 to Y = 200 hours for all channels, but only Channels 25 and 26 have changes calculated from 1 to Y = 600 hours. The decreasing magnitude of the I_{Dmax} and I_{DSS} changes are explained by the positive slope as time progresses toward 600 hours in Figure 52.

TABLE 19. PARAMETER PERCENTAGE CHANGES BY CHANNEL AND STRESS TIME IN 600-HOUR TEST (T_{BP} = 245 °C; T = 1 HOUR VS. T = Y HOURS)

Y (hours)	Channel	g_{mp}	V_T	I_{Dmax}	I_{DSS}
200	25	-0.99%	8.90%	-5.79%	-9.68%
	26	-1.02%	5.44%	-4.07%	-6.41%
	27	-1.18%	4.15%	-3.88%	-5.45%
	Average	-1.07%	6.16%	-4.58%	-7.18%
600	25	-1.72%	7.04%	-5.27%	-8.32%
	26	-1.69%	2.80%	-3.04%	-4.29%
	Average	-1.71%	4.92%	-4.15%	-6.31%

Figure 52 shows the normalized values (to the 1-hour measurements) of I_{Dmax} over time for the devices tested in the 600-hour test. (The 0-hour data point for Channel 25 is behind the 0-hour data points of the other two channels. These points illustrate the burn-in effect for these devices.) One of the three channels used in this test became unusable after the first 200 hours. Hence, only 200 hours of Channel 27 are shown in Figure 52. Using the means of the Channel-25 and Channel-26 model parameters as parameters, a plot of the model output is also shown in Figure 52. Interestingly, after initially degrading, the devices began to recover during stress.

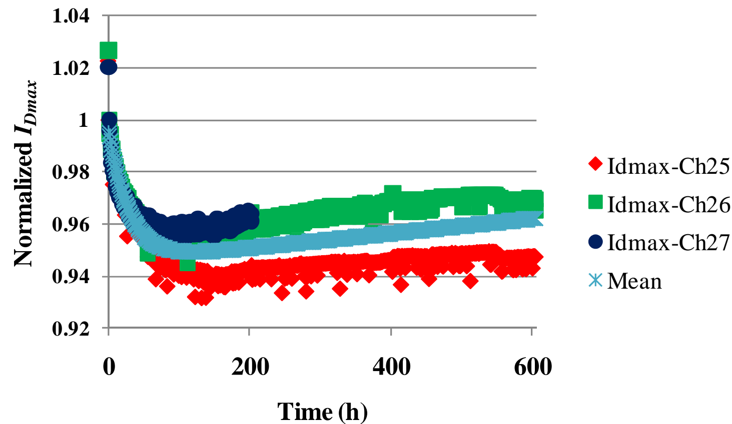

Figure 52. Normalized values (to the 1-hour measurements) of I_{Dmax} over time during the 600-hour test.

The 600-hour test data were fitted to Equation (19). Figure 53 is an example of the qualitative superiority of Equation (19) to the stretched exponential. The stretched-exponential fit is nearly a horizontal line from about 50 hours to 600 hours, while the fit to Equation (19) continues to follow the data. The R-squared value of the stretched exponential was 0.2159 and that from Equation (19) was 0.8696.

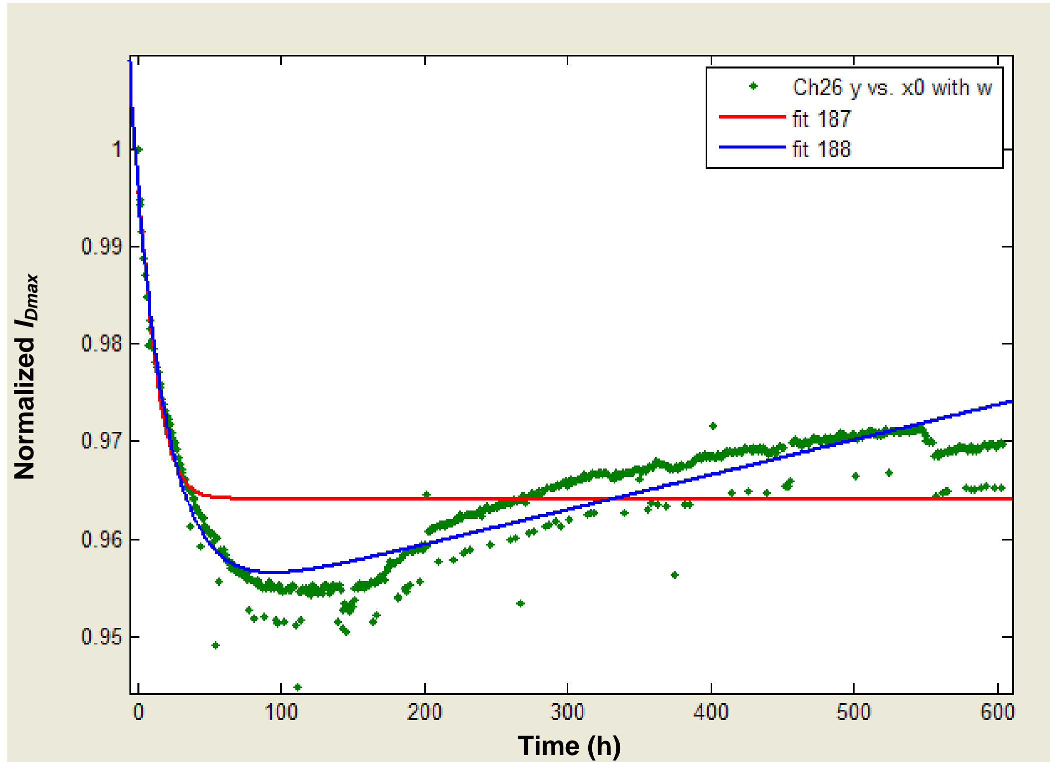

Figure 53. Fits of Channel 26 normalized I_{Dmax} data to Equation (19) in blue (fit 188) and the stretched exponential in red (fit 187).

Table 20 contains the model parameters as calculated by MATLAB for all channels to 200 hours, and for Channels 25 and 26 to 600 hours. The means of the Channel-25 and Channel-26 parameter values were the model parameters used for the "Mean" curve of Figure 52.

The percentage changes between the characterizations conducted at 245 °C at 0 and 200 or 600 hours for each individual channel and the average for the condition are

listed in Table 21. (The 0-hour characterizations are to enable a comparison to the characterizations conducted at 70 °C.) The percentage changes between the characterizations conducted at 70 °C at 0 and 200 or 600 hours for each individual channel and the average for the condition are listed in Table 22. The values highlighted in yellow are those for which the 245-°C parameter value is greater than 10% different than the 70-°C parameter value. The data of the 600-hour test corroborates the data of the 1000-hour test that using one temperature for device characterizations may lead to different failure times than another characterization temperature would generate.

TABLE 20. MODEL PARAMETER SOLUTIONS AND STATISTICS FOR FITTING 600-HOUR NORMALIZED I_{DMAX} DATA TO EQUATION (19)

		Parameter	**Parameter**	**Parameter**	**Parameter**
Y (hours)	**Channel**	**A**	**B**	**C**	**D**
200	25	0.05585	-0.02774	0.9394	1.22E-05
	26	0.04847	-0.02340	0.9417	8.75E-05
	27	0.03945	-0.03732	0.9512	5.58E-05
	Min	0.03945	-0.03732	0.9394	1.22E-05
	Max	0.05585	-0.02340	0.9512	8.75E-05
	Mean	0.04792	-0.02949	0.9441	5.19E-05
	Median	0.04847	-0.02774	0.9417	5.58E-05
600	25	0.05733	-0.02745	0.9382	2.18E-05
	26	0.04609	-0.04172	0.9523	3.70E-05

TABLE 21. PARAMETER PERCENTAGE CHANGES BY CHANNEL AND STRESS TIME IN 600-HOUR TEST (T_{BP} = 245 °C; T = 0 HOURS VS. T = Y HOURS)

Y (hours)	**Channel**	g_{mp}	V_T	I_{Dmax}	I_{DSS}
200	25	-0.885%	12.336%	-7.886%	-13.142%
	26	-0.406%	9.890%	-6.557%	-10.128%
	27	-1.230%	7.888%	-5.785%	-9.338%
	Average	-0.841%	10.038%	-6.743%	-10.869%
600	25	-1.617%	10.554%	-7.377%	-11.836%
	26	-1.078%	7.370%	-5.547%	-8.089%
	Average	-1.348%	8.962%	-6.462%	-9.962%

Table 22. Parameter Percentage Changes by Channel and Stress Time in 600-hour Test (T_{BP} = 70 °C; T = 0 hours vs. T = Y hours)

Y (hours)	Channel	g_{mp}	V_T	I_{Dmax}	I_{DSS}
200	25	-4.099%	10.467%	-10.363%	-13.523%
	26	-3.164%	8.570%	-8.130%	-10.613%
	27	-2.392%	8.034%	-7.119%	-9.703%
	Average	-3.218%	9.024%	-8.537%	-11.280%
600	25	-3.157%	8.289%	-8.276%	-10.863%
	26	-2.425%	5.956%	-5.834%	-7.305%
	Average	-2.791%	7.122%	-7.055%	-9.084%

8.3.4. Discussion

Several observations from the data are notable. Interestingly, the 1000-hour data decreases while the 600-hour data increases, despite the significantly greater power dissipation during the 600-hour test.

The data indicate the need for a burn-in period. What is not clear is whether a burn-in designed to eliminate the increasing transfer curves in high-voltage testing would also eliminate the initial rapid degradation in high-power testing. Likewise, a burn-in designed to eliminate the initial rapid degradation in high-power testing may or may not eliminate the increasing transfer curves in high-voltage testing.

8.4. Conclusion

Studied in this report was the degradation of AlGaN/GaN HEMTs subjected to the conditions of high DC power and high voltage with the gate pinched off. A discovery was made that an exponential model fit the data better than other models previously presented in the literature. If a correlation between DC and RF degradation is desired and the data each fit a different model, then a transformation of the DC fit to the RF data may be required.

Learned from this study was that different conditions cause varying degrees of degradation. In addition, the temperature at which device characterizations are conducted impact the observed level of degradation. Therefore, care must be taken to choose appropriate DC conditions, or combinations of conditions, and characterization temperatures to enable a correlation between DC stress data and RF performance.

IX. Comparison of Pulsed- and Continuous-DC Stressing of AlGaN/GaN HEMTs

9.1. Introduction

This chapter presents a continuation of the results generated from the joint research project with the Naval Postgraduate School (NPS). This chapter contains results produced by both AFIT and NPS.

The DoD seeks perceptivity of the degradation mechanisms of GaN HEMTs. In addition, having a correlation between DC tests and RF performance is desirable. Characterizing GaN HEMTs over time during testing is important to gaining that perceptivity. Understanding the time-dependence of DC degradation is necessary to be able to correlate DC to RF stress. Having the time dependence of degradation is also useful for creating models from which further insight can be obtained.

In this chapter, I present a comparison of the effects of continuous and pulsed DC stress on AlGaN/GaN HEMTs.

9.2. Experiment Description

The test procedures that pertain to the continuous DC stressing are Section 4.1 and Section 4.3, Condition 2 for 300 hours. Three devices were tested at AFRL.

The test conditions that pertain to the pulsed DC stressing (conducted at Naval Surface Warfare Center, Crane Division [NAVSEA Crane], Crane, Indiana) are Section 4.1and Section 4.3, Condition 2. Eight devices were stressed for over 1000 hours each and characterized every 2 hours with a measurement of I_{Dmax} (at $V_G = 1$ V and $V_D = 10$ V) at the stress baseplate temperature. Appropriate times are selected to make relevant comparisons to the continuous DC data. Three devices were pulsed at Pulsed

Condition A (PCA) with a square wave of 100 μs ON and 100 μs OFF (in pinch-off at V_G = −8 V). Three devices were pulsed with a square wave of 250 μs ON and 250 μs OFF (Pulsed Condition B [PCB]). Two devices were pulsed with a square wave of 250 μs ON and 50 μs OFF (Pulsed Condition C [PCC]).

9.3. Results and Discussion

First, the observations of the continuous-DC Condition 2 (Section 4.3) and the pulsed conditions are compared. This comparison uses equivalent times to compare the devices stressed at the same bias condition. The devices stressed by continuous DC were characterized at 0 and 300 hours at a baseplate temperature of 70 °C. The devices stressed by pulsed DC were characterized at 0 and every 2 hours afterward at the stress baseplate temperature of 133 °C. To find the equivalent times for the devices stressed by pulsed DC, 300 hours was divided by the duty cycle of the pulsed condition. For example, the equivalent time of 360 hours for PCC was found by dividing 300 hours by [(250 μs ON) / (300 μs total)]. The I_{Dmax} values of PCA, PCB, and PCC at the respective equivalent times are used for comparison.

Table 23 lists the average degradation in I_{Dmax} for the continuous- and pulsed-DC tests for comparison of the devices at the same bias condition (Section 4.3, Condition 2). Although all devices experienced the same biases for equivalent times, the different conditions produced different amounts of degradation. Pulsed Condition A experienced the least amount of degradation, while Pulsed Conditions B and C experienced the most. Thus, PCA appears to have been less stressful than continuous DC, and PCB and PCC appear to have been more stressful than continuous DC.

TABLE 23. AVERAGE I_{DMAX} DEGRADATION IN CONTINUOUS- AND PULSED-DC, SAME-BIAS TESTS

Condition	***Number of Devices***	***Test Time (hours)***	***ON Time (hours)***	I_{Dmax}
2	3	300	300	−10.9%
		Equivalent Test Time (hours)		
PCA	3	600	300	−9.04%
PCB	3	600	300	−12.8%
PCC	2	360	300	−12.7%

Although all devices nominally had the same channel temperature (392 °C) according to Table 3, the devices tested under PCA may not have reached the steady-state temperature within the 100-μs ON time (Heller, 2011b). Hence, the PCA-tested devices may have been less stressed thermally than the devices tested under continuous DC, PCB, and PCC, resulting in less degradation.

The PCB- and PCC-tested devices may have degraded more than the devices of the other conditions due to the thermal cycling between the endpoints of the temperature range. The continuous-DC-tested devices did not experience thermal cycling during stressing, and the PCA-tested devices may not have reached the estimated channel temperature, as explained in the paragraph above, during their thermal cycling. Of particular note is that the additional 200 μs of OFF time in PCB do not to appear to have reduced degradation compared to PCC.

9.4. Conclusion

Devices were stressed under continuous- and pulsed-DC conditions at AFRL and NAVSEA Crane, respectively. When the observations from stressing at the same bias condition for equivalent times were compared, the devices that experienced the shortest ON pulse were seen to have degraded less than the other devices. This smaller amount of

degradation may have been caused by the devices not reaching the higher steady-state channel temperature that the other devices did. The devices that experienced the longest ON pulse degraded more than the other devices, possibly due to thermal cycling over a greater range of temperatures.

X. Conclusions

10.1. Overall Summary

AlGaN/GaN HEMT technology has the potential to provide the DoD with increased capability at a reduced cost in high-temperature and high-voltage sensor and communications applications. The HEMTs tested in this research exhibited robustness to high forward gate voltage and current, when the drain voltage is zero. In addition, the HEMTs demonstrated resilience against high drain voltages with the gated pinched off, contrary to published reports. The different behavior demonstrated by the tested devices may indicate that the degradation seen in other devices is not an intrinsic failure mode to GaN HEMTs, but may be due to materials, fabrication processes, or device structure. The minimal degradation to the mentioned high drain and gate voltages displayed by the tested devices provides incentive to continue to pursue GaN HEMT technology for DoD systems.

Despite this potential, caution is still warranted with respect to inserting GaN HEMT technology into DoD weapons systems. Lifetime estimates in the literature that are based on the Arrhenius temperature-accelerated degradation model are exceptionally long. However, this research showed that other factors besides temperature, most notably voltage, affect the degradation of these transistors. Therefore, prudence is required when considering such Arrhenius lifetime extrapolations.

10.2. Contributions

The contributions from the multi-stressor accelerated testing are the:

1. Revelation of different failure mechanisms than are in the literature and that failure mechanisms depend on the test conditions. High drain voltage did not degrade the devices tested for this research as is reported for other devices. The parts tested herein did not exhibit significant drain current degradation or gate-edge pits when subjected to high drain voltages at gate pinch-off. Reasons for the difference are the technological maturity of, and the source-connected field plate structure in, the tested devices. Different test conditions revealed different failure mechanisms.
2. Determination that different stressors cause different lifetimes. Voltage and temperature cause different rates of degradation. Different test conditions produced different degradation rates, even at similar channel temperature estimates.
3. Determination that voltage can be used as an accelerant. In connection with Contribution 2, voltage was shown to be a prime candidate for further accelerated-life testing.
4. Fitting of experimental degradation data to a mathematical model. Test data were fit to a model that is the sum of two exponentials. Fitting this model suggests two degradation mechanisms at work during device operation.
5. Comparison of continuous-DC test results to pulsed-DC test results. The comparison indicates that a pulse width of sufficient brevity is less stressful than continuous DC, possibly due to the device not reaching a higher steady-state channel temperature within the pulse ON time. For

longer pulse widths that may attain the higher steady-state channel temperature, thermal cycling between the extremes of the temperature range may induce more degradation than continuous DC.

The contribution from the modeling research is the creation of a framework that modifies a device model during operation and based on operating conditions.

10.3. Ideas for Future Research

Future research could include the following topics and experiments:

1. A designed experiment (Montgomery, 2009) to investigate further the voltage acceleration and its interaction with temperature. Different levels of current may also be incorporated in the test. By designing the test, the analysis of the test data will indicate which stressors, and the interactions thereof, have a significant effect on the life of a GaN HEMT. The execution of the test will also be more efficient. A challenge for this experiment will be choosing the appropriate combinations of factor levels due to their interaction that affects channel temperature through self-heating.
2. Thermal storage tests to understand whether degradation requires stress. These tests will complement the designed experiment above by helping to distinguish the degradation caused by temperature alone and the degradation caused by other factors.
3. An investigation of the effects of characterization temperature on reliability estimates. The results of Chapter 8 indicate that reliability

estimates are dependent on the temperature at which characterizations are conducted. Therefore, a controlled experiment would be useful to quantify more precisely the effect of characterization temperature on lifetime estimates. A group of devices could be stressed and characterized at the stress temperature, while another group of devices could be stressed at the same stress temperature but characterized at a lower temperature.

4. A comparison of the effects of two thicknesses of the GaN buffer. While conducting this research, the thickness of the GaN buffer in the tested devices was revealed to be different than in previous lots. Testing devices from both lots would reveal the effects of the different thicknesses on channel temperature and reliability.
5. A thorough examination of the causes of initial negative threshold voltage shift in high-voltage-tested parts. Most tested devices that experienced high drain voltage stress with the gate pinched off exhibited a negative threshold voltage shift at the first post-stress characterization. This phenomenon is shared with devices without source-connected field plates. Studying this phenomenon may reveal an intrinsic behavior of GaN HEMTs that may be a precursor to degradation.
6. An exploration into the effects of different biases that produce the same drain-to-gate voltages. Most authors who claim that a “critical voltage” causes degradation in GaN HEMTs use the drain-to-gate voltage when the drain voltage is zero and the gate voltage is extremely negative. Conducting an experiment with multiple combinations of drain and gate

voltages, but equaling the same drain-to-gate voltage, would demonstrate that all drain-to-gate voltage combinations do not generate the same degradation.

7. A determination of an appropriate burn-in process that could be applied prior to any test. The devices tested for this research indicated the need for a burn-in protocol prior to testing or operation. Such a burn-in procedure should be applicable to all testing and operation, so that only one process is required. A burn-in designed for high-voltage testing may not appropriately burn-in a device scheduled for high-power testing, and vice versa.
8. Additional investigations of the time-temperature-V_G trade space under DC and RF stress. As stated in Section 7.4, the GaN HEMTs in this research were stressed at high DC gate bias, DC drain current, and baseplate temperature for hundreds of hours in one test and at extremely high DC gate bias but low DC drain current and baseplate temperature for tens of hours in another test. Further investigations could be conducted to understand the time-temperature-V_G trade space and the full extent of degradation due to high forward bias and current under RF operation and over very long time periods (thousands of hours) (Christiansen, 2011c).
9. Size scaling as a means to accelerate GaN HEMT life testing. A possible way to accelerate GaN HEMT reliability testing is to use devices of the same design with proportionally larger feature sizes. Nelson states, "Generally large specimens fail sooner than small ones," and gives

capacitors and microelectronics conductors as examples (Nelson, 1990:17, 385). Initially, GaN HEMTs of both sizes would have to be tested to determine an acceleration factor. In subsequent tests, large devices would be tested and the lifetimes of smaller devices would be extrapolated using the size acceleration factor. The advantage of accelerated testing with size would be that the devices could be tested at lower temperatures, but test times would remain reasonable.

Appendix A. Pictorial Presentation of Test Preparation and Setup

The following images are a pictorial description of the accelerated-life testing preparation and setup.

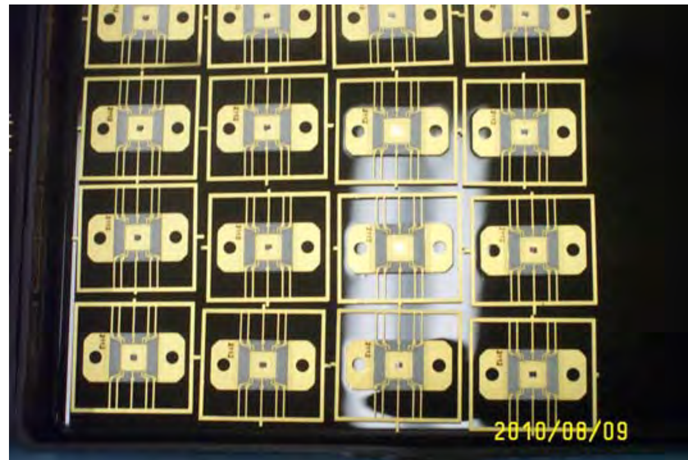

Figure 54. Packaged devices as sent from vendor

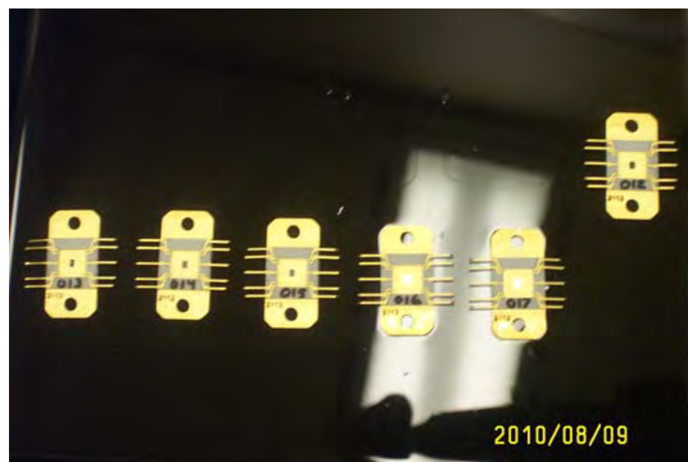

Figure 55. Packaged devices with lead frames removed

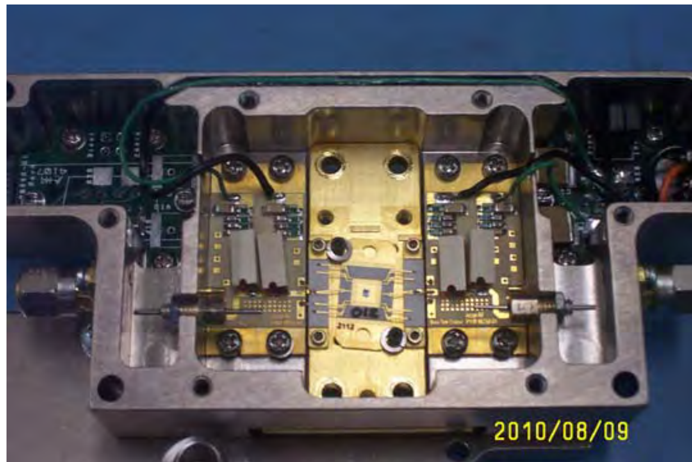

Figure 56. Packaged device attached to test module

Figure 57. Heater bar for three test modules

Figure 58. Clamps attached above devices and test modules attached to heater bar

Figure 59. Test module covers and nitrogen tubes attached

Figure 60. DC test station

Figure 61. Thermal and photoemission imaging system

Appendix B. Scripts, Command Files, and Macros

B.1. Modeling

B.1.1. Unix script

try4.sh

```
#! /bin/bash
# check for _xy.dat file size of 0 (if caught in MATLAB macro)
# or 50 (if MATLAB macro is left to do first fprintf in _xy.dat file)
j=1
contd=1
while [ "$contd" -eq "1" ]
do
	i=`expr $j - 1`
	k=`expr $j + 1`

	sed s/n${i}/n${j}/g sde${i}_end_dvs.cmd > sde${j}_end_dvs.cmd
	cat sde${j}_beg_dvs.cmd sde${j}_mid_dvs.cmd > temp_dvs.cmd
	cat temp_dvs.cmd sde${j}_end_dvs.cmd > sde${j}_dvs.cmd
	mv temp_dvs.cmd sde${k}_beg_dvs.cmd
	sde -e -l sde${j}_dvs.cmd &
	wait

	sed s/n${i}/n${j}/g sdevice${i}_des.cmd > sdevice${j}_des.cmd
	sdevice sdevice${j}_des.cmd &
	wait

	sed s/n${i}/n${j}/g tdr2dat${i}.mcr > tdr2dat${j}.mcr
	tecplot_sv -p tdr2dat${j}.mcr &
	wait

	sed s/n${i}/n${j}/g DESSIS2COMSOLscript_bdc${i}.m >
DESSIS2COMSOLscript_bdc${j}.m
	matlab -r DESSIS2COMSOLscript_bdc${j} &
	wait

	if [ `du -b n${j}_xy.dat | awk '{ print $1 }'` -eq "0" ]
	then
		contd=0
	else
		cp n${j}_xy.dat sde${k}_mid_dvs.cmd
		j=$k
	fi
done
```

B.1.2. Sentaurus Structure Editor command files

sde1_beg_dvs.cmd

```
(sde:clear)

;-----------------------------------------------------------------------
; Setting parameters
; - lateral
(define  L  10.0) ; [um] length
(define  W  1.0)  ; [um] width
(define  D  1.0)  ; [um] depth, if doing 3D
(define  Th_ext 0.01)   ; [um] extension length of thermal contact
(define  Lth      (+ L Th_ext)); [um] end length of thermal contact

(define  Lmid     (/ L 2.0))  ; [um] length midpoint
(define  Wmid     (/ W 2.0))  ; [um] width midpoint
(define  Dmid     (/ D 2.0))  ; [um] depth midpoint
(define  Thmid    (+ L (/ Th_ext 2.0))) ; [um] thermal contact midpoint

;-----------------------------------------------------------------------
; Overlap resolution: New replaces Old
(sdegeo:set-default-boolean "ABA")

;-----------------------------------------------------------------------
; Create wire region
; bulk pieces
(sdegeo:create-rectangle
  (position  0.0  0.0  0.0)
  (position  4.6   W   0.0)
   "Metal" "R.WireL"
)

(sdegeo:create-rectangle
  (position  5.4  0.0  0.0)
  (position   L    W   0.0)
   "Metal" "R.WireR"
)

; create divot
;-------------------------row 1
(sdegeo:create-rectangle
  (position  4.6  0.0  0.0)
  (position  4.7  0.1  0.0)
   "Metal" "R.1"
)

(sdegeo:create-rectangle
  (position  4.7  0.0  0.0)
  (position  4.8  0.1  0.0)
   "Metal" "R.2"
)

(sdegeo:create-rectangle
  (position  4.8  0.0  0.0)
  (position  4.9  0.1  0.0)
   "Metal" "R.3"
)
```

```
(sdegeo:create-rectangle
  (position  5.1  0.0  0.0)
  (position  5.2  0.1  0.0)
   "Metal" "R.6"
)

(sdegeo:create-rectangle
  (position  5.2  0.0  0.0)
  (position  5.3  0.1  0.0)
   "Metal" "R.7"
)

(sdegeo:create-rectangle
  (position  5.3  0.0  0.0)
  (position  5.4  0.1  0.0)
   "Metal" "R.8"
)

;-------------------------row 2
(sdegeo:create-rectangle
  (position  4.6  0.1  0.0)
  (position  4.7  0.2  0.0)
   "Metal" "R.9"
)

(sdegeo:create-rectangle
  (position  4.7  0.1  0.0)
  (position  4.8  0.2  0.0)
   "Metal" "R.10"
)

(sdegeo:create-rectangle
  (position  4.8  0.1  0.0)
  (position  4.9  0.2  0.0)
   "Metal" "R.11"
)

(sdegeo:create-rectangle
  (position  5.1  0.1  0.0)
  (position  5.2  0.2  0.0)
   "Metal" "R.14"
)

(sdegeo:create-rectangle
  (position  5.2  0.1  0.0)
  (position  5.3  0.2  0.0)
   "Metal" "R.15"
)

(sdegeo:create-rectangle
  (position  5.3  0.1  0.0)
  (position  5.4  0.2  0.0)
   "Metal" "R.16"
)
```

```
;-------------------------row 3
(sdegeo:create-rectangle
  (position  4.6  0.2  0.0)
  (position  4.7  0.3  0.0)
   "Metal" "R.17"
)

(sdegeo:create-rectangle
  (position  4.7  0.2  0.0)
  (position  4.8  0.3  0.0)
   "Metal" "R.18"
)

(sdegeo:create-rectangle
  (position  4.8  0.2  0.0)
  (position  4.9  0.3  0.0)
   "Metal" "R.19"
)

(sdegeo:create-rectangle
  (position  5.1  0.2  0.0)
  (position  5.2  0.3  0.0)
   "Metal" "R.22"
)

(sdegeo:create-rectangle
  (position  5.2  0.2  0.0)
  (position  5.3  0.3  0.0)
   "Metal" "R.23"
)

(sdegeo:create-rectangle
  (position  5.3  0.2  0.0)
  (position  5.4  0.3  0.0)
   "Metal" "R.24"
)

;-------------------------row 4
(sdegeo:create-rectangle
  (position  4.6  0.3  0.0)
  (position  4.7  0.4  0.0)
   "Metal" "R.25"
)

(sdegeo:create-rectangle
  (position  4.7  0.3  0.0)
  (position  4.8  0.4  0.0)
   "Metal" "R.26"
)

(sdegeo:create-rectangle
  (position  4.8  0.3  0.0)
  (position  4.9  0.4  0.0)
   "Metal" "R.27"
)
```

```
(sdegeo:create-rectangle
  (position  5.1  0.3  0.0)
  (position  5.2  0.4  0.0)
   "Metal" "R.30"
)

(sdegeo:create-rectangle
  (position  5.2  0.3  0.0)
  (position  5.3  0.4  0.0)
   "Metal" "R.31"
)

(sdegeo:create-rectangle
  (position  5.3  0.3  0.0)
  (position  5.4  0.4  0.0)
   "Metal" "R.32"
)

;--------------------------row 5
(sdegeo:create-rectangle
  (position  4.6  0.4  0.0)
  (position  4.7  0.5  0.0)
   "Metal" "R.33"
)

(sdegeo:create-rectangle
  (position  4.7  0.4  0.0)
  (position  4.8  0.5  0.0)
   "Metal" "R.34"
)

(sdegeo:create-rectangle
  (position  4.8  0.4  0.0)
  (position  4.9  0.5  0.0)
   "Metal" "R.35"
)

(sdegeo:create-rectangle
  (position  5.1  0.4  0.0)
  (position  5.2  0.5  0.0)
   "Metal" "R.38"
)

(sdegeo:create-rectangle
  (position  5.2  0.4  0.0)
  (position  5.3  0.5  0.0)
   "Metal" "R.39"
)

(sdegeo:create-rectangle
  (position  5.3  0.4  0.0)
  (position  5.4  0.5  0.0)
   "Metal" "R.40"
)
```

```
;-------------------------row 6
(sdegeo:create-rectangle
  (position  4.6  0.5  0.0)
  (position  4.7  0.6  0.0)
   "Metal" "R.41"
)

(sdegeo:create-rectangle
  (position  4.7  0.5  0.0)
  (position  4.8  0.6  0.0)
   "Metal" "R.42"
)

(sdegeo:create-rectangle
  (position  4.8  0.5  0.0)
  (position  4.9  0.6  0.0)
   "Metal" "R.43"
)

(sdegeo:create-rectangle
  (position  4.9  0.5  0.0)
  (position  5.0  0.6  0.0)
   "Metal" "R.44"
)

(sdegeo:create-rectangle
  (position  5.0  0.5  0.0)
  (position  5.1  0.6  0.0)
   "Metal" "R.45"
)

(sdegeo:create-rectangle
  (position  5.1  0.5  0.0)
  (position  5.2  0.6  0.0)
   "Metal" "R.46"
)

(sdegeo:create-rectangle
  (position  5.2  0.5  0.0)
  (position  5.3  0.6  0.0)
   "Metal" "R.47"
)

(sdegeo:create-rectangle
  (position  5.3  0.5  0.0)
  (position  5.4  0.6  0.0)
   "Metal" "R.48"
)

;-------------------------row 7
(sdegeo:create-rectangle
  (position  4.6  0.6  0.0)
  (position  4.7  0.7  0.0)
   "Metal" "R.49"
```

```
)

(sdegeo:create-rectangle
  (position  4.7  0.6  0.0)
  (position  4.8  0.7  0.0)
   "Metal" "R.50"
)

(sdegeo:create-rectangle
  (position  4.8  0.6  0.0)
  (position  4.9  0.7  0.0)
   "Metal" "R.51"
)

(sdegeo:create-rectangle
  (position  4.9  0.6  0.0)
  (position  5.0  0.7  0.0)
   "Metal" "R.52"
)

(sdegeo:create-rectangle
  (position  5.0  0.6  0.0)
  (position  5.1  0.7  0.0)
   "Metal" "R.53"
)

(sdegeo:create-rectangle
  (position  5.1  0.6  0.0)
  (position  5.2  0.7  0.0)
   "Metal" "R.54"
)

(sdegeo:create-rectangle
  (position  5.2  0.6  0.0)
  (position  5.3  0.7  0.0)
   "Metal" "R.55"
)

(sdegeo:create-rectangle
  (position  5.3  0.6  0.0)
  (position  5.4  0.7  0.0)
   "Metal" "R.56"
)

;--------------------------row 8
(sdegeo:create-rectangle
  (position  4.6  0.7  0.0)
  (position  4.7  0.8  0.0)
   "Metal" "R.57"
)

(sdegeo:create-rectangle
  (position  4.7  0.7  0.0)
  (position  4.8  0.8  0.0)
   "Metal" "R.58"
```

```
)

(sdegeo:create-rectangle
  (position  4.8  0.7  0.0)
  (position  4.9  0.8  0.0)
   "Metal" "R.59"
)

(sdegeo:create-rectangle
  (position  4.9  0.7  0.0)
  (position  5.0  0.8  0.0)
   "Metal" "R.60"
)

(sdegeo:create-rectangle
  (position  5.0  0.7  0.0)
  (position  5.1  0.8  0.0)
   "Metal" "R.61"
)

(sdegeo:create-rectangle
  (position  5.1  0.7  0.0)
  (position  5.2  0.8  0.0)
   "Metal" "R.62"
)

(sdegeo:create-rectangle
  (position  5.2  0.7  0.0)
  (position  5.3  0.8  0.0)
   "Metal" "R.63"
)

(sdegeo:create-rectangle
  (position  5.3  0.7  0.0)
  (position  5.4  0.8  0.0)
   "Metal" "R.64"
)

;--------------------------row 9
(sdegeo:create-rectangle
  (position  4.6  0.8  0.0)
  (position  4.7  0.9  0.0)
   "Metal" "R.65"
)

(sdegeo:create-rectangle
  (position  4.7  0.8  0.0)
  (position  4.8  0.9  0.0)
   "Metal" "R.66"
)

(sdegeo:create-rectangle
  (position  4.8  0.8  0.0)
  (position  4.9  0.9  0.0)
   "Metal" "R.67"
```

```
)

(sdegeo:create-rectangle
  (position  4.9  0.8  0.0)
  (position  5.0  0.9  0.0)
   "Metal" "R.68"
)

(sdegeo:create-rectangle
  (position  5.0  0.8  0.0)
  (position  5.1  0.9  0.0)
   "Metal" "R.69"
)

(sdegeo:create-rectangle
  (position  5.1  0.8  0.0)
  (position  5.2  0.9  0.0)
   "Metal" "R.70"
)

(sdegeo:create-rectangle
  (position  5.2  0.8  0.0)
  (position  5.3  0.9  0.0)
   "Metal" "R.71"
)

(sdegeo:create-rectangle
  (position  5.3  0.8  0.0)
  (position  5.4  0.9  0.0)
   "Metal" "R.72"
)

;--------------------------row 10
(sdegeo:create-rectangle
  (position  4.6  0.9  0.0)
  (position  4.7  1.0  0.0)
   "Metal" "R.73"
)

(sdegeo:create-rectangle
  (position  4.7  0.9  0.0)
  (position  4.8  1.0  0.0)
   "Metal" "R.74"
)

(sdegeo:create-rectangle
  (position  4.8  0.9  0.0)
  (position  4.9  1.0  0.0)
   "Metal" "R.75"
)

(sdegeo:create-rectangle
  (position  4.9  0.9  0.0)
  (position  5.0  1.0  0.0)
   "Metal" "R.76"
```

```
)

(sdegeo:create-rectangle
  (position  5.0  0.9  0.0)
  (position  5.1  1.0  0.0)
   "Metal" "R.77"
)

(sdegeo:create-rectangle
  (position  5.1  0.9  0.0)
  (position  5.2  1.0  0.0)
   "Metal" "R.78"
)

(sdegeo:create-rectangle
  (position  5.2  0.9  0.0)
  (position  5.3  1.0  0.0)
   "Metal" "R.79"
)

(sdegeo:create-rectangle
  (position  5.3  0.9  0.0)
  (position  5.4  1.0  0.0)
   "Metal" "R.80"
)

;-------------------------- Create thermal contact region
(sdegeo:create-rectangle
  (position   L   0.0  0.0)
  (position  Lth   W   0.0)
   "Metal" "R.Thermal"
)

;--------------------------electromigration
(define test (find-body-id (position 5 0.1 0)) )
```

sde1_mid_dvs.cmd

sde1_mid_dvs.cmd is an empty text file. Subsequent *sde#_mid_dvs.cmd* files are created during the device model modification process.

sde0_end_dvs.cmd

```
;-----------------------------------------------------------------------
; Contact declarations
(sdegeo:define-contact-set "left"  ;- source_inn
  4.0  (color:rgb 0.0 1.0 0.0 ) "##"
)
```

```
(sdegeo:define-contact-set "right"  ;- source
  4.0  (color:rgb 0.0 0.0 1.0 ) "##"
)

(sdegeo:define-contact-set "thermal"  ;- Back_Thermal
  4.0  (color:rgb 1.0 0.0 0.0 ) "##"
)

;-----------------------------------------------------------------------
; Contact settings
(sdegeo:define-2d-contact
 (find-edge-id (position  0.0  Wmid  0.0))
 "left"
)

(sdegeo:define-2d-contact
 (find-edge-id (position   L   Wmid  0.0))
 "right"
)

(sdegeo:define-2d-contact
 (find-edge-id (position   Lth   Wmid  0.0))
 "thermal"
)

;-----------------------------------------------------------------------
; Saving BND file
(sdeio:save-tdr-bnd (get-body-list) "n0_bnd.tdr")

;-----------------------------------------------------------------------
; Profile
(sdedr:define-constant-profile
      "Const.Metal"
      "BoronActiveConcentration"
      1e0
)

(sdedr:define-constant-profile-region
      "PlaceCD.Metal"
      "Const.Metal"
      "Metal"
)

;-----------------------------------------------------------------------
; Mesh
(sdedr:define-refinement-size "RefDef.Metal" 0.1 0.1 0.1 0.1 )

(sdedr:define-refinement-material "PlaceRF.Metal" "RefDef.Metal"
"Metal" )

;-----------------------------------------------------------------------
; Save CMD file
(sdedr:write-cmd-file "n0_msh.cmd")
```

```
;-----------------------------------------------------------------------
; Build Mesh
(system:command "snmesh n0_msh")
```

B.1.3. Sentaurus Device command file

sdevice0_des.cmd

```
File {
    *- input
    Grid    = "n0_msh.tdr"
    Param   = "sdevice.par"

    *- output
    Current = "n0_des.plt"
    Plot    = "n0_des.tdr"
    Output  = "n0_des.log"
    Save    = "n0_des.sav"
}


Electrode {
      { Name = "left"         Voltage = 0.0 }
      { Name = "right"  Voltage = 0.0 }
}


Thermode {
      { Name = "thermal"      Temperature = 300 SurfaceResistance=5e-4
} *- T in C; surf res in (cm^3 * K / W)
}


Physics {
      Thermodynamic
      RecGenHeat
      Mobility(
            eHighFieldsaturation( GradQuasiFermi )
            hHighFieldsaturation( GradQuasiFermi )
            Enormal
      )
      Recombination(
            SRH( TempDependence )
      )
}


Plot {
      Temperature
      Current
      hCurrent
      eCurrent
      ConductionCurrent
```

```
      *--Density and Currents, etc
         eDensity hDensity
         TotalCurrent/Vector eCurrent/Vector hCurrent/Vector
         eMobility hMobility
         eVelocity hVelocity

      *--Temperature
         eTemperature hTemperature

      *--Fields and charges
         ElectricField/Vector Potential

      *--Generation/Recombination
         SRH
         AvalancheGeneration eAvalancheGeneration hAvalancheGeneration

      *--Driving forces
         eEparallel hEparallel eENormal hENormal
}


Math {
      Extrapolate
      RelErrControl
}


Solve {
      *- Buildup of initial solution:
      NewCurrentFile="init_"
      Coupled(Iterations=10){ Poisson }
      Coupled{ Poisson Electron Hole Temperature }

      *- bias left to target
      NewCurrentFile=""
      Quasistationary(
            InitialStep=0.01 Increment=1.35
            MinStep=1e-5 MaxStep=0.2
            Goal{ Name = "left"  Voltage = 1 }
      ){ Coupled{ Poisson Electron Hole Temperature }
      CurrentPlot(Time=(Range=(0 2) Intervals=20))
      }
}
```

B.1.4. Sentaurus Device parameter file

sdevice.par

```
HighFieldDependence:
{
   K_dT = 1e-3,  0.2
}
```

```
Material = "Metal" {
Resistivity {
Resist0 = 0.03 # [Ohm*cm].  0.08 here  = 800 as specified in .cmd file.
TempCoef = 0.0 # [1/K]
}
}
```

B.1.5. Tecplot macro

tdr2dat0.mcr

```
#!MC 1120
# Created by Tecplot 360 build 11.2-0-566
$!VarSet |MFBD| = '.'
$!READDATASET  "|MFBD|/n0_des.tdr"
  DATASETREADER = 'SWB-Loader'
$!WRITEDATASET  "|MFBD|/n0.dat"
  INCLUDETEXT = NO
  INCLUDEGEOM = NO
  INCLUDECUSTOMLABELS = NO
  ASSOCIATELAYOUTWITHDATAFILE = NO
  VARPOSITIONLIST =  [1-2,5] # 1=X, 2=Y, 4=LatticeTemperature,
5=TotalCurrentDensity
  BINARY = NO
  USEPOINTFORMAT = YES
  PRECISION = 9
$!RemoveVar |MFBD|
# $!QUIT
```

B.1.6. MATLAB files

DESSIS2COMSOLscript_bdc0.m

```
% Reads in data from TecPlot and interpolates onto a grid
% By Martha Gallivan, 26 July 2006
% Modified by Brad Christiansen, November 2010

datapath = '/'; %-bdc

Vd{4}='10V';

    fname = 'n0'; %-bdc

    datapath
    fname

    y = striptext_bdc(datapath,fname, [0:72]);

    A = importdata([fname '_notext.dat']);
```

```
    B = [];
    count = 1;
    for i = 1:length(A)
        if (A(i, 3) >= 1e5)
            B(count, 1) = A(i, 1);
            B(count, 2) = A(i, 2);
            count = count + 1;
        end
    end

    fid = fopen([fname '_xy.dat'],'w');
% if B is not empty do the following
    if not (isempty (B))
      for j = 1:length(B)
            fprintf(fid, '(define resp (find-body-id (position %6.4f
%6.4f 0)) ) \n', B(j,1), B(j,2));
            fprintf(fid, '(if (not (equal? test resp)) \n');
            fprintf(fid, '   (begin \n');
            fprintf(fid, '      (sdegeo:delete-region (list (car (find-
body-id (position %6.4f %6.4f 0))))) \n', B(j,1), B(j,2));
            fprintf(fid, '   ) \n');
            fprintf(fid, ') \n');
      end
   end
% otherwise, write an empty _xy.dat file

    quit
```

striptext_bdc.m

```
function y = striptext_bdc(pname,fname, reg)
% Input file name (.dat), reg is the list of regions to include in the
% new file
% By Martha Gallivan, 26 July 2006
% Modified by Brad Christiansen, November 2010

fid1 = fopen([pname fname '.dat'],'r');
fid2 = fopen([fname '_notext.dat'],'w');
tline = fgets(fid1);
while (tline ~= -1)
    if (tline(2:5) == 'Node') % for original data file
           nregstr = tline(8:14);
           for i = 7:-1:2
               if (nregstr(i) == ',')
                   nregstr = nregstr(1:i-1);
               end
           end
           nreg = str2num(nregstr);
    elseif (length(tline) >= 25)

        if (tline(2:25) == 'AUXDATA Tdr.Region.Index')
            upperIndex = length(tline)-2; % for original data file
            regnum = str2num(tline(28:upperIndex));
```

```
            if (ismember(regnum,reg))
            % Found a region in reg to write to the file
               %[regnum nreg]
               for i = 1:7
                  tline = fgets(fid1);
               end
               for i = 1:nreg
                    tline = fgets(fid1);
                    fprintf(fid2,'%s',tline);
               end
            end
        end
    end
    tline = fgets(fid1);
end

y = 1;
```

B.2. Data Processing

B.2.1. Unix scripts

all.sh

A Unix script of the following form was written to process the data from all channels. The code segment below was repeated and changed for each channel. Some channels did not have “245C” data.

```
cd Ch15-014/070C
./proc070_1.sh
cd ../245C
./proc245_1.sh
cd ../..
wait
```

proc070_1.sh

```
#! /bin/bash

# Remove spaces from file names.
for a in *\ *; do mv -i "$a" ${a// /_};done

# Remove .XLS extension
for i in `ls *.XLS`; do filename=`basename $i .XLS`; mv $i $filename;
done
```

```
# Create list of files.
ls -tr *.070.*.SS.SPADATA > list

# Process files with MATLAB.
matlab -r script7 &
```

proc245_1.sh

The only difference between the *proc070_1.sh* and *proc245_1.sh* files is “245” in place of “070” in the line beginning “ls”.

B.2.2. MATLAB files

script7.m

```
format long;

% Load list of filenames.
A = importdata('list');
A_length = length(A);

% Variables for checking for duplicate times.
old_hours_int = '-1';
count = 1;

% Preallocate memory.
TIME_VARY = zeros(A_length, 5);

for list_row = 1:(A_length)
    % Load data of file @ row list_row. File is tab-delimited. Look for
numbers after 23 lines.
    B = importdata(char(A(list_row,1)), '\t', 23);

    % Get elapsed time. Store entire elapsed-time line as string.
    timestr = char(B.textdata(6,1));
    % Get the ending index number of elapsed hours.
    i = 42;
    while (timestr(i) ~= 'H')
        i = i + 1;
    end
    % Change hours string to number.
    hours = str2num(timestr(42:(i-2)));

    % Change Id to mA/mm. Calculate gm and (Vg for gm).
    WORK = B.data;
    for i = 1:(length(WORK) - 1)
        WORK(i,5) = WORK(i,3) * 10 * 1000; % Id in mA/mm
```

```
        WORK(i,6) = (WORK(i,3) - WORK((i + 1),3)) / (WORK(i,2) -
WORK((i + 1),2)) * 10 * 1000; % gm
        WORK(i,7) = (WORK(i,2) + WORK((i + 1),2)) / 2; % Vg for gm
    end
    i = i + 1;
    WORK(i,5) = WORK(i,3) * 10 * 1000; % Id for last line.

    % Calculate gm2.
    WORK(1,8) = (((WORK(2,3) - WORK(1,3))) / ((WORK(2,2) - WORK(1,2))))
* 10 * 1000;
    [a] = lsf(3,1,WORK);
    WORK(2,8) = a;

    len_WORK = length(WORK);

    WORK(len_WORK,8) = (((WORK(len_WORK,3) - WORK(len_WORK-1,3))) /
((WORK(len_WORK,2) - WORK(len_WORK-1,2)))) * 10 * 1000;
    [a] = lsf(3,len_WORK-2,WORK);
    WORK(len_WORK-1,8) = a;

    for j = (3:1:len_WORK - 2)
        [a] = lsf(5,j-2,WORK);
        WORK(j,8) = a;
    end

    % Get gmp and row number of gmp.
    [gmp,gmp_index] = max(WORK(1:length(WORK),6));
    % Calculate Vt.
    Vt = WORK(gmp_index,2) - (WORK(gmp_index,3) / (gmp/10/1000));
    % Get Idmax.
    Idmax = WORK(1,3);
    % Get Idss.
    if length(WORK) == 19
        Idss = WORK(4,3);
    elseif length(WORK) == 25
        Idss = WORK(5,3);
    end
    % Get gmp2 and row number of gmp2.
    [gmp2,gmp2_index] = max(WORK(1:length(WORK),8));
    % Calculate difference between gmp and gmp2.
    gmp_diff = gmp - gmp2;
    % Calculate Vt2.
    Vt2 = WORK(gmp2_index,2) - (WORK(gmp2_index,3) / (gmp2/10/1000));
    % Calculate difference between Vt and Vt2.
    Vt_diff = Vt - Vt2;

    % Check for duplicate timestamps.  Save processed files with
different names.
    hours_int = sprintf('%04u', round(hours));
    if strcmp(old_hours_int, hours_int)
        count_int = sprintf('%u', count);
        fname = ['xfer.' hours_int '-' count_int '.xls'];
        count = count + 1;
    else
        fname = ['xfer.' hours_int '-0.xls'];
```

```
    end
    old_hours_int = hours_int;

    % Save processed file with header data.
    fid_xf = fopen(fname, 'w');
    fprintf(fid_xf, '%s\t%f\n', 'Time', hours);
    fprintf(fid_xf, '%s\t%s\t%s\t%s\t%s\t%s\t%s\t%s\n', 'VBias1',
'VBias2', 'IBias1', 'IBias2', 'Id', 'gm', 'Vg for gm', 'gm2');
    fprintf(fid_xf, '%f\t%f\t%f\t%f\t%f\t%f\t%f\t%f\n', WORK');
    fclose(fid_xf);

    % Write elapsed time, gmp, Vt, Idmax, and Idss to matrix.
    TIME_VARY(list_row,1) = hours;
    TIME_VARY(list_row,2) = gmp;
    TIME_VARY(list_row,3) = Vt;
    TIME_VARY(list_row,4) = Idmax;
    TIME_VARY(list_row,5) = Idss;
    TIME_VARY(list_row,6) = gmp2;
    TIME_VARY(list_row,7) = gmp_diff;
    TIME_VARY(list_row,8) = Vt2;
    TIME_VARY(list_row,9) = Vt_diff;

end

% Save TIME_VARY matrix with header data.
fid_tv = fopen('time_vary.xls', 'w');
fprintf(fid_tv, '%s\t%s\t%s\t%s\t%s\t%s\t%s\t%s\t%s\n', 'Time', 'gmp',
'Vt', 'Idmax', 'Idss', 'gmp2', 'gmp_diff', 'Vt2', 'Vt_diff');
fprintf(fid_tv, '%f\t%f\t%f\t%f\t%f\t%f\t%f\t%f\t%f\n', TIME_VARY');
fclose(fid_tv);
```

lsf.m

```
% Original algorithm written in C by Ross Dettmer
% Modified and written for MATLAB by Brad Christiansen

function [a] = lsf(num, beg, A)
      cps=0;
      xss=0;
      xs=0;
      ys=0;

      for i=beg:1:(beg + num - 1)
          xs = xs + A(i,2);
          ys = ys + A(i,3);
          xss = xss + (A(i,2) * A(i,2));
          cps = cps + (A(i,2) * A(i,3));
      end

        den = (num*xss - xs*xs);
        if (den > 0.000)
              a = ((num*cps - xs*ys)/den) * 10 * 1000;
      else
```

```
                a = 0.00;
        end
end
```

B.3. Voltage step-stress Excel macro

```
Sub BradsMacro()
' by Brad Christiansen
' using calls originally written by Eric Heller

'Init Vg
Vg_iv_start = -6
Vg_iv_end = 1
Vg_idvg_step = 0.25
Vg_stress = -10

'Init Vd
Vd_iv_end = 10
Vd_stress_start = 50
Vd_stress_end = 200
Vd_stress_step = 10

'Init compliances
QS_C_Drain = 0.05
QS_C_Drain_iv = 1
QS_C_Gate = 0.01

Number_of_Datas = 30
QS_WaitTime = 60 'minutes

'Init Agilent
Call ClearAgilent

'init variables
Dim udGPIB0 As Integer
Dim udDevice As Integer
Dim iDeviceNumber As Integer
Dim sBuffer As String

'get device address from worksheet
iDeviceNumber = 12

'get unit descriptors
Call ibfind("GPIB0", udGPIB0)
Call ibdev(0, iDeviceNumber, 0, 10, 1, 10, udDevice)

'get system control by sending interface clear
Call ibsic(udGPIB0)

' Set D/A to high resolution mode for both channels.
Call ibwrt(udDevice, "AAD 1,1" & Chr(13) & Chr(10))
Call ibwrt(udDevice, "AAD 2,1" & Chr(13) & Chr(10))
```

```
Call ibwrt(udDevice, "CN" & Chr(13) & Chr(10))


'counter for MacroSheet data
stress_count = 27

'Outer loop
i = Vd_stress_start - Vd_stress_step    ' i is Stress drain bias
Do While i < Vd_stress_end
i = i + Vd_stress_step

    'Id-Vg
    Count = 1

    'Set Vd to Vd_iv_end
    Call ibwrt(udDevice, "DV2,0," & Vd_iv_end & "," & QS_C_Drain_iv &
Chr(13) & Chr(10))

        'Ramp Vg
        k = Vg_iv_start - Vg_idvg_step    ' k is Id-Vg gate bias
        Do While k < Vg_iv_end
        k = k + Vg_idvg_step
        Count = Count + 1

        'Set Vg
        Call ibwrt(udDevice, "DV1,0," & k & "," & QS_C_Gate & Chr(13) &
Chr(10))

        'Wait one second
        Application.Wait (Now + TimeValue("0:00:01"))

        'read time and store it
        Worksheets("IdVg pre " & i).Range("E" & Count).value = Now

        'read Drain voltage
        Call ibwrt(udDevice, "BC" & Chr(13) & Chr(10))
        Call ibwrt(udDevice, "FMT1" & Chr(13) & Chr(10))
        Call ibwrt(udDevice, "TV2,0" & Chr(13) & Chr(10))
        'read response and store in sBuffer
        sBuffer = Space$(100)
        Call ibrd(udDevice, sBuffer)
        Worksheets("IdVg pre " & i).Range("A" & Count).value =
Mid(sBuffer, 4, 12)

        'read Gate voltage
        Call ibwrt(udDevice, "BC" & Chr(13) & Chr(10))
        Call ibwrt(udDevice, "FMT1" & Chr(13) & Chr(10))
        Call ibwrt(udDevice, "TV1,0" & Chr(13) & Chr(10))
        'read response and store in sBuffer
        sBuffer = Space$(100)
        Call ibrd(udDevice, sBuffer)
        Worksheets("IdVg pre " & i).Range("B" & Count).value =
Mid(sBuffer, 4, 12)
```

```
        'read Drain current
        Call ibwrt(udDevice, "BC" & Chr(13) & Chr(10))
        Call ibwrt(udDevice, "FMT1" & Chr(13) & Chr(10))
        Call ibwrt(udDevice, "TI2,0" & Chr(13) & Chr(10))
        'Read response and store in sBuffer
        sBuffer = Space$(100)
        Call ibrd(udDevice, sBuffer)
        Worksheets("IdVg pre " & i).Range("C" & Count).value =
Mid(sBuffer, 4, 12) * 1000

        'read Gate current
        Call ibwrt(udDevice, "BC" & Chr(13) & Chr(10))
        Call ibwrt(udDevice, "FMT1" & Chr(13) & Chr(10))
        Call ibwrt(udDevice, "TI1,0" & Chr(13) & Chr(10))
        'Read response and store in sBuffer
        sBuffer = Space$(100)
        Call ibrd(udDevice, sBuffer)
        Worksheets("IdVg pre " & i).Range("D" & Count).value =
Mid(sBuffer, 4, 12) * 1000000

        'TEST
        Worksheets("IdVg pre " & i).Range("F" & Count).value = ("Test-"
& k)

        Sheets("IdVg pre " & i).Select
        Application.Goto Reference:=("R" & Count & "C1")

        'Id-Vg - Vg Ramp
        Loop


'Set Vd to 0V
Call ibwrt(udDevice, "DV2,0,0," & QS_C_Drain_iv & Chr(13) & Chr(10))

'Set Vg to 0V
Call ibwrt(udDevice, "DV1,0,0," & QS_C_Gate & Chr(13) & Chr(10))

'Wait one minute
Application.Wait (Now + TimeValue("0:01:00"))


    'Ig measurement

    'Set Vg to -10V
    Call ibwrt(udDevice, "DV1,0,-10," & QS_C_Gate & Chr(13) & Chr(10))

    'Set Vd to 40
    Call ibwrt(udDevice, "DV2,0,40," & QS_C_Drain_iv & Chr(13) &
Chr(10))

    ig_step = 1
    Do While ig_step < 62
    ig_step = ig_step + 1

        'read time and store it
```

```
        Worksheets("Ig pre " & i).Range("E" & ig_step).value = Now

        'read Drain voltage
        Call ibwrt(udDevice, "BC" & Chr(13) & Chr(10))
        Call ibwrt(udDevice, "FMT1" & Chr(13) & Chr(10))
        Call ibwrt(udDevice, "TV2,0" & Chr(13) & Chr(10))
        'read response and store in sBuffer
        sBuffer = Space$(100)
        Call ibrd(udDevice, sBuffer)
        Worksheets("Ig pre " & i).Range("A" & ig_step).value =
Mid(sBuffer, 4, 12)

        'read Gate voltage
        Call ibwrt(udDevice, "BC" & Chr(13) & Chr(10))
        Call ibwrt(udDevice, "FMT1" & Chr(13) & Chr(10))
        Call ibwrt(udDevice, "TV1,0" & Chr(13) & Chr(10))
        'read response and store in sBuffer
        sBuffer = Space$(100)
        Call ibrd(udDevice, sBuffer)
        Worksheets("Ig pre " & i).Range("B" & ig_step).value =
Mid(sBuffer, 4, 12)

        'read Drain current
        Call ibwrt(udDevice, "BC" & Chr(13) & Chr(10))
        Call ibwrt(udDevice, "FMT1" & Chr(13) & Chr(10))
        Call ibwrt(udDevice, "TI2,0" & Chr(13) & Chr(10))
        'Read response and store in sBuffer
        sBuffer = Space$(100)
        Call ibrd(udDevice, sBuffer)
        Worksheets("Ig pre " & i).Range("C" & ig_step).value =
Mid(sBuffer, 4, 12) * 1000

        'read Gate current
        Call ibwrt(udDevice, "BC" & Chr(13) & Chr(10))
        Call ibwrt(udDevice, "FMT1" & Chr(13) & Chr(10))
        Call ibwrt(udDevice, "TI1,0" & Chr(13) & Chr(10))
        'Read response and store in sBuffer
        sBuffer = Space$(100)
        Call ibrd(udDevice, sBuffer)
        Worksheets("Ig pre " & i).Range("D" & ig_step).value =
Mid(sBuffer, 4, 12) * 1000000

        'TEST
        Worksheets("Ig pre " & i).Range("F" & ig_step).value = ("Test-"
& k)

        Sheets("Ig pre " & i).Select
        Application.Goto Reference:=("R" & ig_step & "C1")

        'Wait one second
        Application.Wait (Now + TimeValue("0:00:01"))

        'Ig
        Loop
```

```
'Set Vd to 0V
Call ibwrt(udDevice, "DV2,0,0," & QS_C_Drain_iv & Chr(13) & Chr(10))

'Set Vg to 0V
Call ibwrt(udDevice, "DV1,0,0," & QS_C_Gate & Chr(13) & Chr(10))

'Wait one minute
Application.Wait (Now + TimeValue("0:01:00"))


'Do stress
'Set Vg to Vg_stress
Call ibwrt(udDevice, "DV1,0," & Vg_stress & "," & QS_C_Gate & Chr(13) &
Chr(10))

'Set Vd to i
Call ibwrt(udDevice, "DV2,0," & i & "," & QS_C_Drain & Chr(13) &
Chr(10))

Sheets("MacroSheet").Select

    'Begin process of collecting multiple data points at each stress
level
    j = 0
    Do While j < (Number_of_Datas)
    j = j + 1
    stress_count = stress_count + 1

    'Wait for duration of data point collection step: (QS_WaitTime /
Number_of_Datas) seconds
    newYear = Year(Now())
    newMonth = Month(Now())
    newDay = Day(Now())
    newHour = Hour(Now())
    newMinute = Minute(Now())
    newSecond = Second(Now()) + QS_WaitTime * 60 / Number_of_Datas
    waitTime = DateSerial(newYear, newMonth, newDay) +
TimeSerial(newHour, newMinute, newSecond)
    Application.Wait waitTime

    Worksheets("MacroSheet").Range("H" & stress_count).value = j

    'Store time of measurements
    Worksheets("MacroSheet").Range("G" & stress_count).value = Now

    ' Store voltages of this measurement.  Get them from the Agilent.
    ' Read Drain Voltage from Agilent
    Call ibwrt(udDevice, "BC" & Chr(13) & Chr(10))
    Call ibwrt(udDevice, "FMT1" & Chr(13) & Chr(10))
    Call ibwrt(udDevice, "TV2,0" & Chr(13) & Chr(10))
    'read response and store in sBuffer
    sBuffer = Space$(100)
    Call ibrd(udDevice, sBuffer)
```

```
    Worksheets("MacroSheet").Range("A" & stress_count).value =
Mid(sBuffer, 4, 12)

    ' Read Gate Voltage from Agilent
    Call ibwrt(udDevice, "BC" & Chr(13) & Chr(10))
    Call ibwrt(udDevice, "FMT1" & Chr(13) & Chr(10))
    Call ibwrt(udDevice, "TV1,0" & Chr(13) & Chr(10))
    'read response and store in sBuffer
    sBuffer = Space$(100)
    Call ibrd(udDevice, sBuffer)
    Worksheets("MacroSheet").Range("B" & stress_count).value =
Mid(sBuffer, 4, 12)

    'Read Drain Current
    Call ibwrt(udDevice, "BC" & Chr(13) & Chr(10))
    Call ibwrt(udDevice, "FMT1" & Chr(13) & Chr(10))
    Call ibwrt(udDevice, "TI2,0" & Chr(13) & Chr(10))
    'Read response and store in sBuffer
    sBuffer = Space$(100)
    Call ibrd(udDevice, sBuffer)
    'Display response in appropriate cell
    Worksheets("MacroSheet").Range("C" & stress_count).value = sBuffer
    Worksheets("MacroSheet").Range("D" & stress_count).value =
Mid(sBuffer, 4, 12) * 1000

    'Read Gate Current
    Call ibwrt(udDevice, "BC" & Chr(13) & Chr(10))
    Call ibwrt(udDevice, "FMT1" & Chr(13) & Chr(10))
    Call ibwrt(udDevice, "TI1,0" & Chr(13) & Chr(10))
    'Read response and store in sBuffer
    sBuffer = Space$(100)
    Call ibrd(udDevice, sBuffer)
    'Display response in appropriate cell
    Worksheets("MacroSheet").Range("E" & stress_count).value = sBuffer
    Worksheets("MacroSheet").Range("F" & stress_count).value =
Mid(sBuffer, 4, 12) * 1000000

    Application.Goto Reference:=("R" & stress_count & "C1")

    'end data point collection
    Loop


'Set Vd to 0
Call ibwrt(udDevice, "DV2,0,0," & QS_C_Drain_iv & Chr(13) & Chr(10))

'Set Vg to 0V
Call ibwrt(udDevice, "DV1,0,0," & QS_C_Gate & Chr(13) & Chr(10))

'Wait one minute
Application.Wait (Now + TimeValue("0:01:00"))


stress_count = stress_count + 1
```

```
'End outer loop
Loop


'Do final Id-Vg
    Count = 1

    'Set Vd to Vd_iv_end
    Call ibwrt(udDevice, "DV2,0," & Vd_iv_end & "," & QS_C_Drain_iv &
Chr(13) & Chr(10))

        'Ramp Vg
        k = Vg_iv_start - Vg_idvg_step    ' k is Id-Vg gate bias
        Do While k < Vg_iv_end
        k = k + Vg_idvg_step
        Count = Count + 1

        'Set Vg
        Call ibwrt(udDevice, "DV1,0," & k & "," & QS_C_Gate & Chr(13) &
Chr(10))

        'Wait one second
        Application.Wait (Now + TimeValue("0:00:01"))

        'read time and store it
        Worksheets("IdVg end").Range("E" & Count).value = Now

        'read Drain voltage
        Call ibwrt(udDevice, "BC" & Chr(13) & Chr(10))
        Call ibwrt(udDevice, "FMT1" & Chr(13) & Chr(10))
        Call ibwrt(udDevice, "TV2,0" & Chr(13) & Chr(10))
        'read response and store in sBuffer
        sBuffer = Space$(100)
        Call ibrd(udDevice, sBuffer)
        Worksheets("IdVg end").Range("A" & Count).value = Mid(sBuffer,
4, 12)

        'read Gate voltage
        Call ibwrt(udDevice, "BC" & Chr(13) & Chr(10))
        Call ibwrt(udDevice, "FMT1" & Chr(13) & Chr(10))
        Call ibwrt(udDevice, "TV1,0" & Chr(13) & Chr(10))
        'read response and store in sBuffer
        sBuffer = Space$(100)
        Call ibrd(udDevice, sBuffer)
        Worksheets("IdVg end").Range("B" & Count).value = Mid(sBuffer,
4, 12)

        'read Drain current
        Call ibwrt(udDevice, "BC" & Chr(13) & Chr(10))
        Call ibwrt(udDevice, "FMT1" & Chr(13) & Chr(10))
        Call ibwrt(udDevice, "TI2,0" & Chr(13) & Chr(10))
        'Read response and store in sBuffer
        sBuffer = Space$(100)
        Call ibrd(udDevice, sBuffer)
```

```
        Worksheets("IdVg end").Range("C" & Count).value = Mid(sBuffer,
4, 12) * 1000

        'read Gate current
        Call ibwrt(udDevice, "BC" & Chr(13) & Chr(10))
        Call ibwrt(udDevice, "FMT1" & Chr(13) & Chr(10))
        Call ibwrt(udDevice, "TI1,0" & Chr(13) & Chr(10))
        'Read response and store in sBuffer
        sBuffer = Space$(100)
        Call ibrd(udDevice, sBuffer)
        Worksheets("IdVg end").Range("D" & Count).value = Mid(sBuffer,
4, 12) * 1000000

        'TEST
        Worksheets("IdVg end").Range("F" & Count).value = ("Test-" & k)

        Sheets("IdVg end").Select
        Application.Goto Reference:=("R" & Count & "C1")

        'Final Id-Vg - Vg Ramp
        Loop


'Set Vd to 0V
Call ibwrt(udDevice, "DV2,0,0," & QS_C_Drain_iv & Chr(13) & Chr(10))

'Set Vg to 0V
Call ibwrt(udDevice, "DV1,0,0," & QS_C_Gate & Chr(13) & Chr(10))

'Wait one minute
Application.Wait (Now + TimeValue("0:01:00"))


    'Do final Ig measurement

    'Set Vg to -10V
    Call ibwrt(udDevice, "DV1,0,-10," & QS_C_Gate & Chr(13) & Chr(10))

    'Set Vd to 40
    Call ibwrt(udDevice, "DV2,0,40," & QS_C_Drain_iv & Chr(13) &
Chr(10))

    ig_step = 1
    Do While ig_step < 62
    ig_step = ig_step + 1

        'read time and store it
        Worksheets("Ig end").Range("E" & ig_step).value = Now

        'read Drain voltage
        Call ibwrt(udDevice, "BC" & Chr(13) & Chr(10))
        Call ibwrt(udDevice, "FMT1" & Chr(13) & Chr(10))
        Call ibwrt(udDevice, "TV2,0" & Chr(13) & Chr(10))
        'read response and store in sBuffer
        sBuffer = Space$(100)
```

```
        Call ibrd(udDevice, sBuffer)
        Worksheets("Ig end").Range("A" & ig_step).value = Mid(sBuffer,
4, 12)

        'read Gate voltage
        Call ibwrt(udDevice, "BC" & Chr(13) & Chr(10))
        Call ibwrt(udDevice, "FMT1" & Chr(13) & Chr(10))
        Call ibwrt(udDevice, "TV1,0" & Chr(13) & Chr(10))
        'read response and store in sBuffer
        sBuffer = Space$(100)
        Call ibrd(udDevice, sBuffer)
        Worksheets("Ig end").Range("B" & ig_step).value = Mid(sBuffer,
4, 12)

        'read Drain current
        Call ibwrt(udDevice, "BC" & Chr(13) & Chr(10))
        Call ibwrt(udDevice, "FMT1" & Chr(13) & Chr(10))
        Call ibwrt(udDevice, "TI2,0" & Chr(13) & Chr(10))
        'Read response and store in sBuffer
        sBuffer = Space$(100)
        Call ibrd(udDevice, sBuffer)
        Worksheets("Ig end").Range("C" & ig_step).value = Mid(sBuffer,
4, 12) * 1000

        'read Gate current
        Call ibwrt(udDevice, "BC" & Chr(13) & Chr(10))
        Call ibwrt(udDevice, "FMT1" & Chr(13) & Chr(10))
        Call ibwrt(udDevice, "TI1,0" & Chr(13) & Chr(10))
        'Read response and store in sBuffer
        sBuffer = Space$(100)
        Call ibrd(udDevice, sBuffer)
        Worksheets("Ig end").Range("D" & ig_step).value = Mid(sBuffer,
4, 12) * 1000000

        'TEST
        Worksheets("Ig end").Range("F" & ig_step).value = ("Test-" & k)

        Sheets("Ig end").Select
        Application.Goto Reference:=("R" & ig_step & "C1")

        'Wait one second
        Application.Wait (Now + TimeValue("0:00:01"))

        'Ig
        Loop


'take device handles offline for cleanup
Call ibonl(udGPIB0, 0)
Call ibonl(udDevice, 0)

' Need to power off the device.
Call ClearAgilent

'Copies plot data to "IV data" sheet.
```

```
    Sheets("IV Data").Select
    Range("A3:D503").Select
    Selection.ClearContents

    Sheets("MacroSheet").Select
    Range("A28:B" & stress_count).Select
    Selection.Copy
    Sheets("IV Data").Select
    Range("A3:B" & (stress_count - 25)).Select
    Selection.PasteSpecial Paste:=xlPasteValues, Operation:=xlNone,
SkipBlanks _
        :=False, Transpose:=False

    Sheets("MacroSheet").Select
    Range("D28:D" & stress_count).Select
    Selection.Copy
    Sheets("IV Data").Select
    Range("C3:C" & (stress_count - 25)).Select
    Selection.PasteSpecial Paste:=xlPasteValues, Operation:=xlNone,
SkipBlanks _
        :=False, Transpose:=False

    Sheets("MacroSheet").Select
    Range("F28:G" & stress_count).Select
    Selection.Copy
    Sheets("IV Data").Select
    Range("D3:E" & (stress_count - 25)).Select
    Selection.PasteSpecial Paste:=xlPasteValues, Operation:=xlNone,
SkipBlanks _
        :=False, Transpose:=False


End Sub
```

An Excel macro similar to the one above was used for step-stressing in a manner similar to that used by del Alamo's group.

B.4. Accel-RF test sequence

_2X50_245C_VD17.5_VG3_200HRS.SEQ

```
1;    SPA Test; Definition File = \_2x50_Gate Leakage Vd=0 to 10V, Vg=-
7V.SPA; Temp = 70.00; Output File Prefix = _2x50_Gate Leakage Vd=0 to
10V, Vg=-7V_pre1

2;    SPA Test; Definition File = \_2x50_Gate Leakage Vd=0 to 10V, Vg=-
7V.SPA; Temp = 70.00; Output File Prefix = _2x50_Gate Leakage Vd=0 to
10V, Vg=-7V_pre2
```

3;   SPA Test; Definition File = _2x50_Gate Leakage Vd=0 to 10V, Vg=-7V.SPA; Temp = 70.00; Output File Prefix = _2x50_Gate Leakage Vd=0 to 10V, Vg=-7V_pre3

4;   SPA Test; Definition File = _2x50_Transconductance Vg=1 to -5V 25 steps, Vd=10V.SPA; Temp = 70.00; Output File Prefix = _2x50_Transconductance Vg=1 to -5V 25 steps, Vd=10V_Pre

5;   SPA Test; Definition File = _2x50_IV_VG=1 TO -5V 7 STEPS, VD=0 TO 10V, hi-power.SPA; Temp = 70.00; Output File Prefix = _2x50_IV_VG=1 TO -5V 7 STEPS, VD=0 TO 10V, hi-power_Pre

6;   SPA Test; Definition File = _2x50_Transconductance Vg=1 to -5V 25 steps, Vd=10V.SPA; Temp = 245.00; Output File Prefix = _2x50_Transconductance Vg=1 to -5V 25 steps, Vd=10V_loop0

7;   For i = 1 to 200

8;   Stress Test; Duration = 0 01:00:00; Temp = 245.00; Limits File = DEFAULT & "LIMITS.245"; Stimulus File = DEFAULT & "STIMULUS.245"

9;   SPA Test; Definition File = _2x50_Transconductance Vg=1 to -5V 25 steps, Vd=10V.SPA; Temp = 245.00; Output File Prefix = _2x50_Transconductance Vg=1 to -5V 25 steps, Vd=10V_loop1

10;   Next

11;   SPA Test; Definition File = _2x50_Gate Leakage Vd=0 to 10V, Vg=-7V.SPA; Temp = 70.00; Output File Prefix = _2x50_Gate Leakage Vd=0 to 10V, Vg=-7V_post1

12;   SPA Test; Definition File = _2x50_Gate Leakage Vd=0 to 10V, Vg=-7V.SPA; Temp = 70.00; Output File Prefix = _2x50_Gate Leakage Vd=0 to 10V, Vg=-7V_post2

13;   SPA Test; Definition File = _2x50_Gate Leakage Vd=0 to 10V, Vg=-7V.SPA; Temp = 70.00; Output File Prefix = _2x50_Gate Leakage Vd=0 to 10V, Vg=-7V_post3

14;   SPA Test; Definition File = _2x50_Transconductance Vg=1 to -5V 25 steps, Vd=10V.SPA; Temp = 70.00; Output File Prefix = _2x50_Transconductance Vg=1 to -5V 25 steps, Vd=10V_POST
15;   SPA Test; Definition File = _2x50_IV_VG=1 TO -5V 7 STEPS, VD=0 TO 10V, hi-power.SPA; Temp = 70.00; Output File Prefix = _2x50_IV_VG=1 TO -5V 7 STEPS, VD=0 TO 10V, hi-power_POST

_2x50_Gate Leakage Vd=0 to 10V, Vg=-7V.SPA

```
SPA Configuration:
Date Created: 5/14/2010 10:17:38 AM
BiasSequence = 0
ActiveBias = No
ControllingSource = Bias1
```

```
MeasurementType = StaircaseSweep
Bias1SourceModule = SMU
Bias1SourceMode = Voltage
Bias1Target = 0.000000E+00
Bias1Compliance = 5.000000E-01
Bias1PowerCompliance = 1.000000E+00
Bias1StartTarget = 0.000000E+00
Bias1StopTarget = 1.000000E+01
Bias1BaseTarget = 0.000000E+00
Bias1HoldTime = 0.000000E+00
Bias1DelayTime = 0.000000E+00
Bias1PulseWidth = 1.000000E-03
Bias1PulsePeriod = 1.000000E-02
Bias1NumSteps = 31
Bias1MeasurementMode = 1
Bias1Range = 0
Bias1SweepMode = Single
Bias1IncrementMode = Linear
Bias1Step = 0.000000E+00
Bias2SourceModule = SMU
Bias2SourceMode = Constant V
Bias2Target = 0.000000E+00
Bias2Compliance = 5.000000E-02
Bias2PowerCompliance = 2.000000E-01
Bias2StartTarget = -7.000000E+00
Bias2StopTarget = -6.000000E+00
Bias2BaseTarget = -2.000000E-01
Bias2HoldTime = 0.000000E+00
Bias2DelayTime = 0.000000E+00
Bias2PulseWidth = 1.000000E-03
Bias2PulsePeriod = 1.000000E-02
Bias2NumSteps = 3
Bias2MeasurementMode = 1
Bias2Range = 0
Bias2SweepMode = Single
Bias2IncrementMode = Linear
Bias2Step = 0.000000E+00
Title = Staircase Sweep
controllingVar = VBias1
xVar = VBias1
yVar = IBias2
VBias1Label = VD
VBias2Label = VG
IBias1Label = ID
IBias2Label = IG
IntegrationType = Auto
IntegrationValue = 1.000000E+03
```

_2x50_Transconductance Vg=1 to -5V 25 steps, Vd=10V.SPA

```
SPA Configuration:
Date Created: 8/9/2010 6:29:32 PM
BiasSequence = 0
```

```
ActiveBias = No
ControllingSource = Bias2
MeasurementType = StaircaseSweep
Bias1SourceModule = SMU
Bias1SourceMode = Constant V
Bias1Target = 0.000000E+00
Bias1Compliance = 1.000000E+00
Bias1PowerCompliance = 3.000000E+00
Bias1StartTarget = 1.000000E+01
Bias1StopTarget = 1.000000E+01
Bias1BaseTarget = 0.000000E+00
Bias1HoldTime = 0.000000E+00
Bias1DelayTime = 0.000000E+00
Bias1PulseWidth = 1.000000E-03
Bias1PulsePeriod = 1.000000E-03
Bias1NumSteps = 31
Bias1MeasurementMode = 1
Bias1Range = 0
Bias1SweepMode = Single
Bias1IncrementMode = Linear
Bias1Step = 3.333333E-01
Bias2SourceModule = SMU
Bias2SourceMode = Voltage
Bias2Target = 0.000000E+00
Bias2Compliance = 5.000000E-02
Bias2PowerCompliance = 2.000000E-01
Bias2StartTarget = 1.000000E+00
Bias2StopTarget = -5.000000E+00
Bias2BaseTarget = -6.000000E+00
Bias2HoldTime = 0.000000E+00
Bias2DelayTime = 0.000000E+00
Bias2PulseWidth = 1.000000E-03
Bias2PulsePeriod = 1.000000E-03
Bias2NumSteps = 25
Bias2MeasurementMode = 1
Bias2Range = 0
Bias2SweepMode = Single
Bias2IncrementMode = Linear
Bias2Step = -1.000000E+00
Title = Staircase Sweep
controllingVar = VBias2
xVar = VBias2
yVar = IBias1
VBias1Label = VD
VBias2Label = VG
IBias1Label = ID
IBias2Label = IG
IntegrationType = Auto
IntegrationValue = 1.000000E+02
```

_2x50_IV_VG=1 TO -5V 7 STEPS, VD=0 TO 10V, hi-power.SPA

```
SPA Configuration:
```

```
Date Created: 9/15/2010 3:15:02 PM
BiasSequence = 0
ActiveBias = No
ControllingSource = Bias2
MeasurementType = TransistorSweep
Bias1SourceModule = SMU
Bias1SourceMode = Voltage
Bias1Target = 0.000000E+00
Bias1Compliance = 1.500000E+00
Bias1PowerCompliance = 3.000000E+01
Bias1StartTarget = 0.000000E+00
Bias1StopTarget = 1.000000E+01
Bias1BaseTarget = 0.000000E+00
Bias1HoldTime = 0.000000E+00
Bias1DelayTime = 0.000000E+00
Bias1PulseWidth = 1.000000E-03
Bias1PulsePeriod = 1.000000E-03
Bias1NumSteps = 19
Bias1MeasurementMode = 1
Bias1Range = 0
Bias1SweepMode = Single
Bias1IncrementMode = Linear
Bias1Step = 5.555556E-01
Bias2SourceModule = SMU
Bias2SourceMode = Voltage
Bias2Target = 0.000000E+00
Bias2Compliance = 5.000000E-02
Bias2PowerCompliance = 1.000000E+01
Bias2StartTarget = 1.000000E+00
Bias2StopTarget = -5.000000E+00
Bias2BaseTarget = -6.000000E+00
Bias2HoldTime = 0.000000E+00
Bias2DelayTime = 0.000000E+00
Bias2PulseWidth = 1.000000E-03
Bias2PulsePeriod = 1.000000E-03
Bias2NumSteps = 7
Bias2MeasurementMode = 1
Bias2Range = 0
Bias2SweepMode = Single
Bias2IncrementMode = Linear
Bias2Step = -1.000000E+00
Title = Staircase Sweep
controllingVar = VBias2
xVar = VBias1
yVar = IBias1
VBias1Label = VD
VBias2Label = VG
IBias1Label = ID
IBias2Label = IG
IntegrationType = Auto
IntegrationValue = 1.000000E+02
```

Appendix C. Data Tables

The following tables present the degradation data for each device, as well as the averages (Avg) and standard deviations (Stdev). The titles contain references to the corresponding tables in the main text.

TABLE 24. ABSOLUTE PERCENTAGE CHANGES IN PARAMETERS AFTER 300 HOURS (SEE TABLE 4)

Condition	Device	g_{mp}			V_T			I_{Dmax}			I_{DSS}			R_{on}		
		%	**Avg**	**Stdev**	**%**	**Avg**	**Stdev**	**%**	**Avg**	**Stdev**	**%**	**Avg**	**Stdev**	**%**	**Avg**	**Stdev**
	55-006	2.01%			8.44%			7.88%			10.1%			7.44%		
1	56-007	0.82%	1.68%	0.75%	11.5%	10.8%	2.04%	8.58%	8.80%	1.05%	11.9%	11.8%	1.77%	7.86%	8.06%	0.74%
	57-008	2.22%			12.3%			9.95%			13.6%			8.88%		
	58-009	1.68%			12.5%			11.6%			14.2%			13.4%		
2	59-010	3.07%	1.98%	0.98%	10.9%	10.9%	1.64%	12.1%	10.9%	1.69%	14.1%	13.2%	1.73%	13.9%	12.2%	2.52%
	60-011	1.18%			9.25%			8.95%			11.2%			9.33%		
	28-003	4.47%			21.7%			18.3%			24.6%			18.2%		
3	29-004[a]		3.53%	1.33%		19.4%	3.19%		15.7%	3.74%		21.5%	4.49%		15.4%	3.90%
	30-005	2.59%			17.1%			13.0%			18.3%			12.7%		
	31-7632	3.60%			5.79%			7.59%			8.88%			2.66%		
4	32-7650[b]		3.45%	0.20%		5.95%	0.24%		4.51%	4.36%		5.09%	5.36%		3.78%	1.59%
	33-002	3.31%			6.12%			1.43%			1.31%			4.90%		
	25-7579	6.94%			2.33%			9.10%			9.25%			6.52%		
6	26-7577	2.44%	4.53%	2.27%	4.27%	6.05%	4.86%	5.62%	5.15%	4.21%	6.39%	7.08%	1.93%	3.12%	5.21%	1.83%
	27-001	4.20%			11.6%			0.72%			5.59%			5.99%		

[a] 29-004 reached the pre-determined failure criteria for I_D at 133 hours.

[b] 32-7650 apparently suffered infant mortality before 100 hours.

TABLE 25. PARAMETER CHANGES BY DEVICE AND CONDITION IN 300-HOUR TEST (SEE TABLE 6)

Condition	Device	g_{mp}			V_T			I_{Dmax}			I_{DSS}		
		%	Avg	Stdev	mV	Avg	Stdev	%	Avg	Stdev	%	Avg	Stdev
1	55-006	-2.37%	-2.05%	0.74%	253	309	56.0	-7.9%	-8.83%	1.07%	-10.1%	-11.9%	1.75%
	56-007	-1.20%			310			-8.6%			-11.9%		
	57-008	-2.57%			365			-10.0%			-13.6%		
2	58-009	-2.29%	-2.48%	0.94%	316	297	29.5	-11.6%	-10.9%	1.66%	-14.2%	-13.2%	1.70%
	59-010	-3.50%			312			-12.1%			-14.1%		
	60-011	-1.64%			263			-9.0%			-11.2%		
3	28-003	-5.37%	-3.37%	1.76%	603	491	125	-18.3%	-14.0%	3.90%	-24.6%	-19.3%	4.92%
	29-004[a]	-2.03%			356			-10.7%			-14.9%		
	30-005[a]	-2.72%			514			-13.0%			-18.3%		
4	31-7632	0.04%	-0.05%	0.13%	49.6	40.7	12.7	-1.3%	-1.0%	0.42%	-1.7%	-1.55%	0.21%
	32-7650[b]												
	33-002	-0.14%			31.7			-0.7%			-1.4%		
6	25-7579	0.01%	-0.51%	0.73%	71.4	41.9	41.8	-1.7%	-1.45%	0.35%	-2.4%	-1.80%	0.85%
	26-7577[b]												
	27-001	-1.02%			12.3			-1.2%			-1.2%		

[a] 29-004 and 30-005 were depowered due to instrumentation issues before 300 hours but after sufficient time that the data collected from these parts are useful, and so will be included.
[b] 32-7650 and 26-7577 did not reach 300 hours due to infant mortality and instrumentation issues; this data is excluded from the data set and discussion.

TABLE 26. SLOPES OF NORMALIZED I_{DMAX} AND I_{DSS} LINES FOR HIGH-POWER CONDITIONS (SEE TABLE 8)

Condition	Device	I_{Dmax} slope (normalized fraction/hr)	I_{Dmax} slope Avg	I_{Dmax} slope Stdev	I_{DSS} slope (normalized fraction/hr)	I_{DSS} slope Avg	I_{DSS} slope Stdev
1	55-006	-2.6E-04	-2.9E-04	3.5E-05	-3.4E-04	-4.0E-04	5.5E-05
	56-007	-2.9E-04			-4.0E-04		
	57-008	-3.3E-04			-4.5E-04		
2	58-009	-3.9E-04	-3.6E-04	5.5E-05	-4.7E-04	-4.4E-04	5.8E-05
	59-010	-4.0E-04			-4.7E-04		
	60-011	-3.0E-04			-3.7E-04		
3	28-003	-6.1E-04	-6.4E-04	1.4E-04	-8.2E-04	-8.8E-04	2.0E-04
	29-004	-8.0E-04			-1.1E-03		
	30-005	-5.2E-04			-7.2E-04		

TABLE 27. SLOPES OF NORMALIZED I_{DMAX} AND I_{DSS} LINES FOR HIGH-VOLTAGE CONDITIONS (SEE TABLE 9)

Condition	Device	I_{Dmax} slope (normalized fraction/hr)	I_{Dmax} slope Avg	I_{Dmax} slope Stdev	I_{DSS} slope (normalized fraction/hr)	I_{DSS} slope Avg	I_{DSS} slope Stdev
4	31-7632	-6.7E-05	-5.0E-05	2.4E-05	-8.5E-05	-7.7E-05	1.2E-05
	33-002	-3.3E-05			-6.8E-05		
6	25-7579	-8.7E-05	-7.3E-05	2.1E-05	-1.2E-04	-9.1E-05	4.1E-05
	27-001	-5.8E-05			-6.2E-05		

TABLE 28. PARAMETER CHANGES BY DEVICE AND STRESS TIME Y IN 600-HOUR TEST (SEE TABLE 13)

Y (hours)	Device	g_{mp}			V_T			I_{Dmax}			I_{DSS}		
		%	Avg	Stdev	mV	Avg	Stdev	%	Avg	Stdev	%	Avg	Stdev
200	25-024	-4.1%	-3.23%	0.85%	311	267	37.9	-10.4%	-8.53%	1.69%	-13.5%	-11.3%	1.99%
	26-025	-3.2%			248			-8.1%			-10.6%		
	27-026[a]	-2.4%			243			-7.1%			-9.7%		
600	25-024	-3.2%	-2.80%	0.57%	246	209	52.3	-8.3%	-7.05%	1.77%	-10.9%	-9.10%	2.55%
	26-025	-2.4%			172			-5.8%			-7.3%		

[a] A test channel became unusable after the first 200 hours. Hence, only 200 hours of Device 27-026 are shown.

TABLE 29. PARAMETER PERCENTAGE CHANGES BY CHANNEL AND CONDITION IN 1000-HOUR TEST (T_{BP} = 245 °C; T = 1 HOUR VS. T = 1000 HOURS) (SEE TABLE 15)

Condition	Device	g_{mp} %	g_{mp} Avg	g_{mp} Stdev	V_T %	V_T Avg	V_T Stdev	I_{Dmax} %	I_{Dmax} Avg	I_{Dmax} Stdev	I_{DSS} %	I_{DSS} Avg	I_{DSS} Stdev
4	13-012	-4.13%	-3.66%	0.63%	3.62%	3.41%	0.21%	-5.37%	-5.29%	0.34%	-7.42%	-6.80%	0.58%
	14-013	-3.91%			3.41%			-5.59%			-6.70%		
	15-014	-2.94%			3.20%			-4.93%			-6.27%		
5	19-015	-3.29%	-3.29%	NA	3.41%	3.41%	NA	-4.94%	-4.94%	NA	-6.76%	-6.76%	NA
	20-016[a]												
	21-017[a]												
6	22-018[b]		-4.27%	0.50%		2.19%	0.05%		-4.84%	0.57%		-6.52%	0.45%
	23-019	-3.92%			2.16%			-4.44%			-6.20%		
	24-020	-4.63%			2.23%			-5.24%			-6.84%		

[a] 20-016 and 21-017 were intended to be stressed at Condition 5. However, the previous channel programming was not cleared before the test, and these devices were not stressed at Condition 5.

[b] 22-018 suffered infant mortality at 1.36 hours.

TABLE 30. PARAMETER PERCENTAGE CHANGES BY CHANNEL AND CONDITION IN 1000-HOUR TEST (T_{BP} = 245 °C; T = 0 HOURS VS. T = 1000 HOURS) (SEE TABLE 17)

Condition	Device	g_{mp} %	g_{mp} Avg	g_{mp} Stdev	V_T %	V_T Avg	V_T Stdev	I_{Dmax} %	I_{Dmax} Avg	I_{Dmax} Stdev	I_{DSS} %	I_{DSS} Avg	I_{DSS} Stdev
4	13-012	-4.388%	-3.257%	1.183%	-5.828%	-3.230%	3.853%	-2.795%	-3.091%	1.087%	0.943%	-0.345%	2.910%
	14-013	-3.355%			-5.059%			-2.181%			1.699%		
	15-014	-2.028%			1.196%			-4.295%			-3.676%		
5	19-015	-3.107%	-3.107%	NA	-12.14%	-12.14%	NA	2.252%	2.252%	NA	8.680%	8.680%	NA
	20-016[a]												
	21-017[a]												
6	22-018[b]		-4.623%	0.166%		-4.911%	1.857%		-3.734%	0.085%		-0.158%	0.941%
	23-019	-4.505%			-3.598%			-3.795%			-0.824%		
	24-020	-4.740%			-6.224%			-3.674%			0.507%		

[a] 20-016 and 21-017 were intended to be stressed at Condition 5. However, the previous channel programming was not cleared before the test, and these devices were not stressed at Condition 5.

[b] 22-018 suffered infant mortality at 1.36 hours.

TABLE 31. PARAMETER PERCENTAGE CHANGES BY CHANNEL AND CONDITION IN 1000-HOUR TEST (T_{BP} = 70 °C; T = 0 HOURS VS. T = 1000 HOURS) (SEE TABLE 18)

Condition	Device	g_{mp}			V_T			I_{Dmax}			I_{DSS}		
		%	**Avg**	**Stdev**	**%**	**Avg**	**Stdev**	**%**	**Avg**	**Stdev**	**%**	**Avg**	**Stdev**
4	13-012	-4.316%	-3.495%	0.712%	-7.271%	-5.598%	4.304%	-2.032%	-2.173%	1.545%	0.845%	0.194%	3.063%
	14-013	-3.049%			-8.814%			-0.704%			2.879%		
	15-014	-3.119%			-0.709%			-3.784%			-3.143%		
5	19-015	-4.196%	-4.196%	NA	-16.67%	-16.67%	NA	2.590%	2.590%	NA	9.035%	9.035%	NA
	20-016[a]												
	21-017[a]												
6	22-018[b]		-4.825%	0.276%		-5.229%	1.957%		-3.728%	0.914%		-1.257%	1.729%
	23-019	-4.630%			-3.845%			-4.375%			-2.480%		
	24-020	-5.020%			-6.613%			-3.082%			-0.035%		

[a] 20-016 and 21-017 were intended to be stressed at Condition 5. However, the previous channel programming was not cleared before the test, and these devices were not stressed at Condition 5.

[b] 22-018 suffered infant mortality at 1.36 hours.

TABLE 32. PARAMETER PERCENTAGE CHANGES BY CHANNEL AND STRESS TIME IN 600-HOUR TEST (T_{BP} = 245 °C; T = 1 HOUR VS. T = Y HOURS) (SEE TABLE 19)

Y (hours)	Device	g_{mp}			V_T			I_{Dmax}			I_{DSS}		
		%	**Avg**	**Stdev**	**%**	**Avg**	**Stdev**	**%**	**Avg**	**Stdev**	**%**	**Avg**	**Stdev**
200	25-024	-0.99%	-1.07%	0.10%	8.90%	6.16%	2.46%	-5.79%	-4.58%	1.05%	-9.68%	-7.18%	2.22%
	26-025	-1.02%			5.44%			-4.07%			-6.41%		
	27-026[a]	-1.18%			4.15%			-3.88%			-5.45%		
600	25-024	-1.72%	-1.71%	0.02%	7.04%	4.92%	3.00%	-5.27%	-4.15%	1.58%	-8.32%	-6.31%	2.85%
	26-025	-1.69%			2.80%			-3.04%			-4.29%		

[a] A test channel became unusable after the first 200 hours. Hence, only 200 hours of Device 27-026 are shown.

TABLE 33. PARAMETER PERCENTAGE CHANGES BY CHANNEL AND STRESS TIME IN 600-HOUR TEST (T_{BP} = 245 °C; T = 0 HOURS VS. T = Y HOURS) (SEE TABLE 21)

Y (hours)	Device	g_{mp}			V_T			I_{Dmax}			I_{DSS}		
		%	Avg	Stdev	%	Avg	Stdev	%	Avg	Stdev	%	Avg	Stdev
200	25-024	-0.885%	-0.841%	0.414%	12.336%	10.038%	2.228%	-7.886%	-6.743%	1.063%	-13.142%	-10.869%	2.007%
	26-025	-0.406%			9.890%			-6.557%			-10.128%		
	27-026[a]	-1.230%			7.888%			-5.785%			-9.338%		
600	25-024	-1.617%	-1.348%	0.381%	10.554%	8.962%	2.251%	-7.377%	-6.462%	1.294%	-11.836%	-9.962%	2.650%
	26-025	-1.078%			7.370%			-5.547%			-8.089%		

[a] A test channel became unusable after the first 200 hours. Hence, only 200 hours of Device 27-026 are shown.

TABLE 34. PARAMETER PERCENTAGE CHANGES BY CHANNEL AND STRESS TIME IN 600-HOUR TEST (T_{BP} = 70 °C; T = 0 HOURS VS. T = Y HOURS) (SEE TABLE 22)

Y (hours)	Device	g_{mp}			V_T			I_{Dmax}			I_{DSS}		
		%	Avg	Stdev	%	Avg	Stdev	%	Avg	Stdev	%	Avg	Stdev
200	25-024	-4.099%	-3.218%	0.855%	10.467%	9.024%	1.278%	-10.363%	-8.537%	1.660%	-13.523%	-11.280%	1.995%
	26-025	-3.164%			8.570%			-8.130%			-10.613%		
	27-026[a]	-2.392%			8.034%			-7.119%			-9.703%		
600	25-024	-3.157%	-2.791%	0.518%	8.289%	7.122%	1.650%	-8.276%	-7.055%	1.727%	-10.863%	-9.084%	2.516%
	26-025	-2.425%			5.956%			-5.834%			-7.305%		

[a] A test channel became unusable after the first 200 hours. Hence, only 200 hours of Device 27-026 are shown.

TABLE 35. I_{DMAX} DEGRADATION IN CONTINUOUS- AND PULSED-DC, SAME-BIAS TESTS (SEE TABLE 23)

Condition	Device	*Test Time (hours)*	*ON Time (hours)*	I_{Dmax} %	Avg	Stdev
2	58-009	300	300	-11.6%	-10.9%	1.69%
	59-010			-12.1%		
	60-011			-8.95%		
		Equivalent Test Time (hours)				
PCA	1	600	300	-6.99%	-9.04%	2.11%
	2			-11.2%		
	3			-8.92%		
PCB	4	600	300	-11.9%	-12.8%	0.77%
	5			-13.2%		
	6			-13.3%		
PCC	7	360	300	-13.4%	-12.7%	1.05%
	8			-11.9%		

Bibliography

(Agilent, 2004) Agilent Technologies. "Agilent E5270B 8 Slot Precision Measurement Mainframe Technical Overview," Sep. 2004. Available: http://cp.literature.agilent.com/litweb/pdf/5989-1355EN.pdf. Accessed July 2011.

(Ali, 1991) Ali, F. and A. Gupta, Eds. *HEMTs & HBTs: Devices, Fabrication, and Circuits*. Norwood, MA: Artech House, 1991.

(Ambacher, 1999) Ambacher, O., *et al*. "Two-dimensional electron gases induced by spontaneous and piezoelectric polarization charges in N- and Ga-face AlGaN/GaN heterostructures," *J. Appl. Phys.*, vol. 85, no. 6, pp. 3222-3333, 1999.

(Ambacher, 2002) Ambacher, O., J. Majewski, C. Miskys, A. Link, M. Hermann, M. Eickhoff, M. Stutzmann, F. Bernardini, V. Fiorentini, V. Tilak, B. Schaff, and L. F. Eastman. "Pyroelectric properties of Al(In)GaN/GaN hetero- and quantum well structures," *J. Phys.: Condensed Matter*, vol. 14, no. 13, pp. 3399-3434, Apr. 2002.

(ANSYS) ANSYS, Inc., Canonsburg, PA. [Online]. Available: www.ANSYS.com

(Asif Khan, 1993) Asif Khan, M., A. Bhattarai, J. N. Kuznia, and D. T. Olson. "High electron mobility transistor based on GaN-$Al_xGa_{1-x}N$ heterojunction," *Appl. Phys. Lett.*, vol. 63, no. 9, p. 1214, 1993.

(Bertoluzza, 2009) Bertoluzza, F., G. Sozzi, N. Delmonte, and R. Menozzi. "Lumped element thermal modeling of GaN-based HEMTs," in *2009 IEEE MTT-S Int. Microw. Symp. Digest*, Boston, MA, pp. 973-976.

(Bettidi, 2009) Bettidi, A., F. Corsaro, A. Cetronio, A. Nanni, M. Peroni, and P. Romanini. "X-band GaN-HEMT LNA performance versus robustness trade-off," *2009 European Microw. Conf.*, Rome, Italy, pp.1792-1795.

(Bozada, 2010a) Bozada, C. A. Private communication, May 2010.

(Bozada, 2010b) Bozada, C. A. Private communication, Aug. 2010.

(Cacho, 2008) Cacho, F., V. Fiori, L. Doyen, C. Chappaz, C. Tavernier, and H. Jaouen. "Electromigration induced failure mechanism: multiphysics model and correlation with experiments," in *9th Int. Conf. Thermal, Mech. and Multiphysics Simulation and Experiments Micro-Electron. and Micro-Syst., EuroSimE 2008*, pp. 1-6.

(Chavarkar, 2003) Chavarkar, P. and U. K. Mishra. "High Electron Mobility Transistors," in *RF and Microwave Semiconductor Device Handbook*, J. M. Golio, Ed., Boca Raton, Fla.: CRC Press, 2003.

(Chou, 2004) Chou, Y. C., D. Leung, I. Smorchkova, M. Wojtowicz, R. Grundbacher, L. Callejo, Q. Kan, R. Lai, P. H. Liu, D. Eng, and A. Oki. "Degradation of AlGaN/GaN HEMTs under elevated temperature lifetesting," *Microelectron. Rel.*, vol. 44, no. 7, pp. 1033-1038, July 2004.

(Chowdhury, 2008) Chowdhury, U., J. L. Jimenez, C. Lee, E. Beam, P. Saunier, T. Balistreri, S.-Y. Park, T. Lee, J. Wang, M. J. Kim, J. Joh, and J. A. del Alamo. "TEM Observation of Crack- and Pit-Shaped Defects in Electrically Degraded GaN HEMTs," *Electron Device Letters, IEEE* , vol.29, no.10, pp.1098-1100, Oct. 2008.

(Christiansen, 2011a) Christiansen, B. D., R. A. Coutu, E. R. Heller, C.A. Bozada, B. S. Poling, G. D. Via, J. P. Theimer, and S. E. Tetlak. "Benefits of considering more than temperature acceleration for GaN HEMT life testing," submitted to *Microeletron. Rel.*, 1 Aug. 2011.

(Christiansen, 2011b) Christiansen, B. D., R. A. Coutu, E. R. Heller, B. S. Poling, G. D. Via, R. Vetury, and J. B. Shealy. "Reliability testing of AlGaN/GaN HEMTs under multiple stressors," in *2011 IEEE Int. Rel. Physics Symp. (IRPS)*, Monterey, CA, pp. CD.2.1-CD.2.5.

(Christiansen, 2011c) Christiansen, B. D., E. R. Heller, R. A. Coutu, R. Vetury, and J. B. Shealy, "A very robust AlGaN/GaN HEMT technology to high forward gate bias and current," submitted to *IEEE Electron Device Lett.*, 23 Aug. 2011.

(Circuits Today, 2010) Circuits Today. "EMOSFET-Enhancement MOSFET," www.circuitstoday.com/emosfet-enhancement-mosfet, accessed Aug. 2010.

(Coffie, 2007) Coffie, R., Y. Chen, I. P. Smorchkova, B. Heying, V. Gambin, W. Sutton, Y.-C. Chou, W.-B. Luo, M. Wojtowicz, and A. Oki. "Temperature and voltage dependent RF degradation study in AlGaN/GaN HEMTs," in *2007 IEEE Int. Rel. Phys. Symp.*, Phoenix, AZ, pp.568-569.

(COMSOL) COMSOL AB, Stockholm, Sweden. [Online]. Available: www.comsol.com

(Conway, 2007) Conway, A. M., M. Chen, P. Hashimoto, P. J. Willadsen, and M. Micovic. "Accelerated RF life testing of GaN HFETs," in *Proc. 2007 IEEE Int. Rel. Phys. Symp.*, Phoenix, AZ, pp.472-475.

(Coutu, 2011) Coutu, Jr., R. A. "FY10 [Sponsor] Program Final Report: Electronic Component Failure Prediction Tool Development," unpublished, Jun. 2011.

(del Alamo, 2009) del Alamo, J. A. and J. Joh. "GaN HEMT reliability," *Microelectron. Rel.*, vol. 49, nos. 9-11, pp. 1200-1206, Sep. -Nov. 2009.

(Dridi, 2010) Dridi, Z., B. Bouhafs, and P. Ruterana. "First-principles investigation of lattice constants and bowing parameters in wurtzite AlxGa1−xN, InxGa1−xN and InxAl1−xN alloys", *Semicond. Sci. Technol.*, vol. 18, no. 9, pp. 850-856, Aug. 2003. Available: iopscience.iop.org/0268-1242/18/9/307/fulltext, accessed Aug. 2010.

(Ebeling, 2005) Ebeling C. E. *An Introduction to Reliability and Maintainability Engineering*, Long Grove, IL: Waveland Press, 2005.

(EENG 596, 2008) EENG 596, Fall 2008, Ch. 8 slides.

(EENG 717, 2009) EENG 717, Summer 2009, "HEMTs" slides.

(Fang, 2009) Fang, Z.-Q., G. C. Farlow, B. Claflin, D. C. Look, and D. S. Green. "Effects of electron-irradiation on electrical properties of AlGaN/GaN Schottky barrier diodes," *J. Appl. Physics*, vol. 105, p. 123704, Jun. 2009.

(Glowacki, 2009) Glowacki, A., P. Laskowski, C. Boit, P. Ivo, E. Bahat-Treidel, R. Pazirandeh, R. Lossy, J. Wurfland, and G. Trankle. "Characterization of stress degradation effects and thermal properties of AlGaN/GaN HEMTs with photon emission spectral signatures," *Microelectron. Rel.*, vol. 49, nos. 9-11, pp. 1211-1215, Sep. -Nov. 2009.

(Green, 2000) Green B. M., *et al*. "The effect of surface passivation on the microwave characteristics of undoped AlGaN/GaN HEMT's," *IEEE Electron Device Letters*, vol. 21, June 2000.

(Hafizi, 1994) Hafizi, M. and M. J. Delaney. "Reliability of InP-based HBT's and HEMT's: experiments, failure mechanisms, and statistics," in *Proc. 6th Int. Conf. Indium Phosphide and Related Materials*, 1994, pp.299-302.

(Heller, 2008a) Heller, E. R. "Simulation of life testing procedures for estimating long-term degradation and lifetime of AlGaN/GaN HEMTs," *IEEE Trans. Electron Devices*, vol. 55, no. 10, pp. 254-2560, Oct. 2008.

(Heller, 2008b) Heller, E. R. and A. Crespo. “Electro-thermal modeling of multifinger AlGaN/GaN HEMT device operation including thermal substrate effects”, *Microelectron. Rel.*, vol. 48, no. 1, pp 45-50, Jan. 2008.

(Heller, 2011a) Heller, E. R. Private communication, Feb. 2011.

(Heller, 2011b) Heller, E. R. Private communication, Apr. 2011.

(Higashiwaki, 2008) Higashiwaki, M., T. Mimura, and T. Matsui. “AlGaN/GaN heterostructure field-effect transistors on 4H-SiC substrates with current-gain cutoff frequency of 190GHz,” *Appl. Phys. Express*, vol. 1, no. 2, pp. 021103-1 to 021103-3, Feb. 2008.

(Joh, 2007) Joh, J., L. Xia, and J. A. del Alamo. “Gate current degradation mechanisms of GaN high electron mobility transistors,” in *2007 IEEE Int. Electron Devices Meeting*, Washington, D.C., pp.385-388.

(Joh, 2008) Joh, J. and J. A. del Alamo. “Critical voltage for electrical degradation of GaN high-electron mobility transistors,” *IEEE Electron Device Lett.*, vol. 29, no. 4, pp. 287-289, Apr. 2008.

(Joh, 2009) Joh, J., F. Gao, T. Palacios, and J. A. del Alamo. “A model for the critical voltage for electrical degradation of GaN high electron mobility transistors,” *2009 Reliability of Compound Semiconductors (ROCS) Digest*, pp.3-6, Oct. 2009.

(Joh, 2011) Joh, J. Private communication, Apr. 2011.

(Joshin, 2006) Joshin, K. and T. Kikkawa. “Recent progress of high power GaN-HEMT for wireless application,” in *2006 Asia-Pacific Microw. Conf.*, Yokohama, Japan, pp.1027-1032.

(Karmalkar, 2001) Karmalkar, S. and U. K. Mishra. “Enhancement of breakdown voltage in AlGaN/GaN high electron mobility transistors using a field plate,” *IEEE Trans. Electron Devices*, vol.48, no.8, pp.1515-1521, Aug. 2001.

(Katzer, 2006) Katzer, D. S., J. A. Mittereder, S. C. Binari, D. F. Storm, J. A. Roussos, and P. B. Klein. “Study of the Impact of Electron Traps on GaN HEMT Reliability,” *ECS Trans.*, vol. 3, no. 5, pp. 151-160, Nov. 2006.

(Kim, 2005) Kim, J., J. A. Freitas, Jr., P. B. Klein, S. Jang, F. Ren, and S. J. Pearton. “The Effect of Thermally Induced Stress on Device Temperature

Measurements by Raman Spectroscopy", Electrochemical and Solid-State Letters, **8** 12 G345-G347 (2005).

(Koley, 2003) Koley, G., V. Tilak, L. F. Eastman, and M. G. Spencer. "Slow transients observed in AlGaN/GaN HFETs: Effects of SiN_x passivation and UV illumination," *IEEE Trans. Electron Devices*, vol. 50, no. 4, pp. 886–893, Apr. 2003.

(Kuball, 2010) Kuball, M., N. Killat, A. Manoi, and J. W. Pomeroy. "Benchmarking of thermal boundary resistance of GaN-SiC interfaces for AlGaN/GaN HEMTs: US, European and Japanese suppliers," in *Tech. Dig. Int. Conf. Compound Semiconductor MANTECH*, 2010, pp. 109-110.

(Kuo, 1999) Kuo W. and T. Kim. "An overview of manufacturing yield and reliability modeling for semiconductor products," *Proc. IEEE*, vol. 87, no. 8, August 1999.

(Leach, 2010) Leach, J. H. and H. Morkoç. "Status of Reliability of GaN-Based Heterojunction Field Effect Transistors," *Proc. IEEE*, vol. 98, pp. 1127-1139, July 2010.

(Lee, 2008) Lee, S., R. Vetury, J. D. Brown, S. R. Gibb, W. Z. Cai, J. Sun, D. S. Green, and J. Shealy. "Reliability assessment of AlGaN/GaN HEMT technology on SiC for 48V applications," in *2008 IEEE Int. Rel. Phys. Symp.*, Phoenix, AZ, pp. 446-449.

(Li, 2009) Li, Y., M. Krishnan, S. Salemi, G. Paradee, and A. Christou. "Strain induced buffer layer defects in GaN HFETs and their evolution during reliability testing," in *2009 IEEE Int. Rel. Phys. Symp.*, Montreal, QC, pp. 718-721.

(Liddle, 2008) Liddle, A. J. "Sensitivity analysis of AlGaN/GaN high electron mobility transistors to process variation," M.S. thesis, Dept. Elec. Comput. Eng, Air Force Inst. Technol., Wright-Patterson AFB, OH, 2008.

(Makaram, 2010) Makaram, P., J. Joh, J. A. del Alamo, T. Palacios, and C. V. Thompson. "Evolution of structural defects associated with electrical degradation in AlGaN/GaN high electron mobility transistors," *Appl. Phys. Lett.*, vol. 96, no. 23, p. 233509, 2010.

(Marcon, 2010) Marcon, D., T. Kauerauf, F. Medjdoub, J. Das, M. Van Hove, P. Srivastava, K. Cheng, M. Leys, R. Mertens, S. Decoutere, G. Meneghesso, E. Zanoni, and G. Borghs. "A comprehensive reliability investigation of the voltage-, temperature- and device geometry-dependence of the gate degradation on state-of-

the-art GaN-on-Si HEMTs," in *2010 IEEE Int. Electron Devices Meeting*, San Francisco, CA, pp. 20.3.1-20.3.4.

(Marcon, 2011) Marcon, D., T. Kauerauf, and S. Decoutere. (2011, June). Unraveling the mysteries of HEMT degradation. *Compound Semiconductor* [Online]. Available: http://content.yudu.com/A1sg95/ComSemiJune2011/resources/14.htm.

(MathWorks) The MathWorks, Inc., Natick, MA. [Online]. Available: www.mathworks.com

(May, 2004) May, G. S. and S. M. Sze. *Fundamentals of Semiconductor Fabrication*, Hoboken, NJ: John Wiley & Sons, 2004.

(McClory, 2008) McClory, J. W. "The effect of radiation on the electrical properties of aluminum gallium nitride/gallium nitride heterostructures," Ph.D. dissertation, Dept. Eng. Phys., Air Force Inst. Technol., Wright-Patterson AFB, OH, 2008.

(McQueary, 2008) McQueary, C. E. "Improving the suitability of systems," *ITEA J.*, vol. 29, no. 3, pp. 211-214, Sep. 2008.

(Meeker, 1998) Meeker, W. Q. and L. A. Escobar. *Statistical Methods for Reliability Data*, New York: John Wiley & Sons, 1998.

(Meneghesso, 2008) Meneghesso, G., G. Verzellesi, F. Danesin, F. Rampazzo, F. Zanon, A. Tazzoli, M. Meneghini, and E. Zanoni. "Reliability of GaN high-electron-mobility transistors: state of the art and perspectives," *IEEE Trans. Dev. Mat. Rel.*, vol. 8, no. 2, June 2008.

(Mishra, 2002) Mishra, U. K., P. Parikh, and Y-F Wu. "AlGaN/GaN HEMTs—an overview of device operation and applications," *Proc. IEEE*, vol. 90, no. 6, pp. 1022-1031, June 2002.

(Montgomery, 2009) Montgomery, D. C. *Design and Analysis of Experiments*, New York: John Wiley & Sons, 2009.

(Neaman, 2003) Neaman, D. A. *Semiconductor Physics and Devices: Basic Principles*, 3rd ed. New York: McGraw-Hill, 2003.

(Nelson, 1990) Nelson, W. *Accelerated Testing: Statistical Models, Test Plans, and Data Analyses*, New York: John Wiley & Sons, 1990.

(NIST, 2010) National Institute of Standards and Technology. “Eyring” in *Engineering Statistics Handbook*, www.itl.nist.gov/div898/handbook/apr/section1/apr152.htm, accessed Aug. 2010.

(Nobelprize.org, 2010) Nobelprize.org. “The History of the Integrated Circuit.” nobelprize.org/educational/physics/integrated_circuit/history/index.html, accessed Aug. 2010.

(Park, 2009) Park, S.Y., C. Floresca, U. Chowdhury, J. L. Jimenez, C. Lee, E. Beam, P. Saunier, T. Balistreri, M. J. Kim. “Physical degradation of GaN HEMT devices under high drain bias reliability testing,” *Microelectron. Rel.*, vol. 49, no. 5, pp. 478-483, May 2009.

(Pavlidis, 2005) Pavlidis, D., P. Valizadeh, and S. H. Hsu. “AlGaN/GaN high electron mobility transistor (HEMT) reliability,” *2005 European Gallium Arsenide and Other Semiconductor Application Symp.*, pp. 265- 268.

(Plexim) Plexim GmbH, Zurich, Switzerland. [Online]. Available: www.plexim.com

(Posternak, 1990) Posternak, M., A. Baldereschi, A. Catellani, and R. Resta. “*Ab Initio* Study of the Spontaneous Polarization of Pyroelectric BeO,” *Phys. Rev. Lett.*, vol. 64, no. 15, pp. 1777-1780, Apr. 1990.

(Puzyrev, 2010) Puzyrev, Y. S., B. R. Tuttle, R. D. Schrimpf, D. M. Fleetwood, and S. T. Pantelides. “Theory of hot-carrier-induced phenomena in GaN high-electron-mobility transistors”, *Appl. Phys. Lett.*, vol. 96, no. 5, pp. 053505:1-3, 2010.

(Puzyrev, 2011) Puzyrev, Y. S., T. Roy, M. Beck, B. R. Tuttle, R. D. Schrimpf, D. M. Fleetwood, and S. T. Pantelides. “Dehydrogenation of defects and hot-electron degradation in GaN high-electron-mobility transistors,” *J. Appl. Phys.*, vol. 109, no. 3, pp. 034501:1-8, 2011.

(Rao, 2010) Rao, H. and G. Bosman. “Device reliability study of high gate electric field effects in AlGaN/GaN high electron mobility transistors using low frequency noise spectroscopy,” *J. Appl. Physics*, vol. 108, p. 053707, Sep. 2010.

(Rashmi, 2002) Rashmi, A. Kranti, S. Haldar, and R. S. Gupta. “An accurate charge control model for spontaneous and piezoelectric polarization dependent two-dimensional electron gas sheet charge density of lattice-mismatched AlGaN/GaN HEMTs,” *Solid State Electronics*, vol. 46, pp. 621-630, 2002.

(ReliaSoft, 2011) ReliaSoft Corporation, Tucson, AZ. http://www.weibull.com/AccelTestWeb/general_log_linear_relationship_chap_.htm, accessed May 2011.

(Roy, 2010) Roy, T., Y. S. Puzyrev, B. R. Tuttle, D. M. Fleetwood, R. D. Schrimpf, D. F. Brown, U. K. Mishra, and S. T. Pantelides. "Electrical-stress-induced degradation in AlGaN/GaN high electron mobility transistors grown under gallium-rich, nitrogen-rich, and ammonia-rich conditions," *Appl. Phys. Lett.*, vol. 96, pp. 133503-1 to 133503-3, 2010.

(SAS Institute) SAS Institute Inc., Cary, NC. [Online]. Available: www.jmp.com

(Schwierz, 2003) Schwierz, F. and J.J. Liou. *Modern Microwave Transistors: Theory, Design, and Performance*, Hoboken, N.J.: Wiley-Interscience, 2003.

(Sedra, 1991) Sedra, A. S. and K. C. Smith. *Microelectronic Circuits*, 3rd ed. Saunders College Publishing, 1991.

(Silvaco) Silvaco, Inc., Santa Clara, CA. [Online]. Available: www.silvaco.com

(SIMULIA) SIMULIA, Providence, RI. [Online]. Available: www.simulia.com

(Singhal, 2007) Singhal, S., A. W. Hanson, A. Chaudhari, P. Rajagopal, T. Li, J. W. Johnson, W. Nagy, R. Therrien, C. Park, A. P. Edwards, E. L. Piner, K. J. Linthicum, and I. C. Kizilyalli. "Qualification and reliability of a GaN process platform," in *Tech. Dig. Int. Conf. Compound Semiconductor MANTECH*, 2007, pp. 83-86.

(Smith, 2009) Smith, K. V., S. Brierley, R. McAnulty, C. Tilas, D. Zarkh, M. Benedek, P. Phalon, and A. Hooven. "GaN HEMT reliability through the decade," *ECS Trans.*, vol. 19, no. 3, pp. 113-121, May 2009.

(Statemaster.com, 2010) Statemaster.com. www.statemaster.com/encyclopedia/Image:CellPhoneTower-OR.jpg, accessed Aug. 2010.

(Synopsys) Synopsys, Inc., Mountain View, CA. [Online]. Available: www.synopsys.com

(Synopsys, 2008) Synopsys, Inc., Mountain View, CA. *Simulation of NMOSFET Degradation Kinetics with TCAD Sentaurus*, 2008.

(Synopsys, 2010) Synopsys, Inc., Mountain View, CA. *Sentaurus Device User Guide*, ver. D-2010.03, 2010.

(Sze, 2007) Sze, S. M. and K. K. Ng. *Physics of Semiconductor Devices*, 3rd ed. Hoboken, NJ: John Wiley & Sons, 2007.

(Trew, 2005) Trew, R. J., G. L. Bilbro, W. Kuang, Y. Liu, and H. Yin. "Microwave AlGaN/GaN HFETs," *IEEE Microwave*, vol. 6, no. 1, pp. 56-66, Mar. 2005.

(Trew, 2009) Trew, R. J., D. S. Green, and J. B. Shealy. "AlGaN/GaN HFET reliability," *IEEE Microwave*, vol. 10, no. 4, pp. 116-127, June 2009.

(Ullrich, 2010) Ullrich, B. "Semiconductors Optics and Optoelectronics I," kottan-labs.bgsu.edu/teaching/workshop2001/chapter5.htm, accessed Aug. 2010.

(U.S. DoD, 2010) U.S. Department of Defense. "Forward Deployed and/or U.S.-based X-band radars," www.defense.gov/specials/missiledefense/xbr.html, accessed Aug. 2010.

(Vetury, 2001) Vetury, R., N. Q. Zhang, S. Keller, and U. K. Mishra. "The impact of surface states on the DC and RF characteristics of AlGaN/GaN HFETs," *IEEE Trans. Electron Devices*, vol.48, no.3, pp.560-566, Mar. 2001.

(Via, 2010) Via, G. D. Private communication, Aug. 2010.

(Vurgaftman, 2001) Vurgaftman, I., J. R. Meyer, and L. R. Ram-Mohan. "Band parameters for III--V compound semiconductors and their alloys," *J. Appl. Phys.*, vol. 89, no. 11, pp. 5815-5875, June 2001.

(Weatherford, 2010) Weatherford, T. R. Private communication, Jun. 2010.

(Xu, 2004) Xu, H., C. Sanabria, A. Chini, S. Keller, U. K. Mishra, and R. A. York. "A C-band high-dynamic range GaN HEMT low-noise amplifier," *IEEE Microw. Wireless Compon. Lett.*, vol.14, no.6, pp. 262-264, June 2004.

Vita

Bradley D. Christiansen was born in Provo, Utah, in May 1971. His parents relocated soon thereafter to Payson, Utah, where they reared Brad. He graduated from Payson High School in May 1989. In the Fall of that same year, Brad began his pursuit toward a bachelor's degree in electrical engineering at Brigham Young University (BYU) in Provo, Utah. After his freshman year, Brad served a two-year Church mission to Massachusetts among Portuguese-speaking people. Following his mission, he continued his studies at BYU and participated in the Air Force Reserve Officer Training Corps. He graduated and was commissioned a second lieutenant in the United States Air Force in December 1995. Brad entered active duty in February 1996 and had several assignments prior to graduating in March 2006 from the Air Force Institute of Technology (AFIT) with a master's degree in electrical engineering. He returned to AFIT in August 2008 to pursue the doctor of philosophy degree in electrical engineering. Upon graduation, he will be assigned to the Air Force Research Laboratory, Sensors Directorate, Aerospace Components and Subsystems Division.

REPORT DOCUMENTATION PAGE			*Form Approved* *OMB No. 0704-0188*

The public reporting burden for this collection of information is estimated to average 1 hour per response, including the time for reviewing instructions, searching existing data sources, gathering and maintaining the data needed, and completing and reviewing the collection of information. Send comments regarding this burden estimate or any other aspect of this collection of information, including suggestions for reducing the burden, to Department of Defense, Washington Headquarters Services, Directorate for Information Operations and Reports (0704-0188), 1215 Jefferson Davis Highway, Suite 1204, Arlington, VA 22202-4302. Respondents should be aware that notwithstanding any other provision of law, no person shall be subject to any penalty for failing to comply with a collection of information if it does not display a currently valid OMB control number.

PLEASE DO NOT RETURN YOUR FORM TO THE ABOVE ADDRESS.

1. REPORT DATE *(DD-MM-YYYY)*	**2. REPORT TYPE**	**3. DATES COVERED** *(From - To)*
22-12-2011	Doctoral Dissertation	Sep 2008 - Dec 2011

4. TITLE AND SUBTITLE
Investigation of Gallium Nitride Transistor Reliability through Accelerated Life Testing and Modeling

5a. CONTRACT NUMBER

5b. GRANT NUMBER

5c. PROGRAM ELEMENT NUMBER

6. AUTHOR(S)
Christiansen, Bradley D., Lieutenant Colonel, USAF

5d. PROJECT NUMBER
11G179

5e. TASK NUMBER

5f. WORK UNIT NUMBER

7. PERFORMING ORGANIZATION NAME(S) AND ADDRESS(ES)
Air Force Institute of Technology
Graduate School of Engineering and Management (AFIT/EN)
2950 Hobson Way
Wright-Patterson AFB OH 45433-7765

8. PERFORMING ORGANIZATION REPORT NUMBER
AFIT/DEE/ENG/11-04

9. SPONSORING/MONITORING AGENCY NAME(S) AND ADDRESS(ES)
Air Force Research Laboratory – Sensors Directorate
Christopher A. Bozada, Division Technical Advisor
2241 Avionics Circle
Wright-Patterson AFB, OH 45433-7322
Christopher.Bozada@wpafb.af.mil

10. SPONSOR/MONITOR'S ACRONYM(S)
AFRL/RYD

11. SPONSOR/MONITOR'S REPORT NUMBER(S)

12. DISTRIBUTION/AVAILABILITY STATEMENT
APPROVED FOR PUBLIC RELEASE; DISTRIBUTION UNLIMITED

13. SUPPLEMENTARY NOTES

14. ABSTRACT
Gallium nitride high electron mobility transistors are attractive to the DoD for their ability to operate at high frequencies, voltages, temperatures, and power. Yet, there are concerns about the reliability of these devices. Various degradation mechanisms and their causes are proposed in the literature. A variety of reliability tests were conducted to understand these mechanisms and causes. A multi-stressor experiment revealed different failure mechanisms than are in the literature. In particular, the devices tested at high voltage in the OFF state did not degrade significantly as suggested by others' reports. The validity of temperature-accelerated life testing when applied to GaN HEMT lifetime assessments is questioned. Temperature alone could not explain the differences in observed degradation. The tested devices showed excellent robustness to high forward gate stress, exhibiting only a slight change in gate diode characteristic, little decrease in maximum drain current, and a persisting breakdown voltage exceeding 200 V. The time-dependence of degradation was analyzed, and results of continuous- and pulsed-direct current stressing were compared.

15. SUBJECT TERMS
Gallium nitride, High electron mobility transistor, Reliability, Arrhenius, Accelerated life testing

16. SECURITY CLASSIFICATION OF:			**17. LIMITATION OF ABSTRACT**	**18. NUMBER OF PAGES**	**19a. NAME OF RESPONSIBLE PERSON**
a. REPORT	**b. ABSTRACT**	**c. THIS PAGE**			Dr. Ronald A. Coutu, Jr.
U	U	U	UU	209	**19b. TELEPHONE NUMBER** *(Include area code)* (937) 255-3636 x7230 Ronald.Coutu@afit.edu

Standard Form 298 (Rev. 8/98)
Prescribed by ANSI Std. Z39.18